Electronic Supplementary Material (ESI) for Faraday Discussions.

Trends in the Thermal Stability of Two-Dimensional Covalent Organic Frameworks

Austin M. Evans,[1] Matthew R. Ryder,[2] Woojung Ji,[1] Amanda R. Corcos,[1] Michael J. Strauss,[1] Edon Vitaku,[1] Nathan C. Flanders,[1] Ryan P. Bisbey,[1] William R. Dichtel*[,1]

[1]Northwestern University, Department of Chemistry, 2145 Sheridan Road, Evanston, IL 60208
[2]Neutron Scattering Division, Oak Ridge National Laboratory, Oak Ridge, TN, 37831

Supplementary Information

Correspondence Address

Professor William R. Dichtel
Northwestern University
2145 Sheridan Road
Evanston, IL 60208 (USA)
wdichtel@northwestern.edu

Table of Contents

List of Schemes, Tables, and Figures in Supporting Information

Schemes in Supporting Information — Page No.

Tables in Supporting Information — Page No.

Figures in Supporting Information — Page No.

A. Materials and Instrumentation

I. Materials

Reagents were purchased from commercial grade suppliers and used without further purification, unless otherwise described. Anhydrous solvents were obtained from a solvent purification system (JC Meyer System).

II. Instrumentation

Nuclear Magnetic Resonance (NMR) Spectroscopy. ^{1}H and ^{13}C NMR spectra were acquired on a Bruker AvanceIII-500 MHz spectrometer with a CryoProbe 5mm DCH w/ Z-Gradient, or on a 400 MHz Agilent DD MR-400 spectrometer using an AutoX 5mm probe w/ Z-Gradient. All spectra were recorded at 25°C unless specified otherwise. All spectra were calibrated using residual solvent as an internal reference ($CDCl_3$: 7.26 ppm for ^{1}H NMR, 77.00 for ^{13}C NMR; THF-d_8: 3.58, 1.73 ppm for ^{1}H NMR, 67.57, 25.37 ppm for ^{13}C NMR). Data are reported as follows: chemical shift, multiplicity (s = singlet, d = doublet, t = triplet, q = quartet, sep = septet, m = multiplet, *br* = broad, dd = doublet of doublets), coupling constants (Hz), and integration.

High-Resolution Mass Spectrometry (HRMS). High-resolution mass spectra were acquired on an Agilent 6210A LC-TOF Mass Spectrometer, with Atmospheric Pressure Photoionization (APPI) as an ion source. The instrument is equipped with an Agilent Series 1200 HPLC binary pump and autosampler. All samples were run using direct injection.

Sonication. Sonication was performed with a Branson 3510 ultrasonic cleaner with a power output of 100 W and a frequency of 42 kHz.

Critical Point Dryer. The supercritical drying procedure was performed in Tousimis Samdri795 critical point dryer. Prior to the supercritical drying process, all samples were placed in tea bags (ETS Drawstring Tea Filters, sold by English Tea Store, Amazon.com) and then soaked in absolute ethanol to keep the samples wet (typically 5–15 min). The drying chamber is first cooled ('cool' valve meter set to 0.40), and the tea bags containing the samples were then placed in it, and the chamber is filled with absolute ethanol and then sealed. The chamber was then filled with liquid CO_2 ('fill' valve meter set to 0.40), and after 2 min, the samples were purged for 30 min ('purge-vent' valve meter set to 0.15, and 'purge timer' valve meter set to 6). The temperature was then raised to 40°C resulting in a chamber pressure of around 1300 psi, which is well above the critical point of CO_2. The chamber was held above the critical point for 30 min, after which the CO_2 source was turned off, and the pressure was released over a period of 30 min ('bleed' valve meter set at 0.07). The samples were then transferred to vials and their final mass were weighed.

X-Ray Diffraction. Small- and wide-angle X-ray scattering (SAXS/WAXS) patterns were collected at Argonne National Lab's (ANL) Advanced Photon Source (APS) at sector 5-IDD (DND-CAT) in a capillary transmission geometry. Experiments conducted at 5-ID-D were

collected at a beam energy of 13.3 keV. Experiments were conducted by placing COF powders into capilarries filled with quartz wool. These capillaries then had their sealed ends removed and were connected to a constant flow of argon and placed into a heating block. Individual frames were collected on a set of Pilatus detectors, which were then summed and radially integrated to produce a linear XRD pattern using proprietary software available at the APS. Scattering intensity is reported as a function of the modulus of the scattering vector q, related to the scattering angle 2θ by the equation $q = (4\pi/\lambda) \sin \theta$, where λ is the X-ray wavelength. The sample-to-detector distance was adjusted to measure across relevant detection ranges. Capillary experiments were conducted using 2.0 mm OD borosilicate capillaries with 0.2 mm wall thicknesses purchased from Hilgenberg GmbH.

Variable Temperature X-Ray Diffraction Studies. *In operando* X-ray diffraction was performed at sector 17 of the Advanced Photon Source, Argonne National Laboratory. Samples were prepared by packing ~25 mg of COF sample into a thick-walled Kapton capillary and mounted into a sample holder available at the Sector 17. A thermocouple was then mounted in the center of the powder sample, inside of the Kapton capillary. The sample was then placed under a constant stream of helium and heated at a rate of $10°C \cdot min^{-1}$ under a helium atmosphere. Diffraction patterns were collected over the course of this heating on a 2D Pilatus detector approximately every minute by collecting ten frames per minute and averaging the counts of these ten frames. These frames were then radially integrated to produce 1D diffraction patterns, which were then analyzed.

COF Modeling and Structural Refinement. Crystal modeling of the COF structures was carried out using the Materials Studio (ver. 5.0) suite of programs by Accelrys. The initial structures were S5 constructed piecewise starting with a primitive hexagonal unit cell of a P6 space group. The cell parameter was estimated according to the distance between the center of the vertices for each COF, and c parameter was chosen as 3.35 Å, which has been observed for similar materials. [3] Initially, these structures were estimated to be eclipsed. The structures were optimized using a Geometry Optimization routine including energy minimization with cell parameters optimization, using the parameters from the Universal Force Field. Calculation of the simulated powder diffraction patterns and Pawley refinements were performed in the Materials Studio Reflex Plus Module using a Bragg-Brentano geometry. When the first ~2 features were seen to align but relative intensities were seen to be inconsistent, we assigned this to a non-eclipsed structure. If this was the case, supercells of the crystallites were generated and different stackings (AB, ABC, partial AB, etc. were attempted). The intensity profile which matched most closely was used to refine. In the COFs reported here, eclipsed structures were found to be most consistent with the diffraction patterns obtained here. Prior to refinement of functionalized TAPB-PDA-R COFs, the functionalized R component was assigned to have occupancy at both the 2,5 and 2′,5′ position of the phenyl ring it is attached to, so as to account for its prochirality. The observed diffraction patterns were subjected to a polynomial background subtraction and then to Pawley refinement wherein peak profile were refined using the Pseudo-Voigt peak shape function and asymmetry was corrected using the Berar-Baldinozzi function. Crystallite size was then estimated by the LeBail method which was Pawley refined to the experimental data.

Fourier-Transfer Infrared Spectroscopy (FT-IR). Infrared spectra were collected on a Nicolet iS10 FT-IR spectrometer equipped with a ZnSe crystal in attenuated total reflection mode. Spectra were background subtracted to remove contribution from atmospheric species. Spectra as shown were not corrected or calibrated to any IR feature.

Diffuse Reflectance for Infrared Fourier Transform Spectroscopy (DRIFTS). DRIFTS experiments were conducted on a Thermo-fisher 6700 infrared spectrometer with a Harrick Praying Mantis attachment. Powder samples were loaded into the attachment with a KBr carrier to reduce the optical density of the COF powders. These samples were then heated at $5^{\circ}C \bullet min^{-1}$ under a constant argon flow with constant monitoring of their infrared spectra.

Thermal Gravimetric Analysis (TGA). Thermogravimetric analysis (TGA) was performed on a Netzch Simultaneous Thermal Analysis (STA) system using approximately 5 mg of sample. The samples were heated to a designated temperature at a rate of $10°C \bullet min^{-1}$ under a helium atmosphere.

Nitrogen Sorption Measurements. Gas sorption isotherms were conducted on a Micromeritics ASAP 2420 Accelerated Surface Area and Porosity Analyzer. Typically, 20-40 mg samples were transferred to dried and tared analysis tubes and capped with a Transeal. The samples were heated to 40°C at a rate of $1°C \bullet min^{-1}$ and evacuated at 40°C for 20 min, then heated to 100°C at a rate of $1°C \bullet min^{-1}$ heat, and evacuated at 100°C until the outgas rate was ≤ 0.4 $\mu mHg \bullet min^{-1}$, at which point the tube was weighed again to determine the mass of the activated sample. The tube was then transferred to the analysis port of the instrument. UHP-grade (99.999% purity) N_2 was used for all adsorption measurements. N_2 isotherms were generated by incremental exposure to nitrogen up to 760 mmHg (1 atm) in a liquid nitrogen (77 K) bath. Oil-free vacuum pumps and oil-free pressure regulators were used for all measurements. Brunauer-Emmett-Teller (BET) surface areas were calculated from the linear region of the N_2 isotherm at 77 K within the pressure range P/P_0 of 0.05-0.10.

Density Functional Theory (DFT) Calculations. First-principles density functional theory (DFT) calculations were performed using the periodic *ab initio* code CRYSTAL17.[1] The PBE exchange-correlation functional was used with a semi-classical dispersion correction (PBE-D3) to better account for the noncovalent interactions present in the 2D COF structures.[2-3] The dispersion correction included a pairwise and three-body Becke-Johnson (BJ) damping-function.[3] Each of the DFT calculations was performed with all-electron atom-centered Gaussian-type basis sets of triple-zeta quality, similar to our previous work.[4-6]

The all-electron basis sets contained a total of 1,848 and 2,232 basis functions, corresponding to 522 and 618 electrons spread over 972 and 1,188 shells per unit cell for TAPB-PDA and TAPB-PDA-Et respectively. The lattice parameters and atomic coordinates were optimized using a quasi-Newtonian algorithm[7-11] while initially maintaining the space group symmetry (*P6*) and then reducing the symmetry (*P1*) after scanning the resultant vibrational modes. The presence of imaginary modes when performing the DFT vibrational frequency calculations with *P6* symmetry would indicate that the crystallographic space group symmetry for TAPB-PDA and TAPB-PDA-

Et may be reduced from the idealized *P6* space group, primarily when negating thermal effects. However, the size of the basis sets and number of radial and angular points defined for the integration grid have been reported to have an impact on the imaginary nature of the soft modes, and an in-depth analysis is out with the scope of the current work. Therefore, to obtain structural insight into the deformed structures, we analyzed the geometrical changes along the trajectory of the phonon modes, and allowing for the associated symmetry reduction relaxed the resultant geometries.

The infrared (IR) absorption spectra of TAPB-PDA and TAPB PDA-Et are reported in Figure S105. The IR intensities were computed through the Berry Phase approach, by evaluating the Born atomic tensors as polarization differences between the original and the distorted geometries.[12] In the range of 650–3500 cm^{-1}, the spectral features did not change significantly in either position or intensity and are in excellent agreement with experiment data. Therefore, the vibrational modes involved do not appear to be substantially affected by the change from the high symmetry planar phase to the deformed low symmetry phase.

B. Synthetic Procedures

Scheme S1. Synthesis of 2-(2-azido-ethoxy)-ethanol (**S1**).

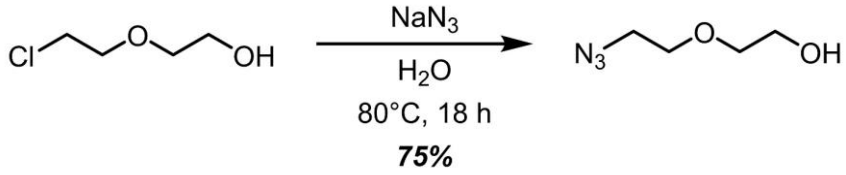

Synthesis of 2-(2-azido-ethoxy)-ethanol.

2-(2-azido-ethoxy)-ethanol was synthesized *via* slight modifications of literature procedures. All spectroscopic data is consistent with what has previously been reported.[13-14]

To a 500 mL flame-dried round bottom flask, a solution of 2-(2-chloro-ethoxy)-ethanol (35.4 g, 284 mmol) in deionized H_2O (180 mL) and NaN_3 (46.2 g, 710 mmol, 2.5 equiv) were added. The reaction mixture was stirred at 80°C under a nitrogen atmosphere for 18 h then poured into a NaOH solution (5% (*w/v*), 300 mL) and extracted with diethyl ether (5 × 300 mL). The organic layer was dried over $MgSO_4$ and evaporated to dryness to afford **S1** (27.7 g, 75%) as a colorless oil. All spectroscopic data is consistent with what has previously been reported.

Scheme S2. Synthesis of 2-(2-azido-ethoxy)-ethyl-4-methylbenzenesulfonate (**S2**).

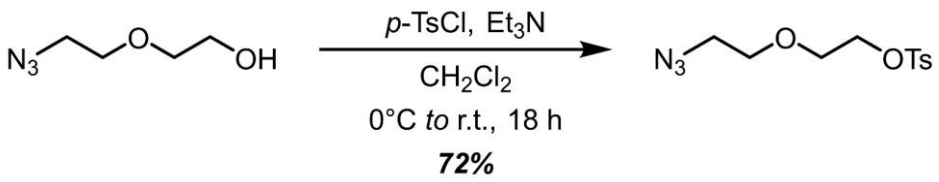

Synthesis of 2-(2-azido-ethoxy)-ethyl-4-methylbenzenesulfonate.

Synthesis of 2-(2-azido-ethoxy)-ethyl-4-methylbenzenesulfonate was prepared *via* slight modifications of literature procedures. All spectroscopic data is consistent with what has previously been reported. [13-14]

To a 1000 mL flame-dried round bottom flask, a solution of 2-(2-azido-ethoxy)-ethanol (**S1**, 20.0 g, 153 mmol) in dry CH_2Cl_2 (600 mL) and Et_3N (27 mL, 184 mmol, 1.5 equiv) were added. The reaction mixture was cooled to 0 ˚C and *p*-TsCl (34.8 g, 184 mmol, 1.2 equiv) was added. The solution was stirred at 0°C for 1 h, allowed to warm to room temperature and stirred for another 17 h under a nitrogen atmosphere. The solution was washed with $NaHCO_3$ (3 × 800 mL), H_2O (3 x 800 mL), and brine (3 × 800 mL), dried over $MgSO_4$, and evaporated to dryness to afford **S2** (31.3 g, 72%) as a colorless oil. All spectroscopic data is consistent with what has previously been reported.

Scheme S3. Synthesis of 2,5-hydroxy-1,4-dibenzaldehyde **(S3)**.

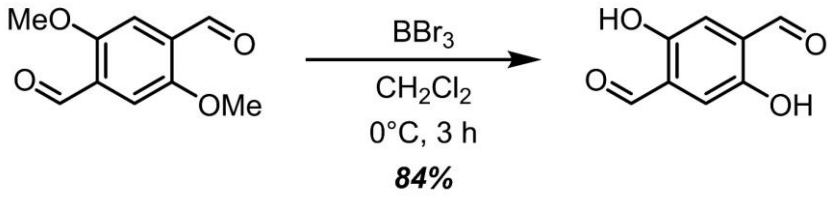

Synthesis of 2,5-hydroxy-1,4-dibenzaldehyde.

Synthesis of 2,5-hydroxy-1,4-dibenzaldehyde was prepared *via* slight modifications of literature procedures. All spectroscopic data is consistent with what has previously been reported.[14-15]

To a flame-dried 250 mL round bottom flask, a solution of 2,5-dimethoxy-1,4-dibenzaldehyde (3.0 g, 15 mmol) in dry CH_2Cl_2 (100 mL) was added. The reaction mixture was cooled to 0°C and BBr_3 (1.0 M in CH_2Cl_2, 42 mL) was added dropwise. The solution was stirred at 0°C for 3 h and diluted with H_2O (150 mL), and the organic layer was separated. The aqueous layer was extracted with hot EtOAc (3 × 120 mL) and the combined organic layer was dried over $MgSO_4$, filtered, and evaporated to dryness. Recrystallization from boiling EtOAc afforded **S3** (2.2 g, 84%) as orange crystals. All spectroscopic data is consistent with what has previously been reported.

Scheme S4. Synthesis of Azide Modified Terephthalaldehyde (**S4**).

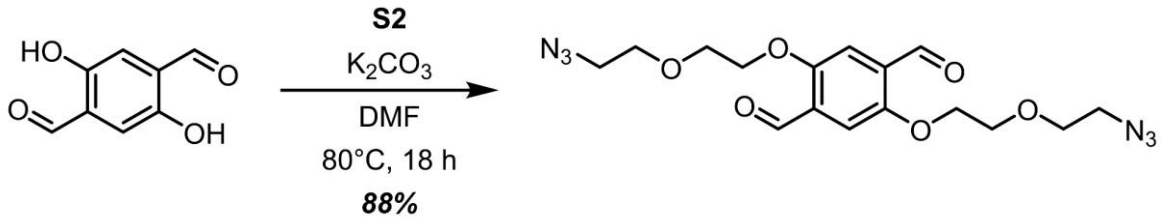

Synthesis of Azide Modified Terephthalaldehyde.

The azide modified terephthalaldehyde was prepared *via* a reported procedure.[14]

To a flame-dried 1000 mL round bottom flask, a solution of 2,5-hydroxy-1,4-dibenzaldehyde (S3, 4.0 g, 24 mmol) and 2-(2-azido-ethoxy)-ethyl-4-methylbenzenesulfonate (S2, 16.4 g, 57 mmol, 2.4 equiv) in dry DMF (400 mL) was added, followed by K_2CO_3 (26.0 g, 193 mmol). The reaction mixture was stirred at 80°C for 18 h, diluted with water (1000 mL), and extracted with hot EtOAc (5 × 600 mL). The combined organic layer was dried over MgSO4, filtered, and evaporated to dryness. Silica gel column chromatography (SiO_2, Hex/EtOAc = 3/2) afforded **S4** (8.2 g, 88%) as yellow crystals.

^{1}H NMR (500 MHz, $CDCl_3$) δ 10.51 (s, 2H), 7.46 (s, 2H), 4.28-4.26 (m, 4H), 3.90-3.88 (m, 4H), 3.73-3.71 (t, *J* = 4.9 Hz, 4H), 3.40-3.38 (t, *J* = 5.0Hz, 4H) ppm.

^{13}C NMR (126 MHz, $CHCl_3$) δ 189.11, 155.10, 129.48, 112.17, 70.34, 69.45, 68.76, 50.65 ppm.

HRMS calculated for $[C_{16}H_{20}NaN_6O_6Na]^+$ 415.1337, found: 415.1348.

Scheme S5. Synthesis of 2,5-dibromoterephthalaldehyde (**S5**).

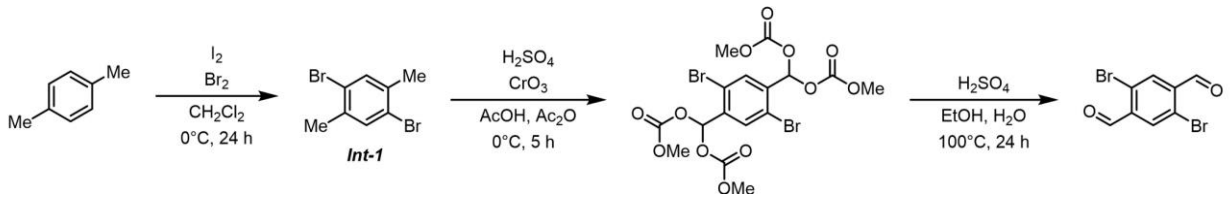

Synthesis of 2,5-dibromoterephthalaldehyde.

2,5-dibromoterephthalaldehyde was prepared *via* the reported synthesis described below. All spectroscopic data is consistent with what has previously been reported.[16]

Bromine (2.05 equiv) was added dropwise over the course of 30 min to an ice-cold solution of *p*-xylene (1.00 equiv) and iodine (0.008 equiv). Caution was taken to exclude light from the reaction mixture during this process. After stirring for 24 h at room temperature, 20% KOH was added to the solution and the reaction was allowed to equilibrate back to room temperature. The aqueous solution was decanted, and the remaining residue was recrystallized from EtOH (3×) to yield ***Int-1***.

To a suspension of ***Int-1*** (8.0 g) in AcOH (40 mL) and Ac_2O (80 mL) was added H_2SO_4 (28 mL) at 0°C. CrO_3 (12 g) was then added to the reaction mixture in portions. After complete addition of CrO_3 the resulting mixture was vigorously stirred at 0°C for 5 h. The green slurry was then poured into ice water and filtered. The collected white solid (diacetate) was washed with water and cold MeOH.

The diacetate was then hydrolyzed by refluxing with a mixture of water (40 mL), EtOH (40 mL), and sulfuric acid (4 mL) for 5 h. After the mixture had cooled, the pale-yellow solid was isolated *via* filtration. This crude product was purified *via* recrystallization from chloroform to yield pure **S5**.

Scheme S6. Synthesis of 2,5-dimethylterephthalaldehyde (**S6**).

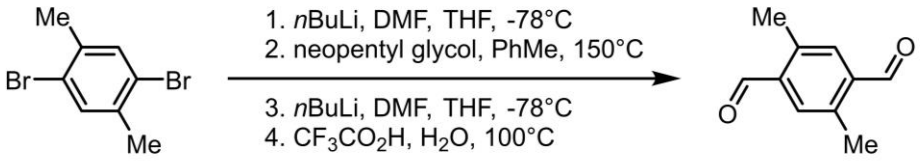

Synthesis of 2,5-dimethylterephthalaldehyde.

2,5-dimethylterephthalaldehyde was prepared *via* a reported literature procedure.[17] All spectroscopic data is consistent with what has previously been reported.[17-18]

In a Schlenk flask, 1,4-dibromo-2,5-dimethylbenzene (A, 18.00 g, 68.19 mmol) was dissolved in dry THF (200 mL) under N_2 and cooled to -78°C. *n*BuLi (2.5 M in hexanes, 30 mL, 75.0 mmol) was added dropwise via cannula. The mixture was allowed to stir at -78°C for 15 min before dry DMF (11 mL) was added. The reaction was allowed to warm to rt while stirring for 2 h, after which it was charged with concentrated HCl. The mixture was extracted with Et_2O two times, and the combined organic layers were washed with brine, dried over MgSO4, and concentrated under reduced pressure. The residue was used without further purification and was refluxed overnight in a Dean-Stark apparatus with toluene (130 mL), neopentyl glycol (14.2 g), and *p*-TsOH (2.42 g). The mixture was washed with a saturated $NaHCO_3$ solution, water, brine, and dried over $MgSO_4$ before concentration under reduced pressure. The residue was treated a second time as described above with the same amounts of *n*BuLi and DMF under the same conditions (the protection using neopentyl glycol was not repeated). After isolation, the product was refluxed in water (16 mL) and TFA (120 mL) for 15 min. The mixture was concentrated under reduced pressure and charged with CH_2Cl_2. It was then washed with saturated $NaHCO_3$ solution, brined, dried over $MgSO_4$, and concentrated under reduced pressure. The resulting liquid (which was a saturated solution of PDA-Me in residual DMF) was placed in a freezer overnight. The resulting **S6** precipitate was isolated *via* filtration and washed with hexanes. Isolated yield of **S6**: 3.34 g (30.2%).

^{1}H NMR (500 MHz, $CDCl_3$) δ 10.33 (s, 2H), 7.69 (s, 2H), 2.69 (s, 6H) ppm.

^{13}C NMR (125 MHz, $CDCl_3$) δ 192.34, 138.30, 137.06, 134.84, 18.95 ppm.

Scheme S7. Synthesis of 2,5-ethylterephthalaldehyde (**S7**).

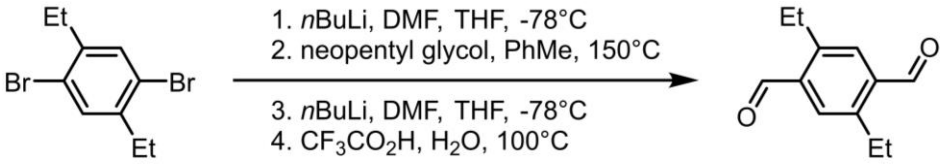

Synthesis of 2,5-ethylterephthalaldehyde.

2,5-diethylterephthalaldehyde was prepared *via* a reported literature procedure.[17]All spectroscopic data is consistent with what has previously been reported.[17]

In a Schlenk flask, 1,4-dibromo-2,5-diethylbenzene (10.00 g, 34.2 mmol) was dissolved in dry THF (100 mL) under N_2 and cooled to -78°C. *n*BuLi (2.5 M in hexanes, 15 mL, 37.5 mmol) was added dropwise via cannula. The mixture was allowed to stir at -78°C for 15 min before dry DMF (6 mL) was added. The reaction was allowed to warm to rt while stirring for 2 h, after which it was charged with concentrated HCl. The mixture was extracted with Et_2O two times, and the combined organic layers were washed with brine, dried over MgSO4, and concentrated under reduced pressure. The residue was used without further purification and was refluxed overnight in a Dean-Stark apparatus with toluene (65 mL), neopentyl glycol (7.13 g), and *p*-TsOH (1.21 g). The mixture was washed with a saturated $NaHCO_3$ solution, water, brine, and dried over $MgSO_4$ before concentration under reduced pressure. The residue was treated a second time as described above with the same amounts of *n*BuLi and DMF under the same conditions (the protection using neopentyl glycol was not repeated). After isolation, the product was refluxed in water (8 mL) and TFA (65 mL) for 15 min. The mixture was concentrated under reduced pressure and charged with CH_2Cl_2. It was then washed with saturated $NaHCO_3$ solution, brined, dried over $MgSO_4$, and concentrated under reduced pressure. The resulting liquid (which was a saturated solution of PDA-Et in residual DMF) was placed in a freezer overnight. The resulting **S7** precipitate was isolated *via* filtration and washed with hexanes. Isolated yield of **S7**: 1.98 g (30.4%).

^{1}H NMR (500 MHz, $CDCl_3$) δ 10.36 (s, 2H), 7.75 (s, 2H), 3.10 (q, 4H), 1.30 (t, 6H) ppm.

^{13}C NMR (125 MHz, $CDCl_3$) δ 191.12, 144.73, 136.87, 132.93, 25.19, 16.35 ppm.

Scheme S8. Synthesis of 2,5-bis(methylthio)terephthaldehyde (**S8**).

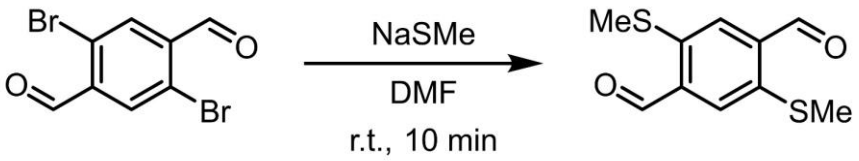

Synthesis of 2,5-bis(methylthio)terephthaldehyde.

2,5-bis(methylthio)terephthaldehyde was prepared *via* a reported procedure. All spectroscopic data is consistent with what has previously been reported.[19]

To a solution of 2,5-dibromoterephthalaldehyde (synthesis previously described) (1.00 equiv) in DMF was added sodium methanethiolate (2.35 equiv), and the resulting mixture was stirred at room temperature for 10 min. The mixture was poured into diluted HCl (*c.a.* 1 M), and extracted into $CHCl_3$ (3×). The combined organic layers were washed with water and brine, dried over $MgSO_4$, and concentrated *in vacuo*. The crude solid was then purified *via* column chromatography (SiO_2, CH_2Cl_2) to yield **S8** as a pale orange solid. All spectroscopic data is consistent with what has previously been reported.

Scheme S9. Synthesis of benzophenoneimine of benzidine (BND) (**S9**).

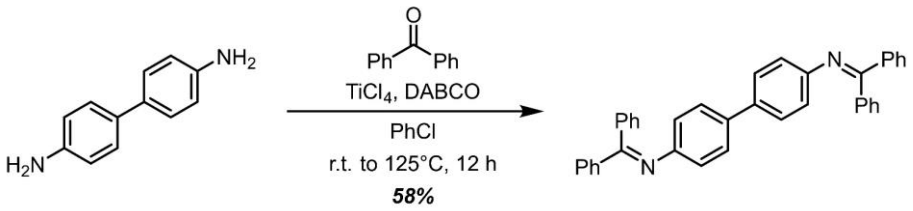

Synthesis of the benzophenoneimine of benzidine.

The benzophenoneimine of benzidine was prepared *via* a reported procedure. All spectroscopic data is consistent with what has previously been reported.[20]

To a 500mL flame-dried round-bottom flask, benzidine (1.70 g, 9.25 mmol), benzophenone (3.37 g, 18.50 mmol, 1.0 equiv per NH2 funcionality), 1,4- diazobicyclo[2.2.2]octane (DABCO) (6.23 g, 55.50 mmol, 6.0 equiv), and PhCl (100 mL) were added and the contents were stirred at room temperature under a nitrogen atmosphere. Titanium(IV) chloride (1.52 mL, 13.88 mmol, 1.5 equiv) was syringed in portions over 15 min (1/4 of the portion at times 0 min, 5 min, 10 min, and 15 min). After the addition was complete, the reaction mixture was stirred for another 20 min at room temperature, then the flask was equipped with a reflux condenser, and the reaction stirred at 125°C overnight (12 h). The reaction mixture was then cooled to about 40°C, and filtered while warm through a Buchner funnel equipped with a filter paper. The filtrate was then concentrated in vacuo, and the crude product (3.89 g) was purified by stirring in a mixture of hot EtOH and $CHCl_3$ (3:1, 400 mL), preforming a hot filtration through a cotton-plugged plastic funnel, and allowing the filtrate to slowly cool to room temperature, at which point the product started to crystallize. The flask was then put in the fridge overnight to induce further crystallization. The solid was then collected via filtration to yield **S9** (2.74 g, 58%) as a yellow/orange solid.

^{1}H NMR (500 MHz, $CDCl_3$) δ 7.76 – 7.70 (m, 4H), 7.47 – 7.41 (m, 2H), 7.38 (dd, J = 8.3, 6.7 Hz, 4H), 7.33 – 7.29 (m, 4H), 7.28 – 7.20 (m, 6H), 7.15 – 7.08 (m, 4H), 6.78 – 6.68 (m, 4H) ppm.

^{13}C NMR (126 MHz, $CDCl_3$) δ 168.11, 150.02, 139.71, 136.25, 135.39, 130.66, 129.50, 129.30, 128.58, 128.16, 128.02, 127.97, 126.55, 121.45 ppm.

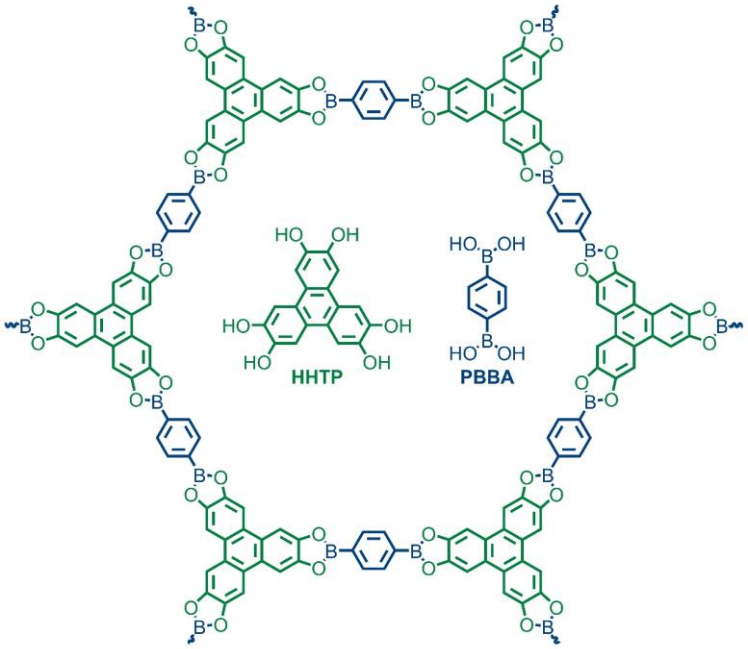

Figure S1. Structure of HHTP-PBBA COF and the monomers from which it is constructed.

Scheme S10. Synthesis of HHTP-PBBA COF (COF-5).

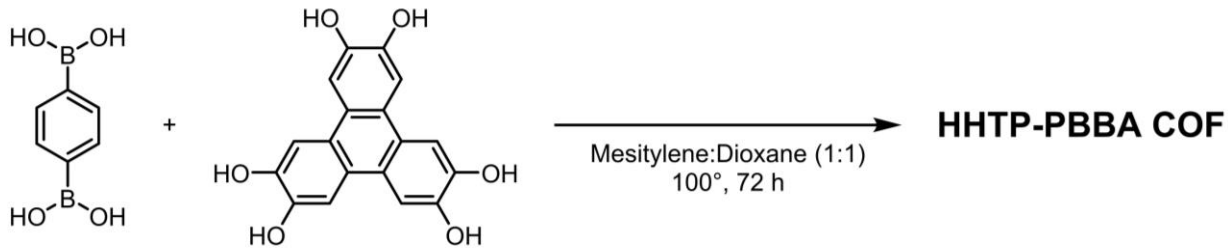

Synthesis of the HHTP-PBBA COF.

HHTP-PBBA COF was prepared *via* a slight modification of a reported literature procedure.[21]

A 20 mL scintillation vial was charged with 1,4-benzene-bisboronic acid (PBBA) (1.5 equiv), 2,3,6,7,10,11-hexahydroxytriphenylene (HHTP) (1.0 equiv), and a mesitylene:dioxane solution (1:1 *v*/*v*). The reaction mixture was heated at 100°C for 72 h to yield a free-flowing gray-purple powder. After 72 h, the reaction was cooled to room temperature and the resulting powder was isolated *via* filtration. The crude material was washed with copious amounts of anhydrous acetone before being dried again under high vacuum.

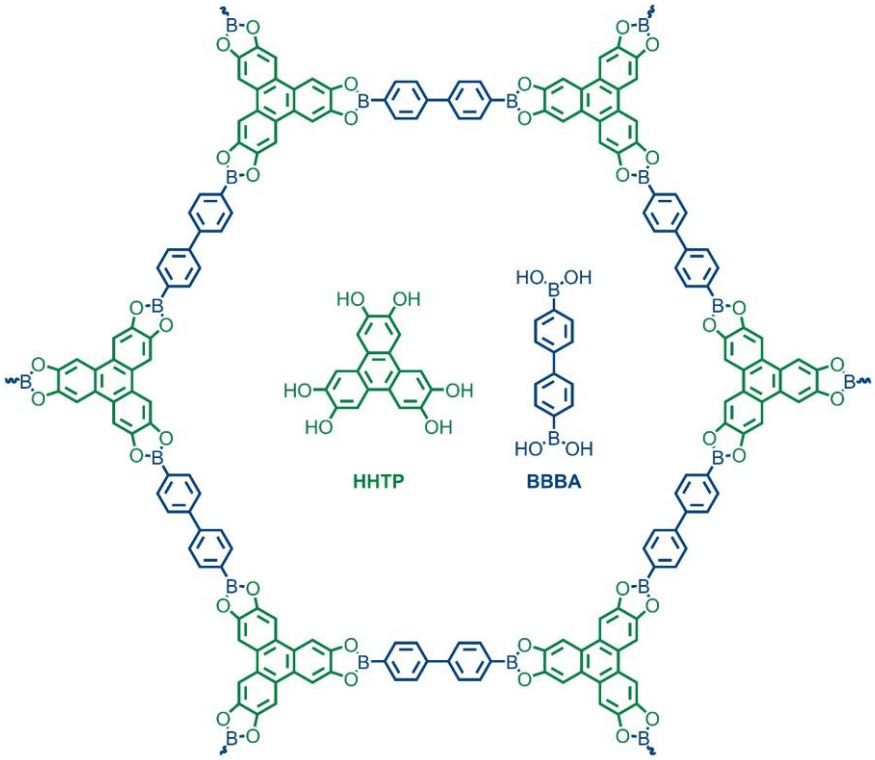

Figure S2. Structure of HHTP-BBBA COF and the monomers from which it is constructed.

Scheme S11. Synthesis of HHTP-BBBA COF (COF-10).

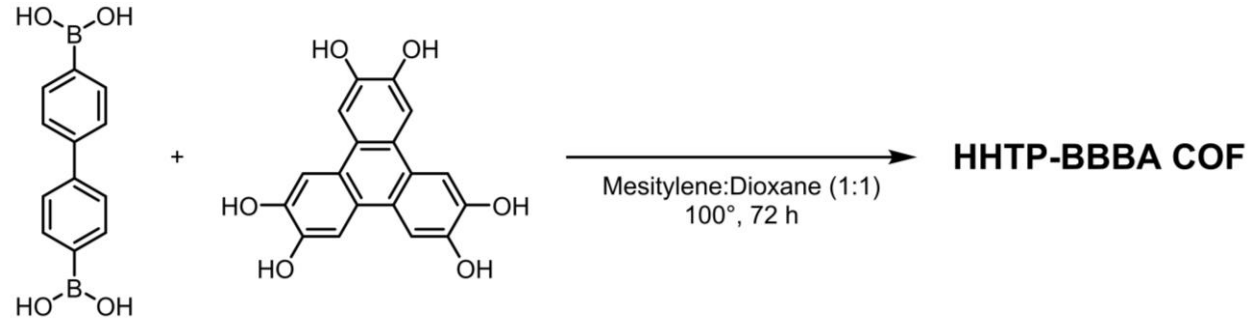

Synthesis of the HHTP-BBBA COF.

HHTP-BBBA COF was prepared *via* a slight modification of a reported literature procedure.[21]

A 20 mL scintillation vial was charged with 1,4-biphenyl-bisboronic acid (BBBA) (1.5 equiv), 2,3,6,7,10,11-hexahydroxytriphenylene (HHTP) (1.0 equiv), and a mesitylene:dioxane solution (1:1 *v*/*v*). The reaction mixture was heated at 100°C for 72 h to yield a free-flowing gray-purple powder. After 72 h, the reaction was cooled to room temperature and the resulting powder was isolated *via* filtration. The crude material was washed with copious amounts of anhydrous acetone before being dried again under high vacuum.

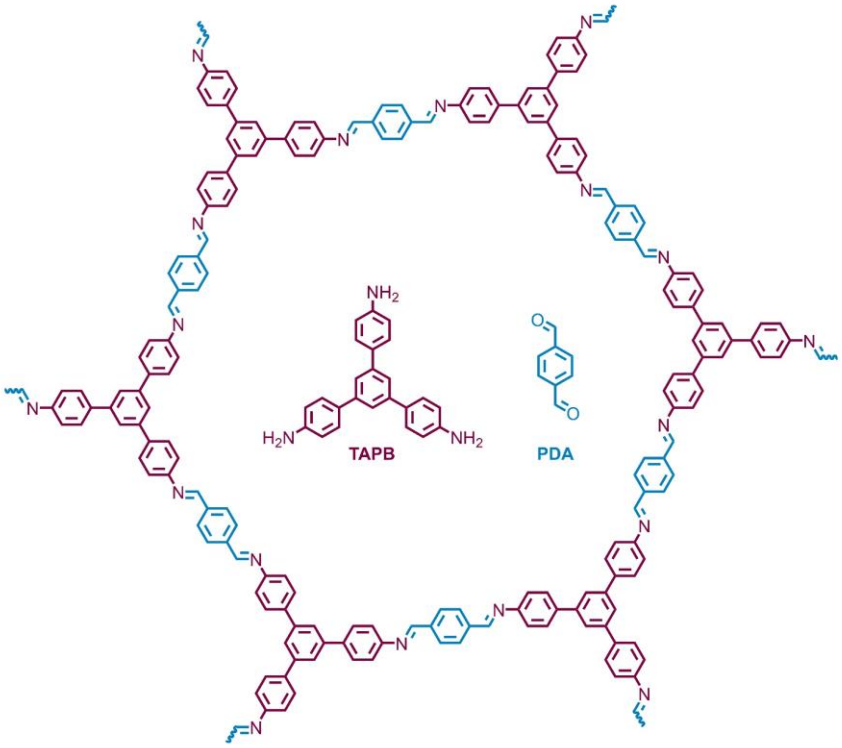

Figure S3. Structure of TAPB-PDA- COF and the monomers from which it is constructed.

Scheme S12. Synthesis of TAPB-PDA- COF.

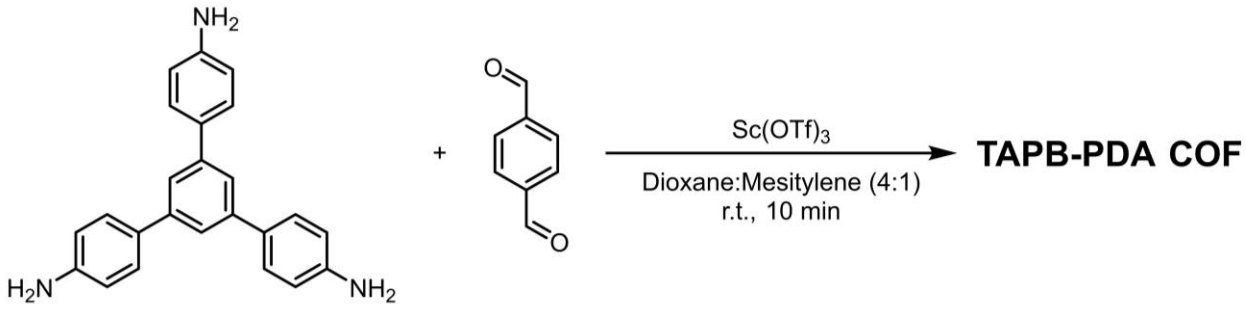

Synthesis of TAPB-PDA COF.

TAPB-PDA COF was prepared *via* a reported literature procedure.[17, 22-23]

A 20 mL scintillation vial was charged with 1,3,5-tris(4-aminophenyl)benzene (1.0 equiv), terephthalaldehyde (1.5 equiv). A 1,4-dioxane/mesitylene solution (4:1 v/v) was added, and the resulting suspension was sonicated at room temperature until the monomers were fully dissolved. Scandium(III) trifluoromethanesulfonate (0.018 equiv) was added, and the resulting suspension was sonicated briefly. The vial was closed with a plastic cap for 10 min. The reaction mixture was transferred to a container and while wet, precipitates were activated by Soxhlet extraction using CH_3OH for 12 h, followed by supercritical CO_2 drying.

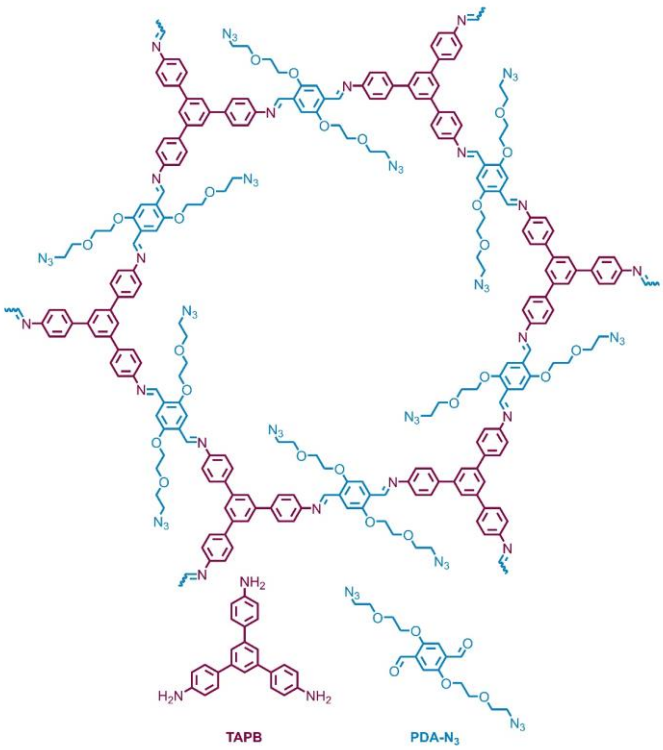

Figure S4. Structure of TAPB-PDA-N_3 COF and the monomers from which it is constructed.

Scheme S13. Synthesis of TAPB-PDA-N_3 COF.

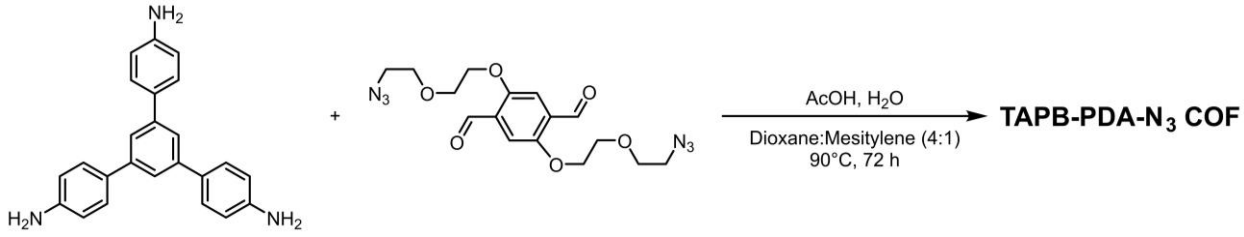

Synthesis of TAPB-PDA-N_3 COF.

TAPB-PDA-N_3 COF was prepared *via* a reported literature procedure.[14]

A 20 mL scintillation vial was charged with 1,3,5-tris(4-aminophenyl)benzene (105 mg, 0.3 mmol) and PDA-N_3 (0.45 mmol). A 1,4-dioxane/mesitylene solution (4:1 *v/v*) was added, and the resulting suspension was sonicated at room temperature until the monomers were fully dissolved. Glacial AcOH (3.6 mL) and H_2O (2.4 mL) were added, and the resulting solution was heated at 90°C for 72 h. The reaction mixture was transferred to a tea bag and washed with methanol in a Soxhlet extractor for 18 h. The material was then activated by supercritical CO_2 followed by drying under vacuum at room temperature for 5 h that afforded the TAPB-PDA-N_3 COF (200 mg, 75%) as a yellow solid.

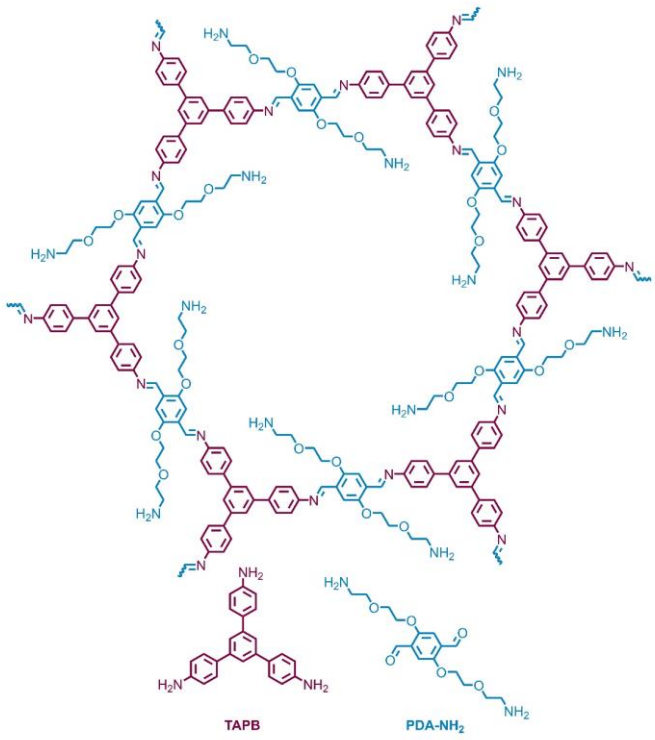

Figure S5. Structure of TAPB-PDA-NH_2 COF and the monomers from which it is constructed.

Scheme S14. Synthesis of TAPB-PDA-NH_2 COF.

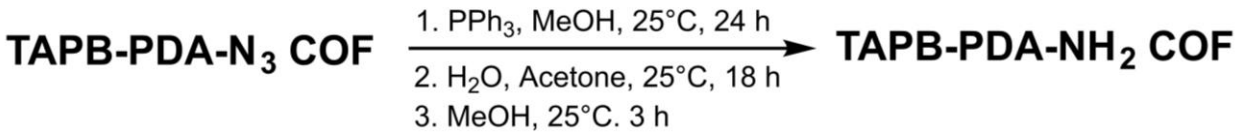

Synthesis of TAPB-PDA-NH_2 COF.

TAPB-PDA-NH_2 COF was prepared *via* a reported literature procedure.[14]

To a flame-dried 25 mL round bottom flask, a suspension of TAPB-PDA-N_3 COF (100 mg, 0.34 mmol by imine) in dry CH_3OH (10 mL) was added, followed by PPh_3 (1.3 g, 5.1 mmol, 15 equiv). After 24 h at 25°C, the suspension was filtered in a tea bag and immersed in 4% (*v/v*) H_2O in acetone for 18 h and in methanol for 3 h. The material was subjected to the supercritical CO_2 drying followed by the vacuum drying at room temperature for 5 h that afforded TAPB-PDA-NH_2 COF (89 mg, 97%) as a yellow solid.

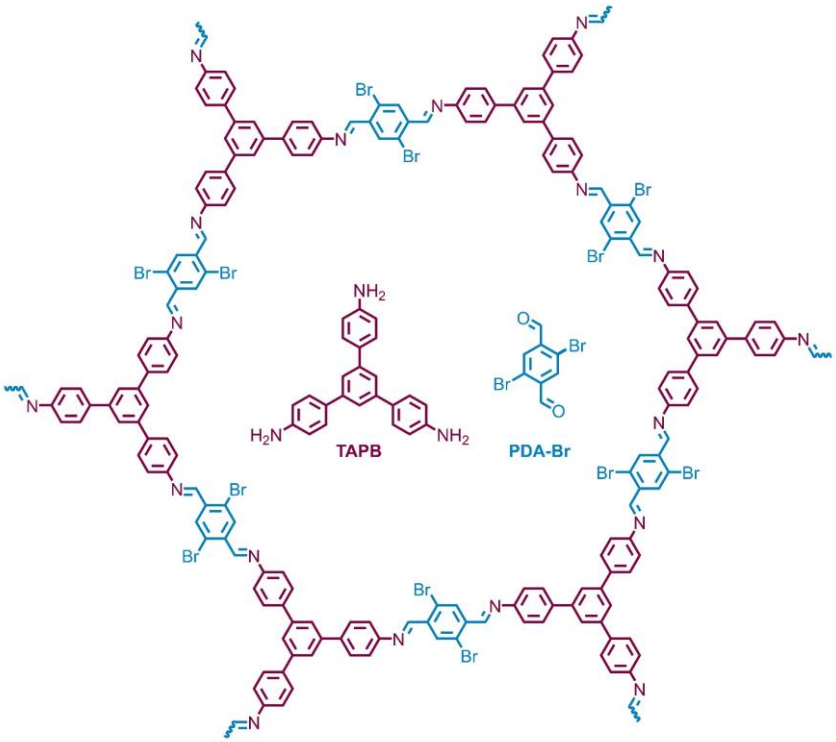

Figure S6. Structure of TAPB-PDA-Br COF and the monomers from which it is constructed.

Scheme S15. Synthesis of TAPB-PDA-Br COF.

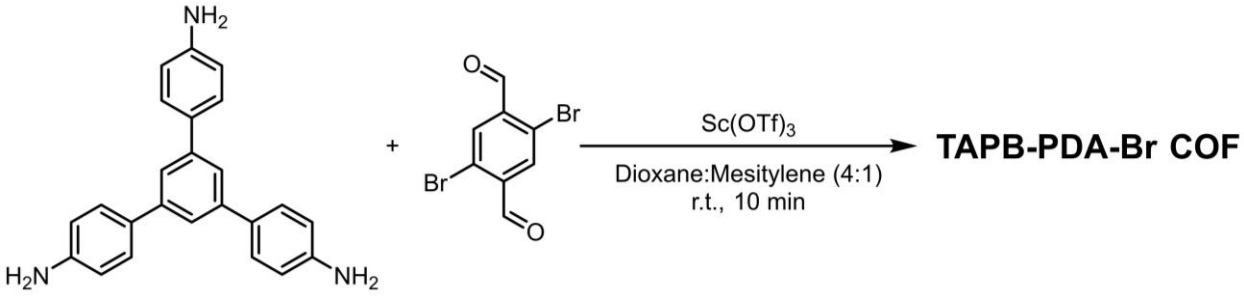

Synthesis of TAPB-PDA-Br COF.

TAPB-PDA-Br COF was prepared *via* a slight modification of a reported literature procedure.[22]

A 20 mL scintillation vial was charged with 1,3,5-tris(4-aminophenyl)benzene (1.0 equiv), 2,5-dibromoterephthalaldehyde (1.5 equiv). A 1,4-dioxane/mesitylene solution (4:1 v/v) was added, and the resulting suspension was sonicated at room temperature until the monomers were fully dissolved. Scandium(III) trifluoromethanesulfonate (0.018 equiv) was added, and the resulting suspension was sonicated briefly. The vial was closed with a plastic cap for 10 min. The reaction mixture was transferred to a container and while wet, precipitates were activated by Soxhlet extraction using CH_3OH for 12 h, followed by supercritical CO_2 drying.

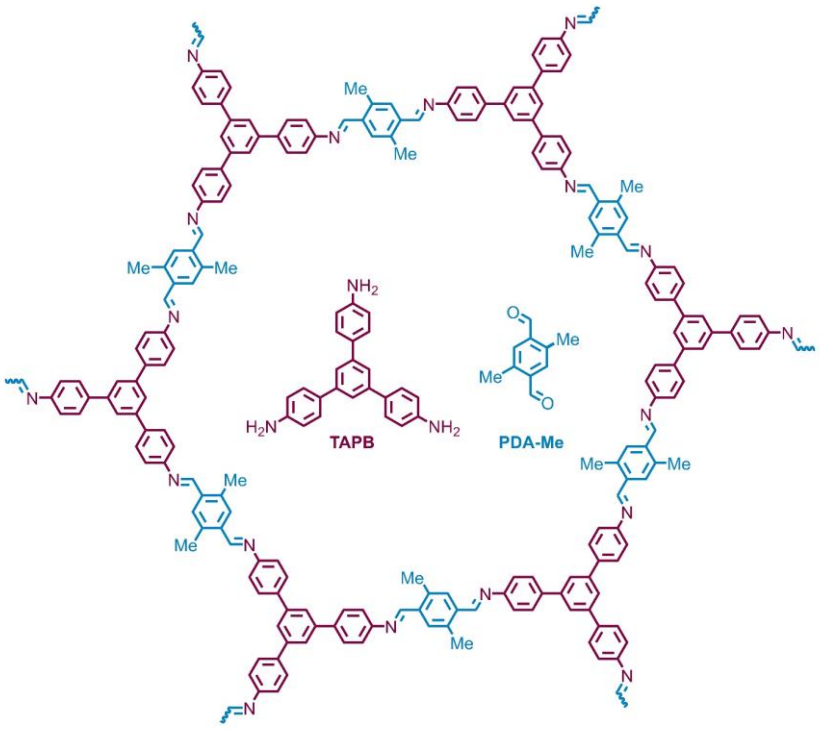

Figure S7. Structure of TAPB-PDA-Me COF and the monomers from which it is constructed.

Scheme S16. Synthesis of TAPB-PDA-Me COF.

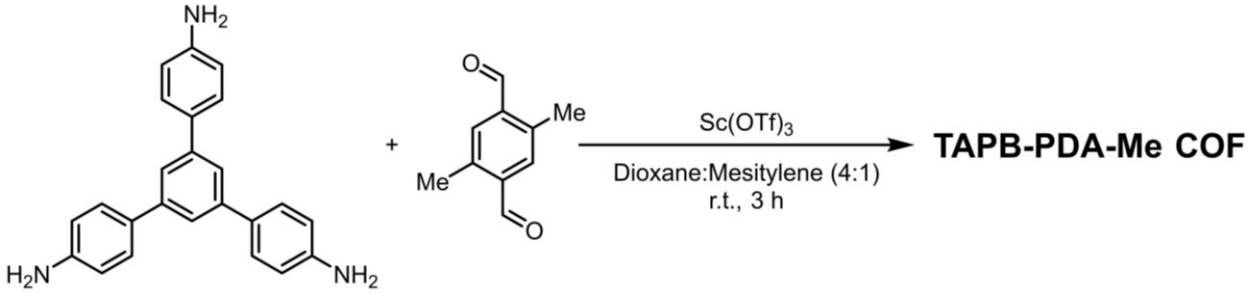

Synthesis of TAPB-PDA-Me COF.

TAPB-PDA-Me COF was prepared *via* a reported literature procedure.[17, 22]

A 20 mL scintillation vial was charged with 1,3,5-tris(4-aminophenyl)benzene (1.0 equiv), 2,5-bis(methylthio)terephthalaldehyde (1.5 equiv). A 1,4-dioxane/mesitylene solution (4:1 v/v) was added, and the resulting suspension was sonicated at room temperature until the monomers were fully dissolved. Scandium(III) trifluoromethanesulfonate (0.018 equiv) was added, and the resulting suspension was sonicated briefly. The vial was closed with a plastic cap for 3 h. The reaction mixture was transferred to a container and while wet, precipitates were activated by Soxhlet extraction using CH_3OH for 12 h, followed by supercritical CO_2 drying.

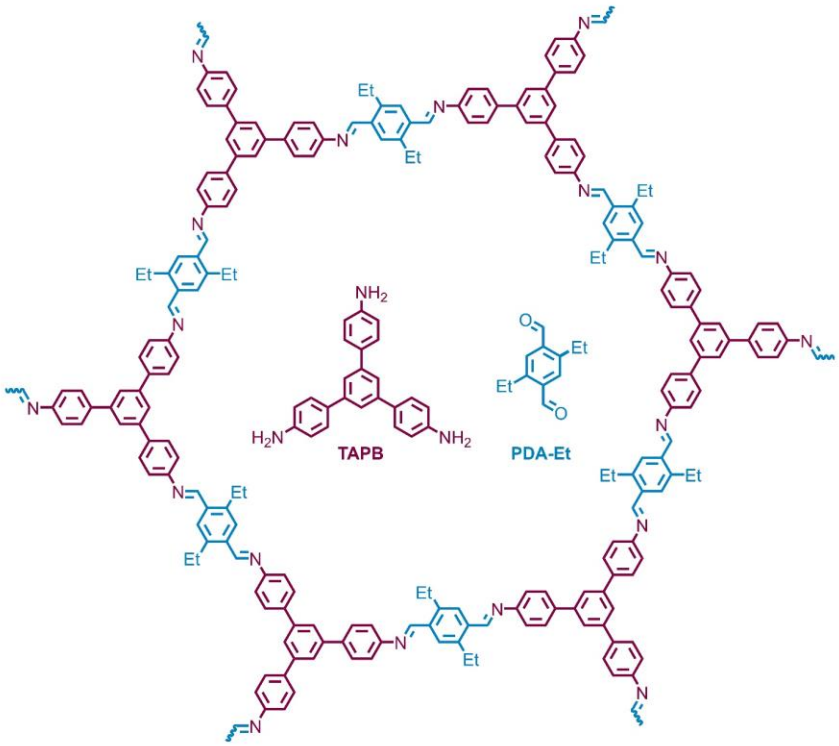

Figure S8. Structure of TAPB-PDA-Et COF and the monomers from which it is constructed.

Scheme S17. Synthesis of TAPB-PDA-Et COF.

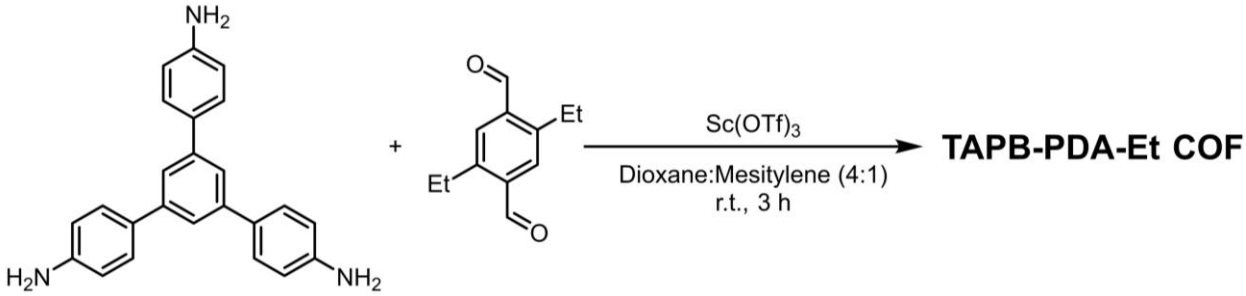

Synthesis of TAPB-PDA-Et COF.

TAPB-PDA-Et COF was prepared *via* a reported literature procedure.[17, 22]

A 20 mL scintillation vial was charged with 1,3,5-tris(4-aminophenyl)benzene (1.0 equiv), 2,5-bis(methylthio)terephthalaldehyde (1.5 equiv). A 1,4-dioxane/mesitylene solution (4:1 v/v) was added, and the resulting suspension was sonicated at room temperature until the monomers were fully dissolved. Scandium(III) trifluoromethanesulfonate (0.018 equiv) was added, and the resulting suspension was sonicated briefly. The vial was closed with a plastic cap for 3 h. The reaction mixture was transferred to a container and while wet, precipitates were activated by Soxhlet extraction using CH_3OH for 12 h, followed by supercritical CO_2 drying.

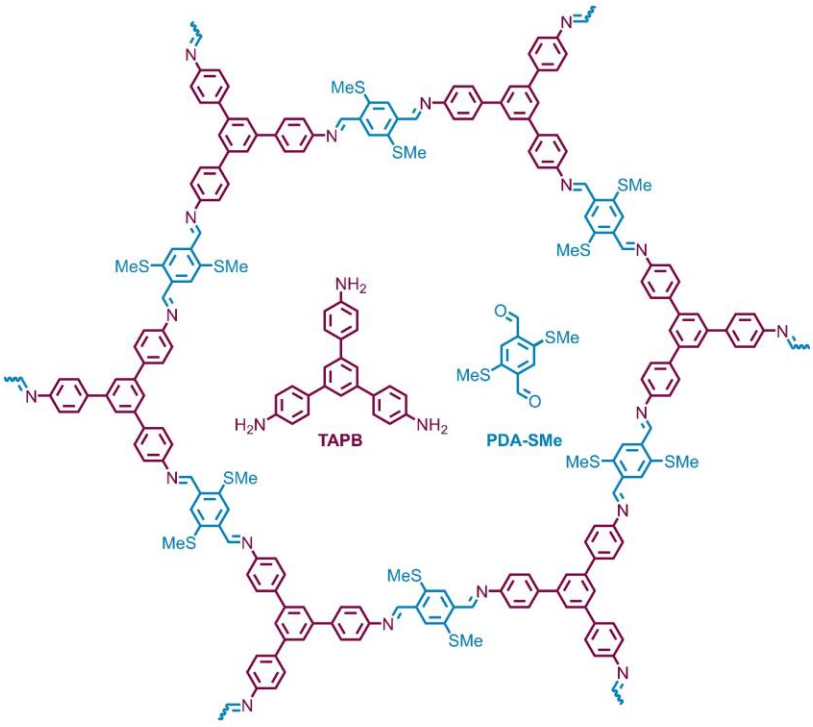

Figure S9. Structure of TAPB-PDA-SMe COF and the monomers from which it is constructed.

Scheme S18. Synthesis of TAPB-PDA-SMe COF.

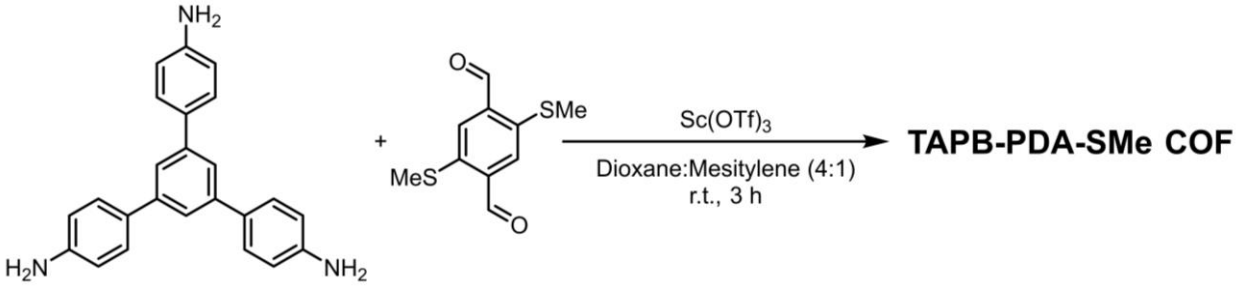

Synthesis of TAPB-PDA-SMe COF.

TAPB-PDA-SMe COF was prepared *via* a slight modification of a reported literature procedure.[17, 22]

A 20 mL scintillation vial was charged with 1,3,5-tris(4-aminophenyl)benzene (1.0 equiv), 2,5-bis(methylthio)terephthalaldehyde (1.5 equiv). A 1,4-dioxane/mesitylene solution (4:1 v/v) was added, and the resulting suspension was sonicated at room temperature until the monomers were fully dissolved. Scandium(III) trifluoromethanesulfonate (0.018 equiv) was added, and the resulting suspension was sonicated briefly. The vial was closed with a plastic cap for 3 h. The reaction mixture was transferred to a container and while wet, precipitates were activated by Soxhlet extraction using CH_3OH for 12 h, followed by supercritical CO_2 drying.

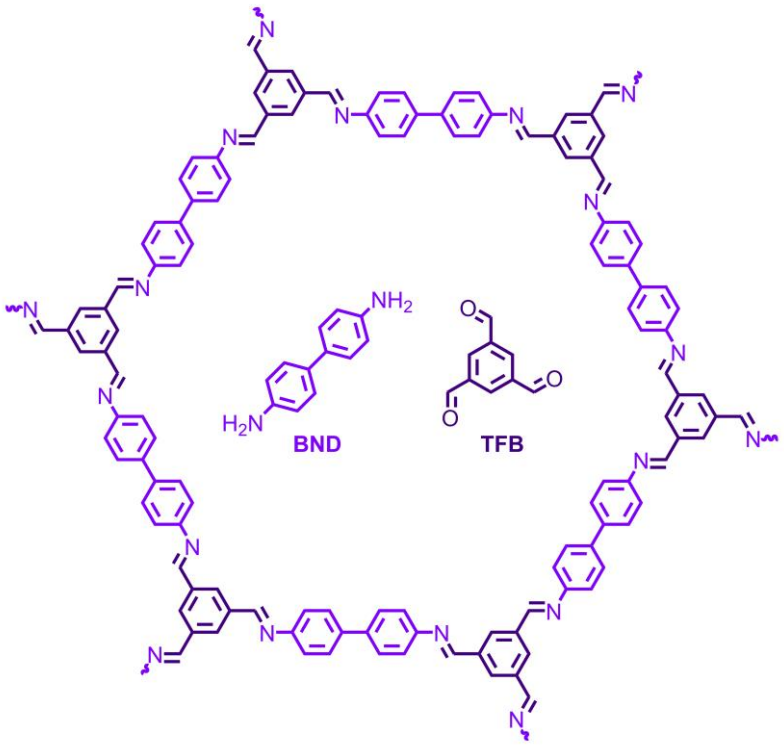

Figure S10. Structure of BND-TFB COF and the monomers from which it is constructed.

Scheme S19. Synthesis of BND-TFB COF.

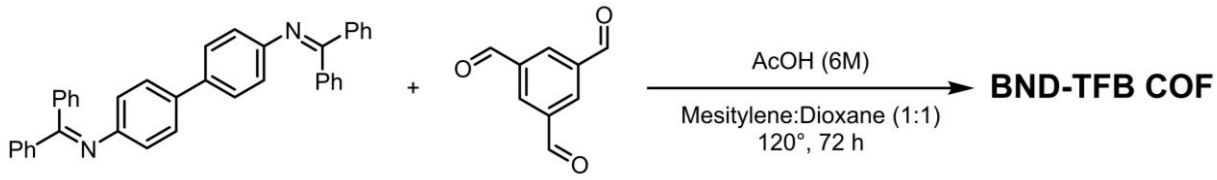

Synthesis of BND-TFB COF.

BND-TFB COF was prepared *via* a reported literature procedure.[20]

To a flame-dried 250 mL high-pressure flask with vacuum valve, 1,3,5-triformylbenzene (0.97 g, 6.0 mmol, 1.5 equiv) and benzidine-benzophenone (4.61 g, 9.0 mmol, 1.5 equiv) were added, followed by mesitylene:dioxane (1:1, 60.0 mL) along the walls of the flask (to push down any remaining solids remaining atop of the flask). The flask was sealed and sonicated at room temperature for 10 min, and then 6M acetic acid (10 mL) was added, and the flask was sealed again. The reaction mixture was then degassed through three freeze-pump-thaw cycles (vacuum <50 mTorr), after which the vacuum valve was switched to N_2, and the flask was charged with N_2 and sealed under positive N_2 pressure. The flask was then placed (no stirring) in a 120 °C pre-

heated oil bath for three days. The flask was removed from the oil bath, allowed to cool, and filtered through a Buchner funnel equipped with a filter paper. Acetone was used to ensure all of the material is filtered from the flask to the Buchner funnel. The solid was collected and stirred in an Erlenmeyer flask in hot DMF (600 mL at 90°C for 30min), and filtered while hot. This procedure was repeated two more times in DMF (600 mL at 90°C for 30min), once in absolute ethanol (600 mL at 80°C for 30min), and lastly once in acetone (600 mL at 60°C). The material was then filtered, collected, placed in a vacuum chamber, and dried at 120°C for 24 h under vacuum to give an orange solid (1.98 g, 86%).

C. Ambient X-Ray Diffraction

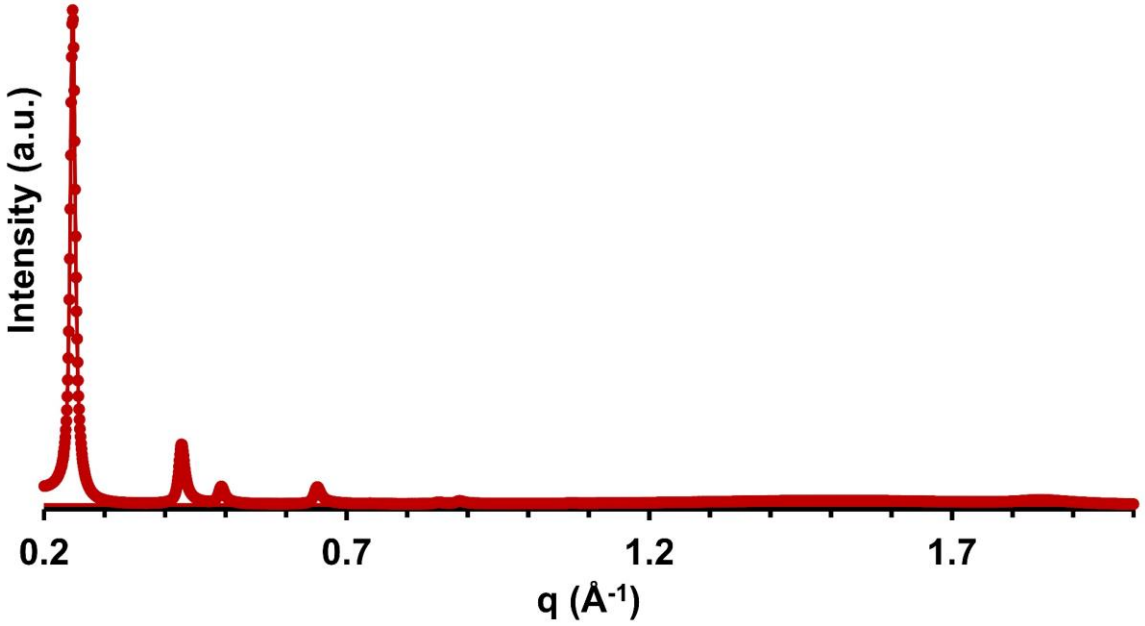

Figure S11. Ambient X-ray diffraction pattern of HHTP-PBBA COF.

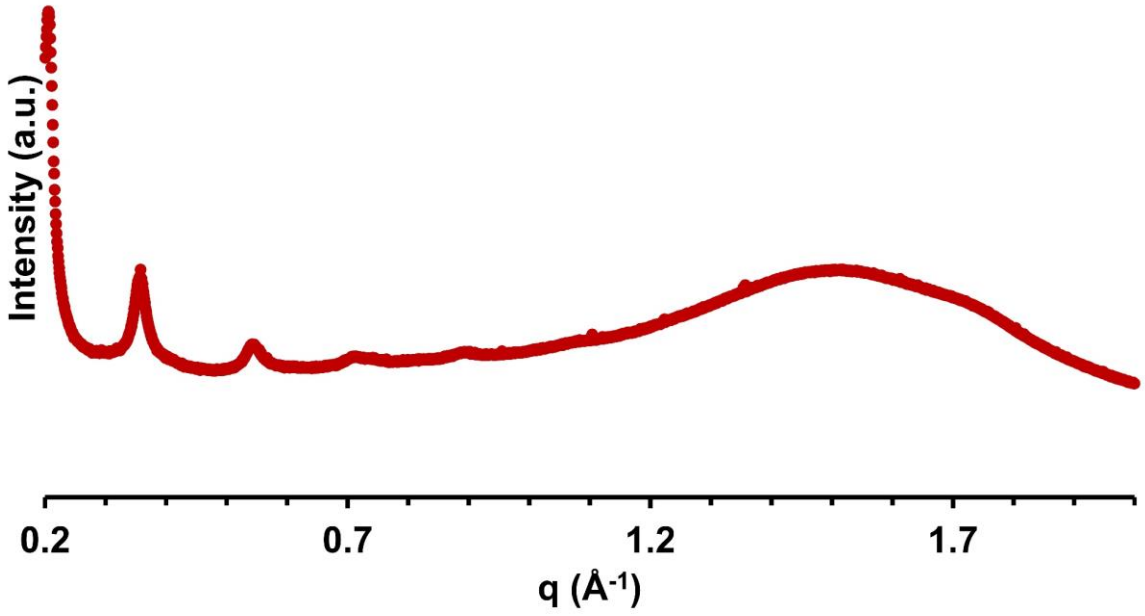

Figure S12. Ambient X-ray diffraction pattern of HHTP-BBBA COF.

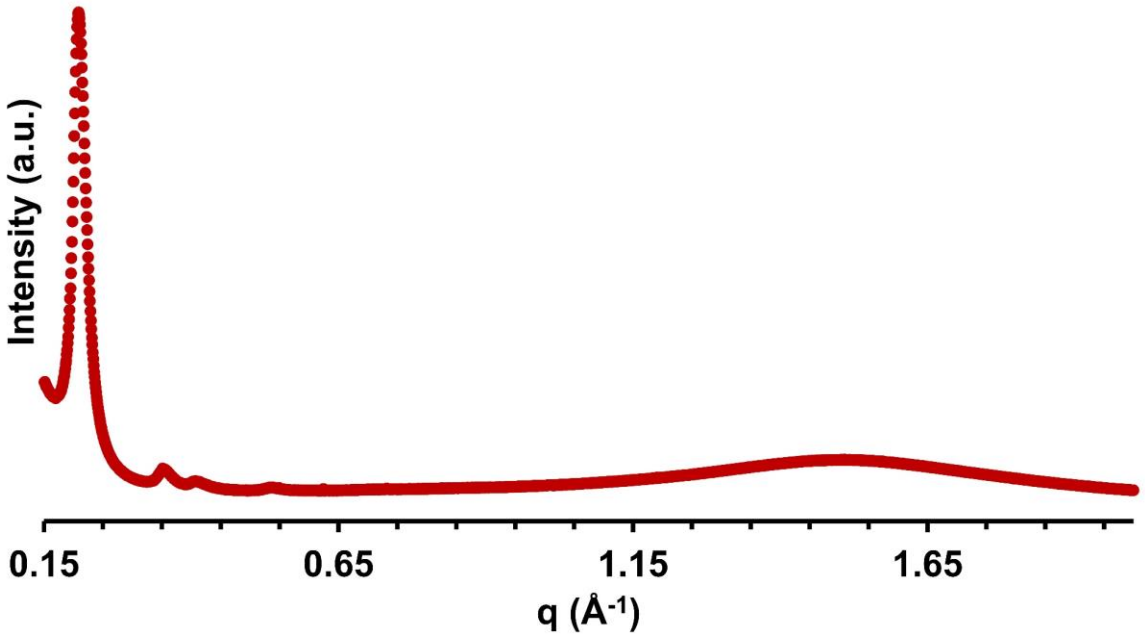

Figure S13. Ambient X-ray diffraction pattern of TAPB-PDA COF.

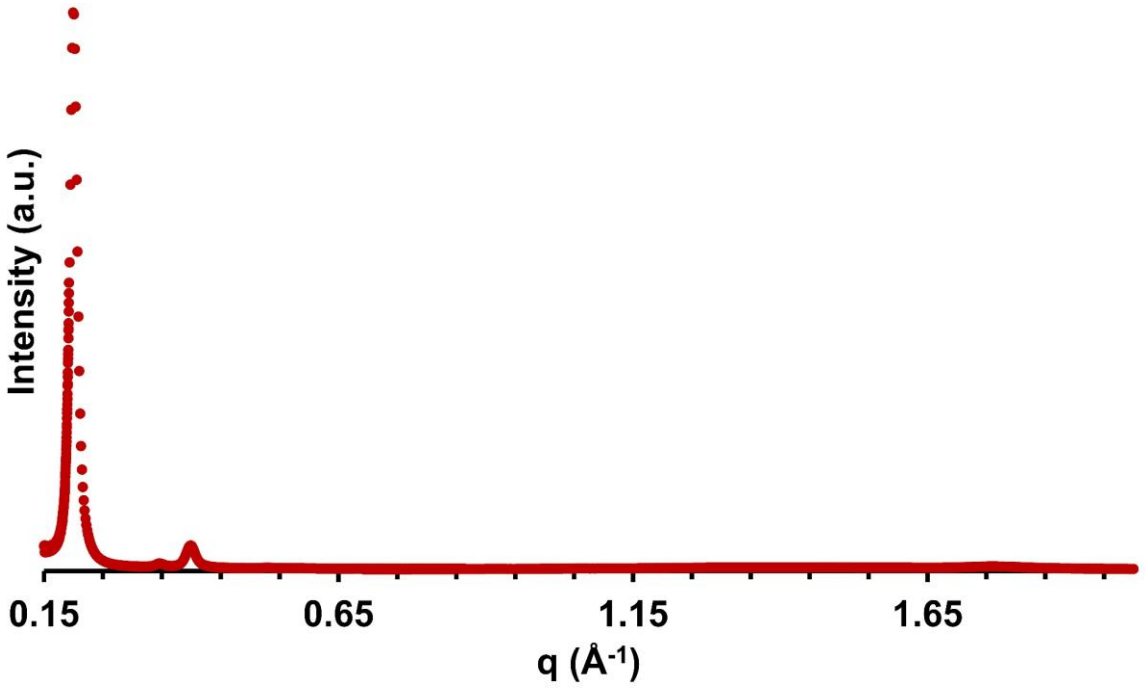

Figure S14. Ambient X-ray diffraction pattern of TAPB-PDA-N_3 COF.

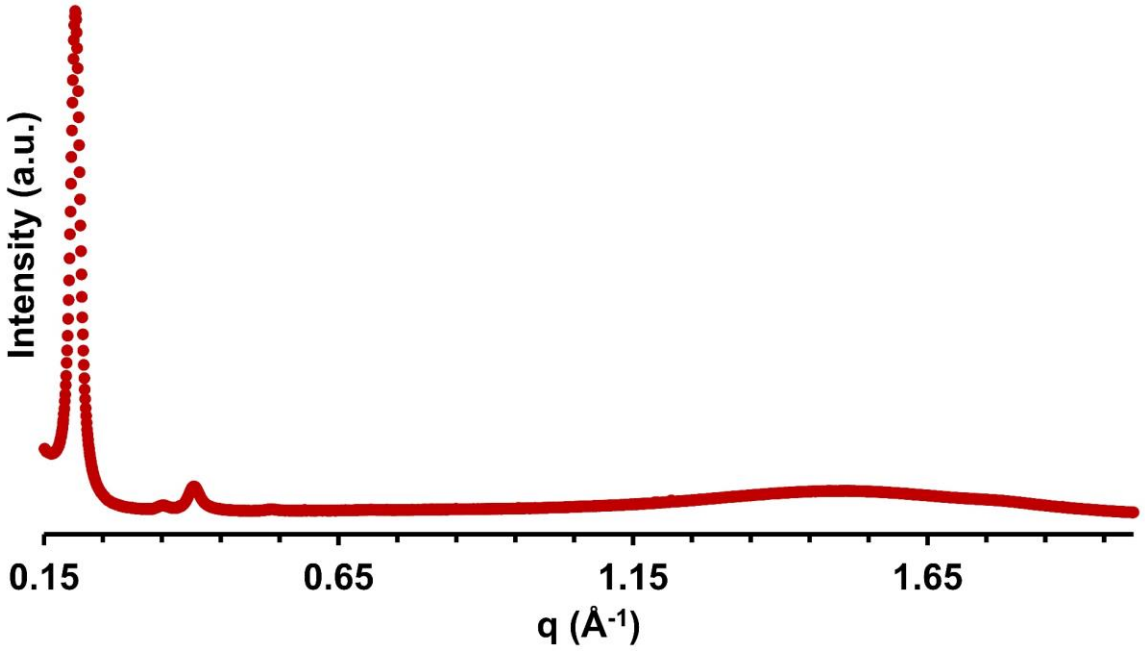

Figure S15. Ambient X-ray diffraction pattern of TAPB-PDA-NH_2 COF.

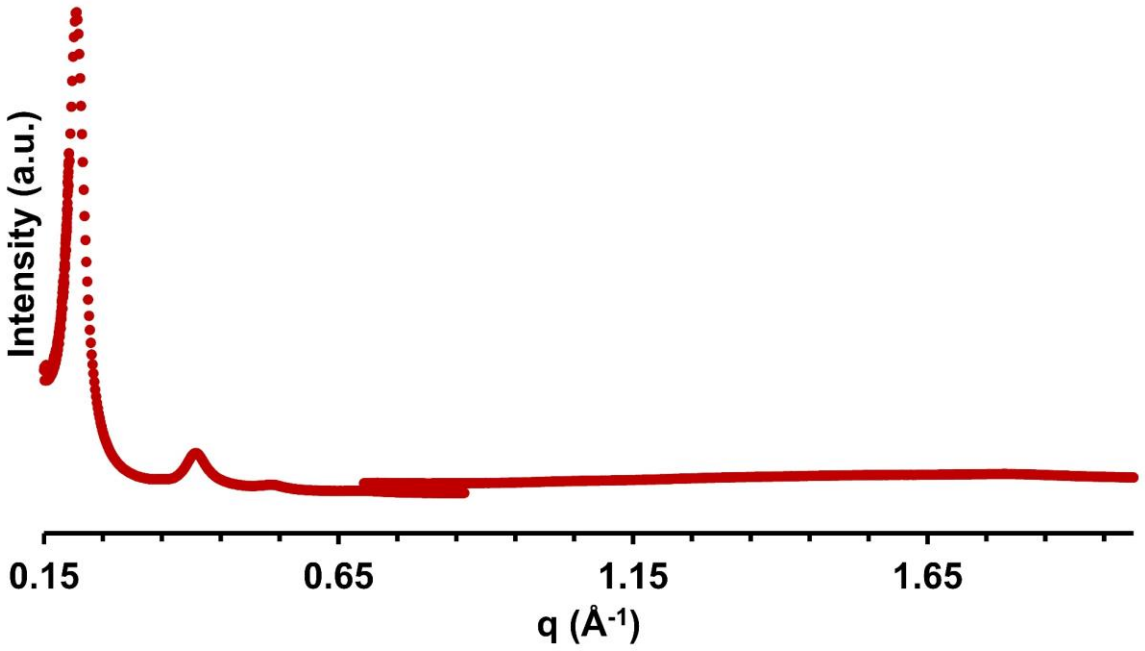

Figure S16. Ambient X-ray diffraction pattern of TAPB-PDA-Br COF.

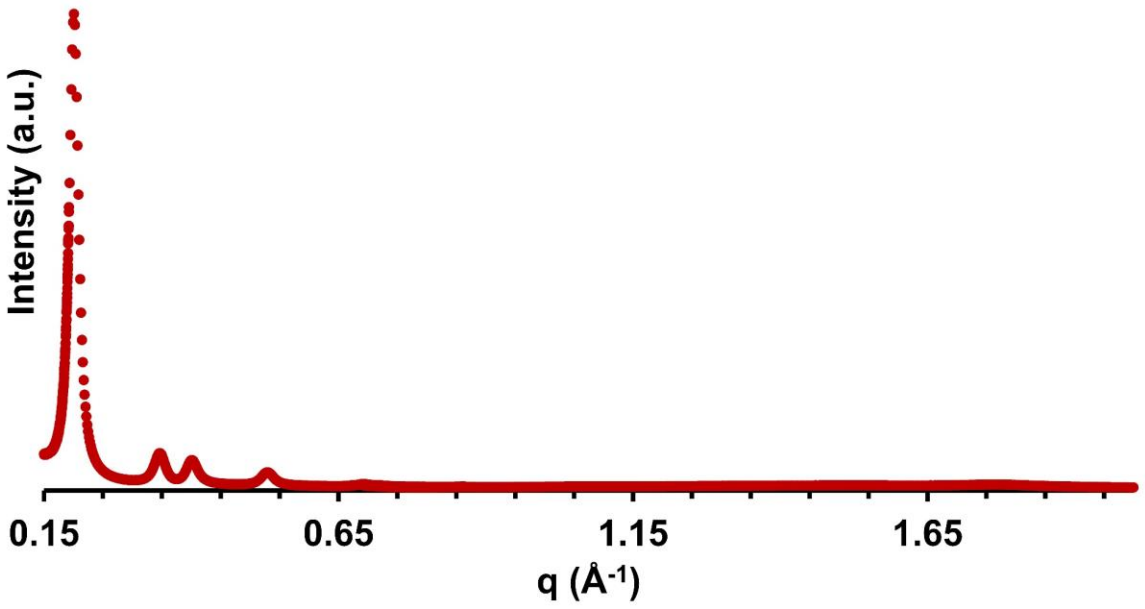

Figure S17. Ambient X-ray diffraction pattern of TAPB-PDA-Me COF.

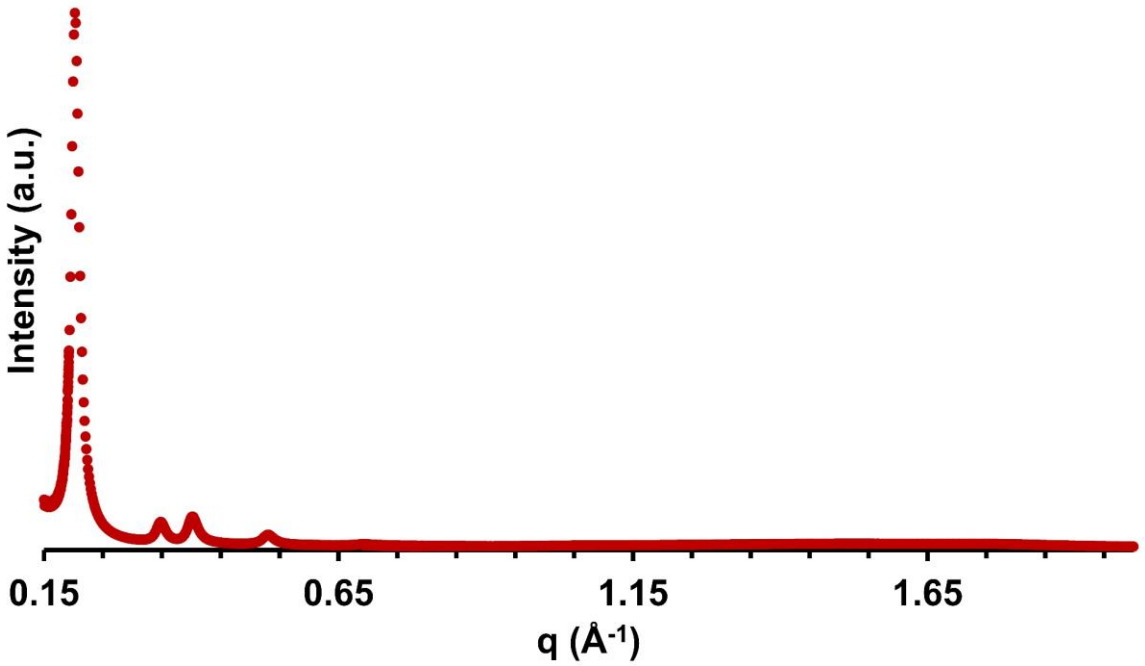

Figure S18. Ambient X-ray diffraction pattern of TAPB-PDA-Et COF.

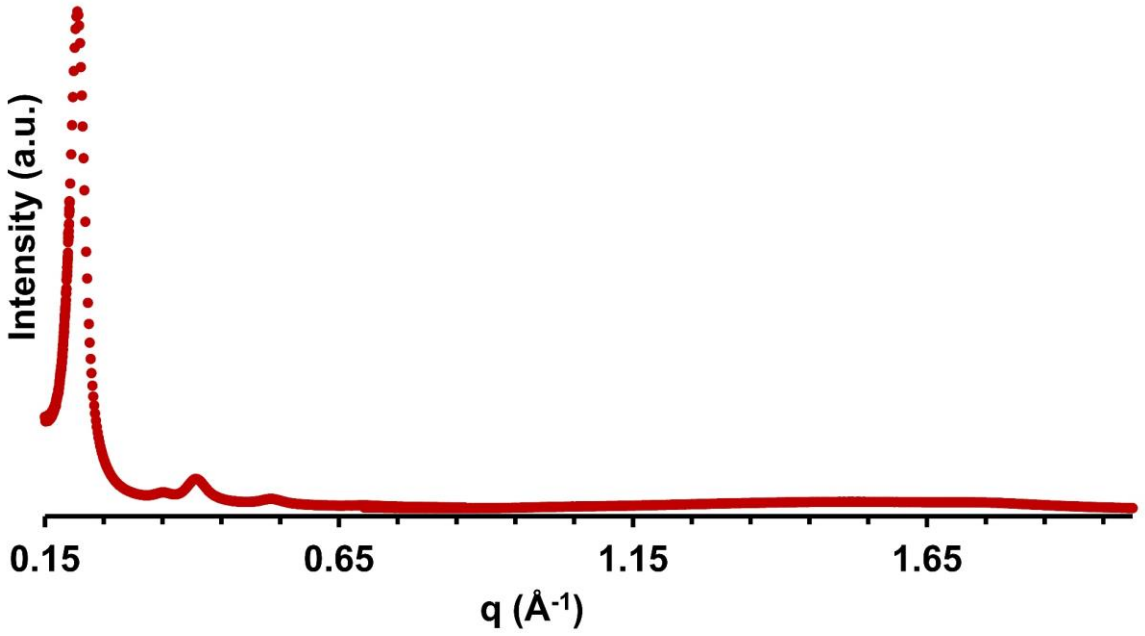

Figure S19. Ambient X-ray diffraction pattern of TAPB-PDA-SMe COF.

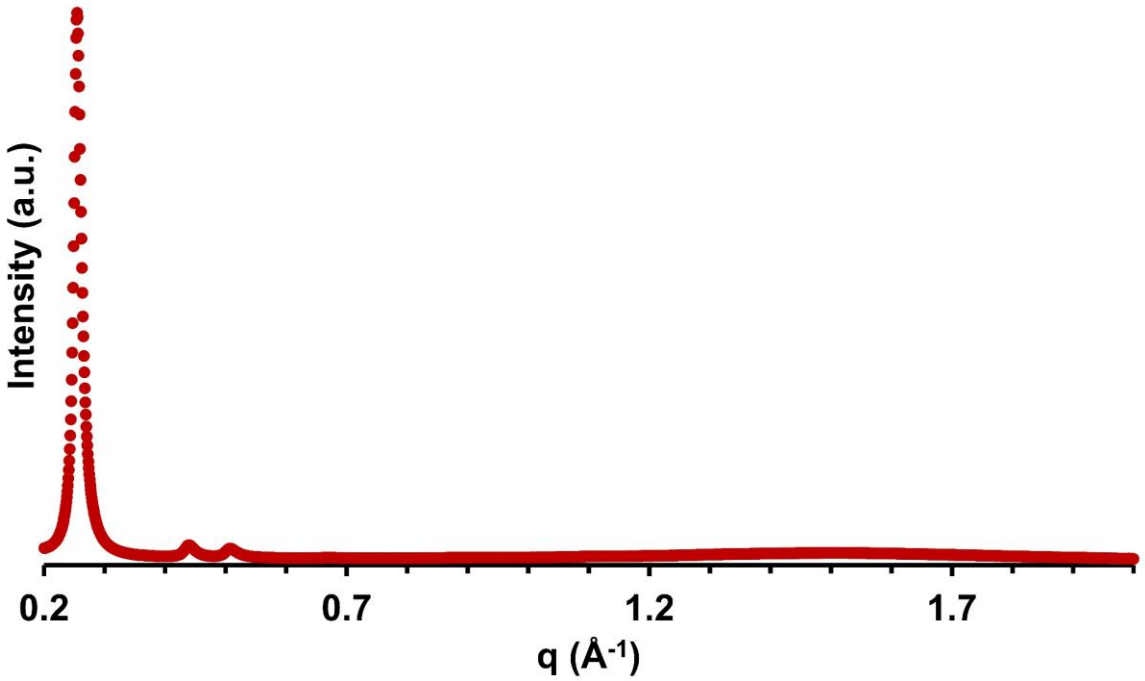

Figure S20. Ambient X-ray diffraction pattern of BND-TFB COF.

D. Refined Diffraction Patterns

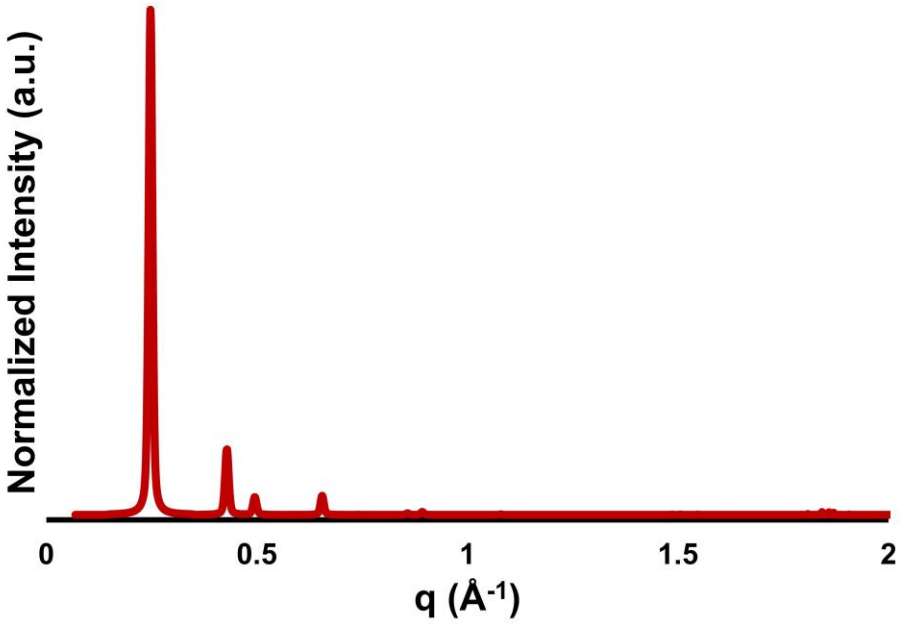

Figure S21. Refined diffraction pattern of HHTP-PBBA COF.

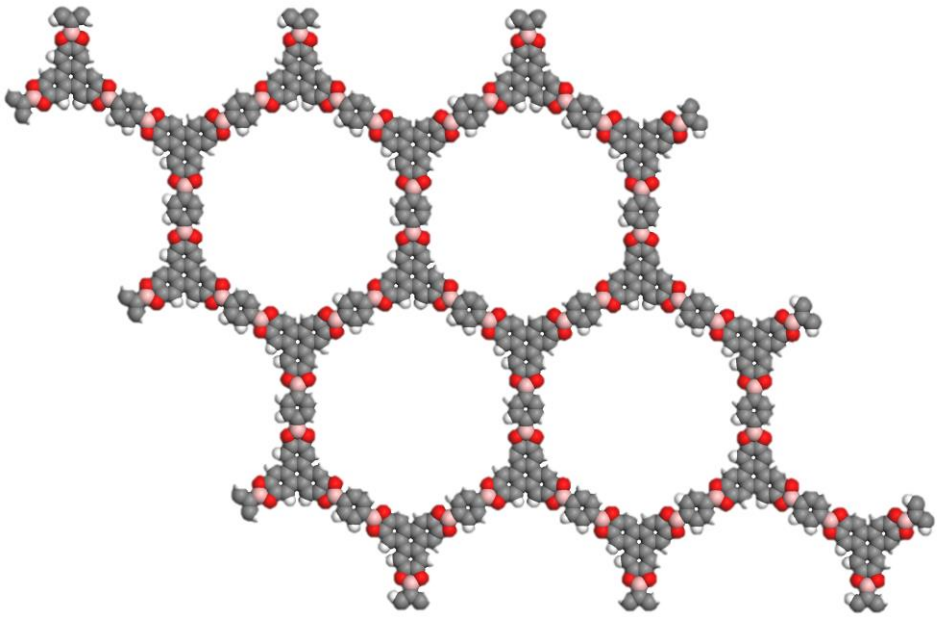

Figure S22. Refined structure of HHTP-PBBA COF.

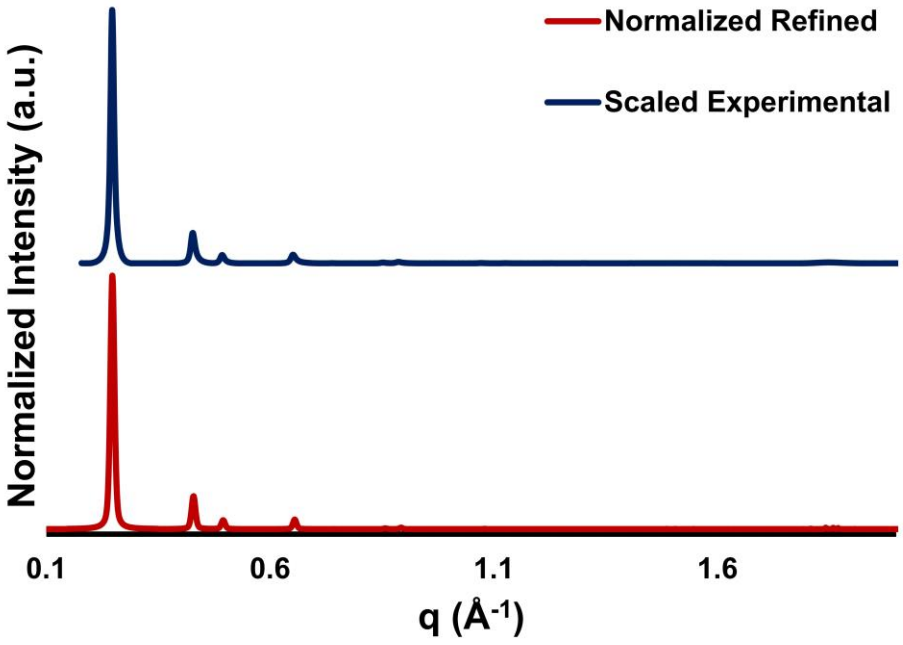

Figure S23. Comparison of refined diffraction pattern of HHTP-PBBA COF.

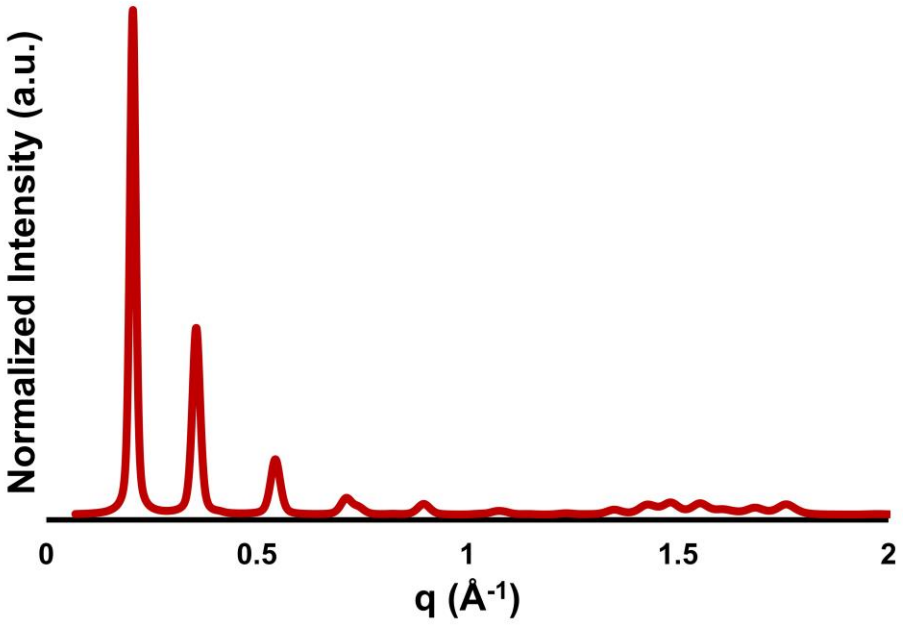

Figure S24. Refined diffraction pattern of HHTP-BBBA COF.

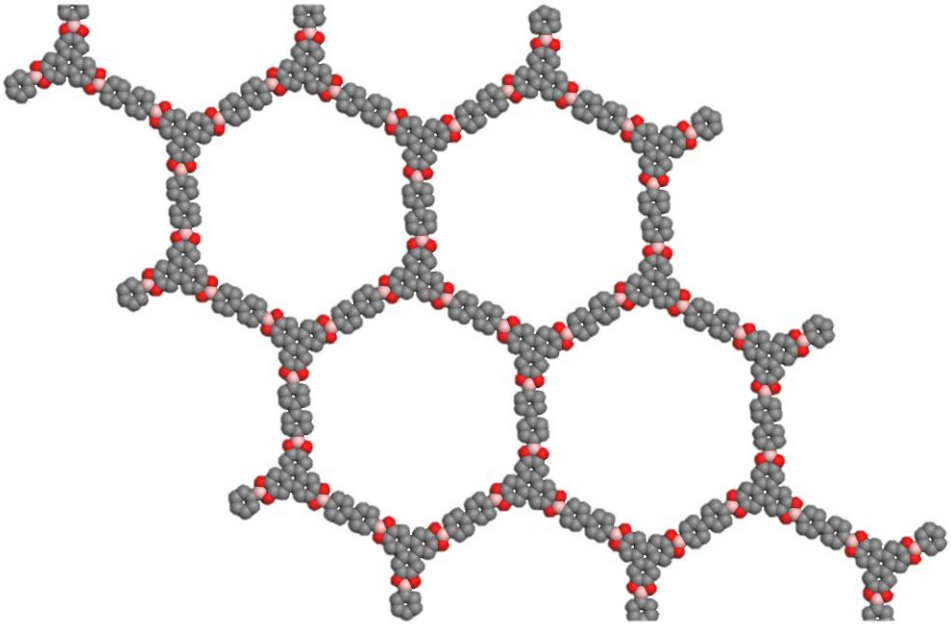

Figure S25. Refined structure of HHTP-BBBA COF

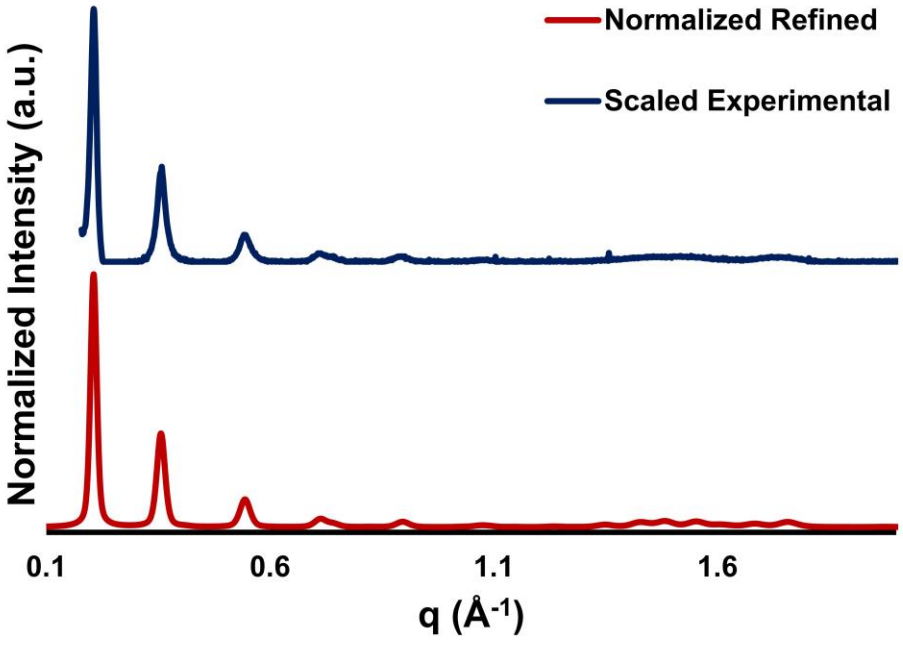

Figure S26. Comparison of refined diffraction pattern of HHTP-BBBA COF.

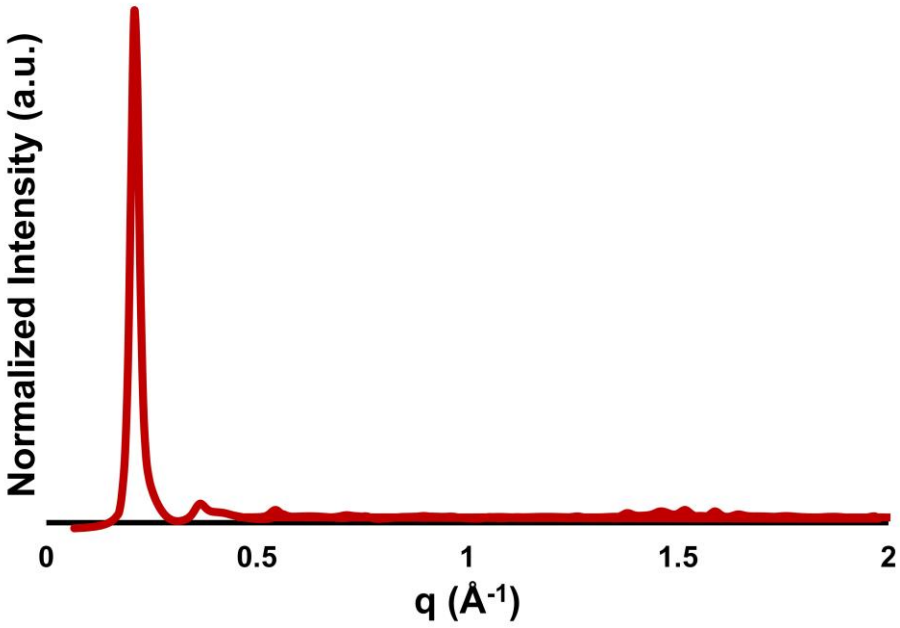

Figure S27. Refined diffraction pattern of TAPB-PDA COF.

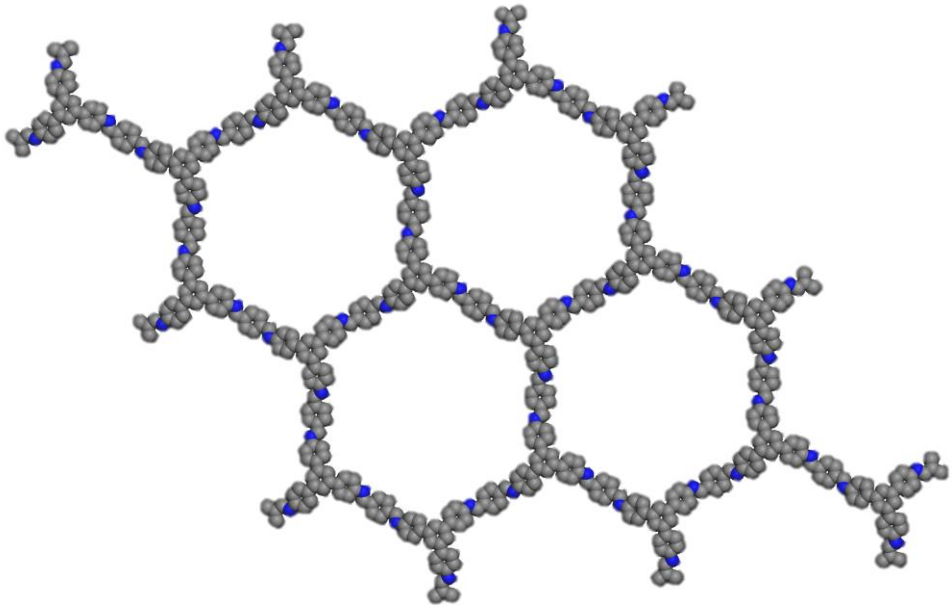

Figure S28. Refined structure of TAPB-PDA COF.

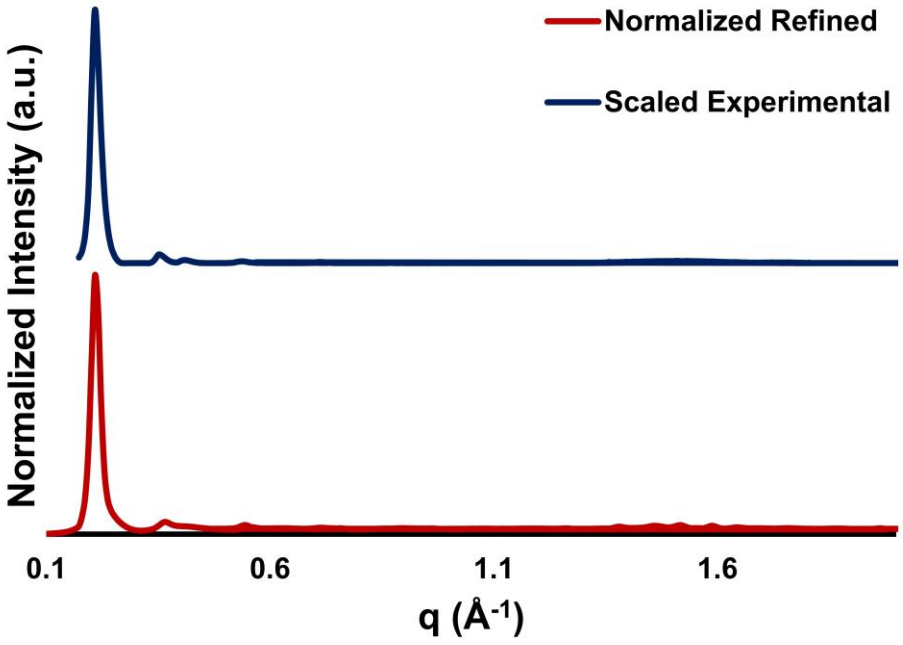

Figure S29. Comparison of refined diffraction pattern of TAPB-PDA COF.

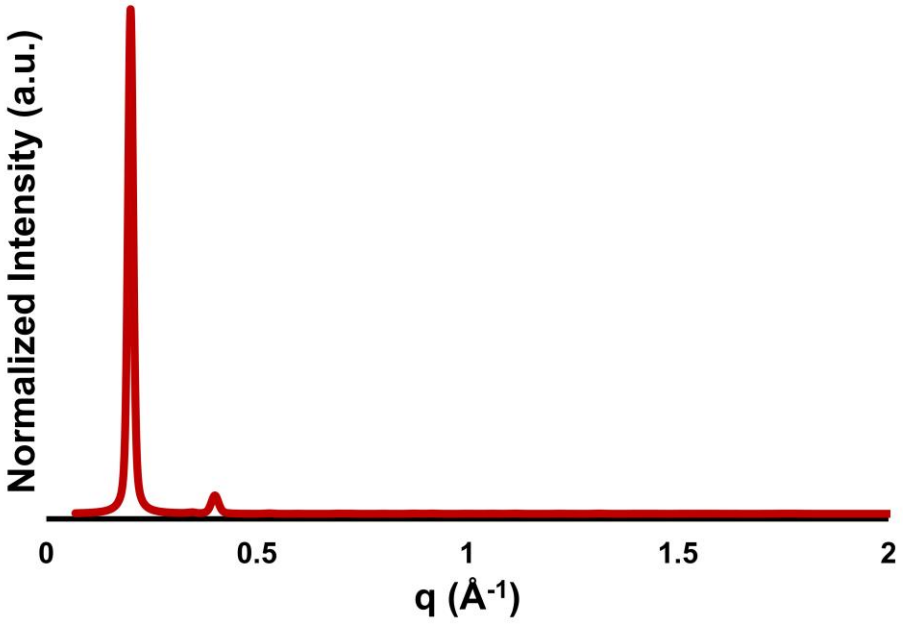

Figure S30. Refined diffraction pattern of TAPB-PDA-N_3 COF.

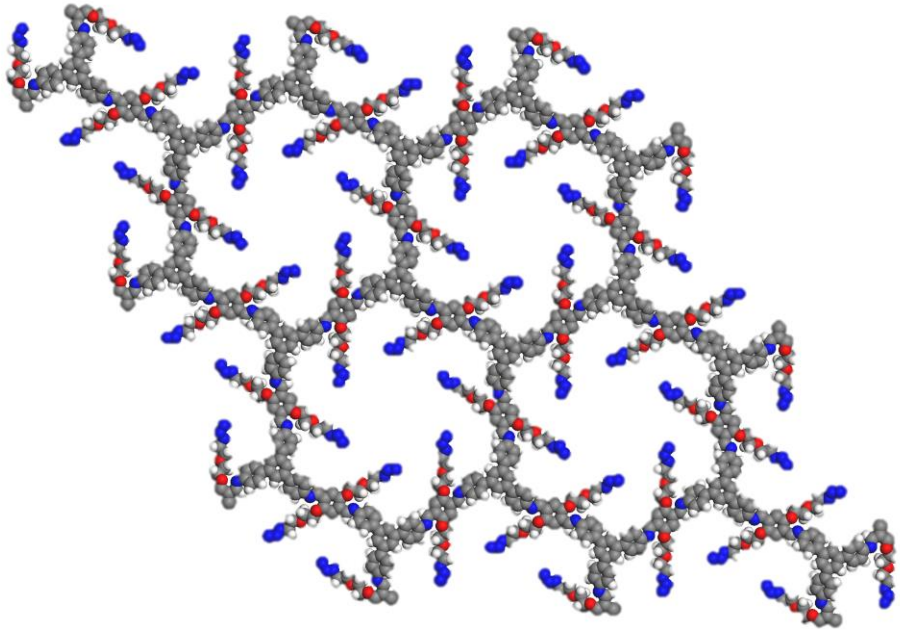

Figure S31. Refined structure of TAPB-PDA-N_3 COF.

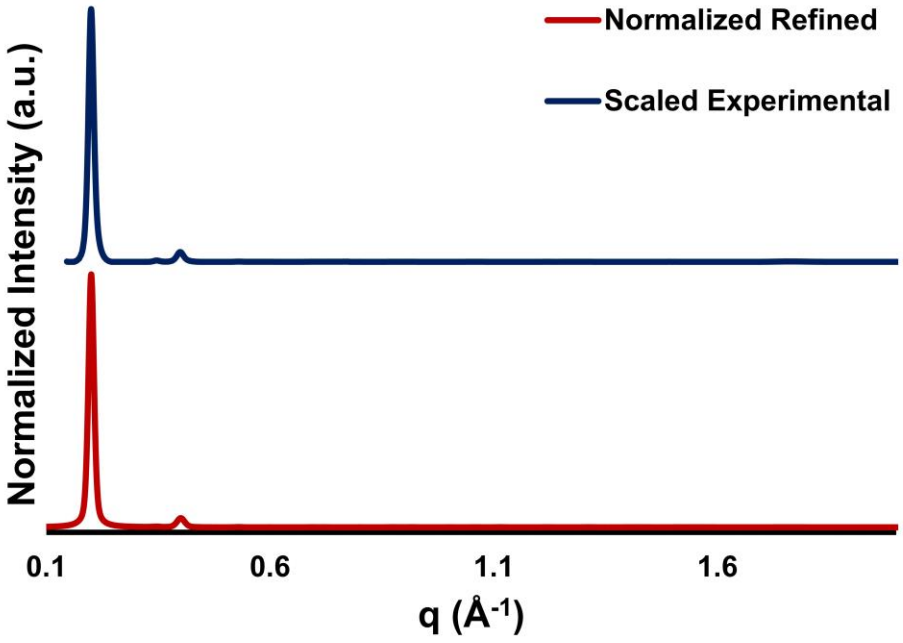

Figure S32. Comparison of refined diffraction pattern of TAPB-PDA-N_3 COF.

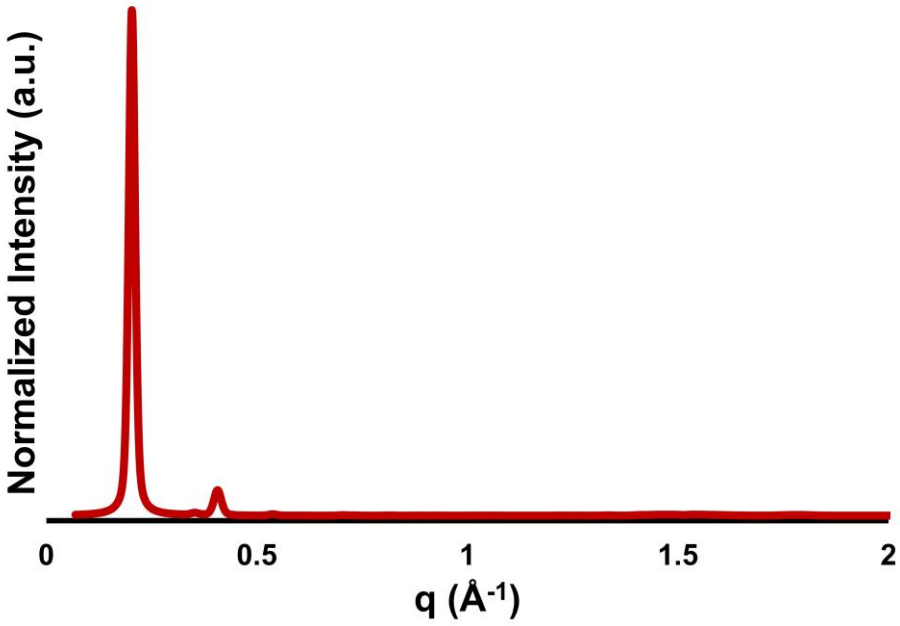

Figure S33. Refined diffraction pattern of TAPB-PDA-NH_2 COF.

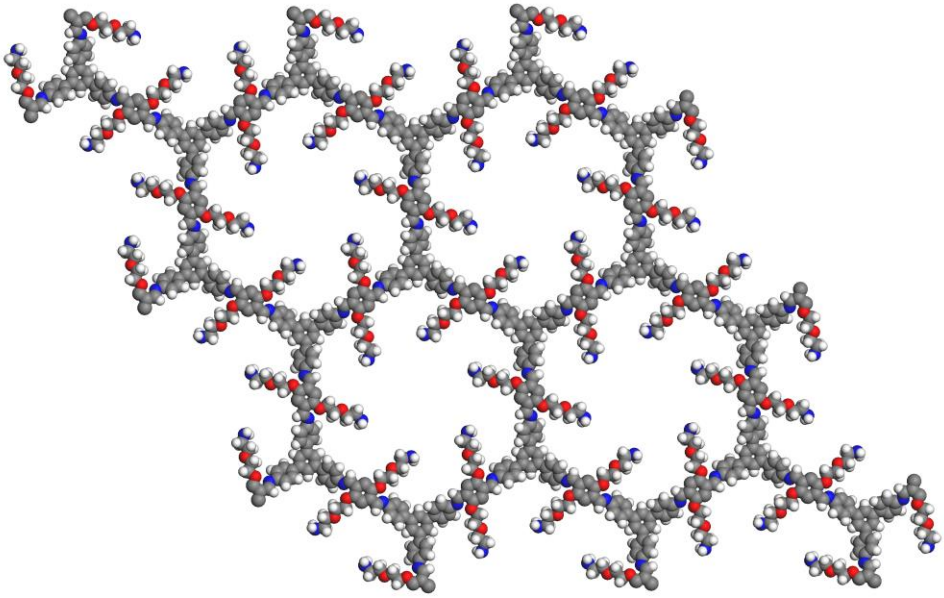

Figure S34. Refined structure of TAPB-PDA-NH_2 COF.

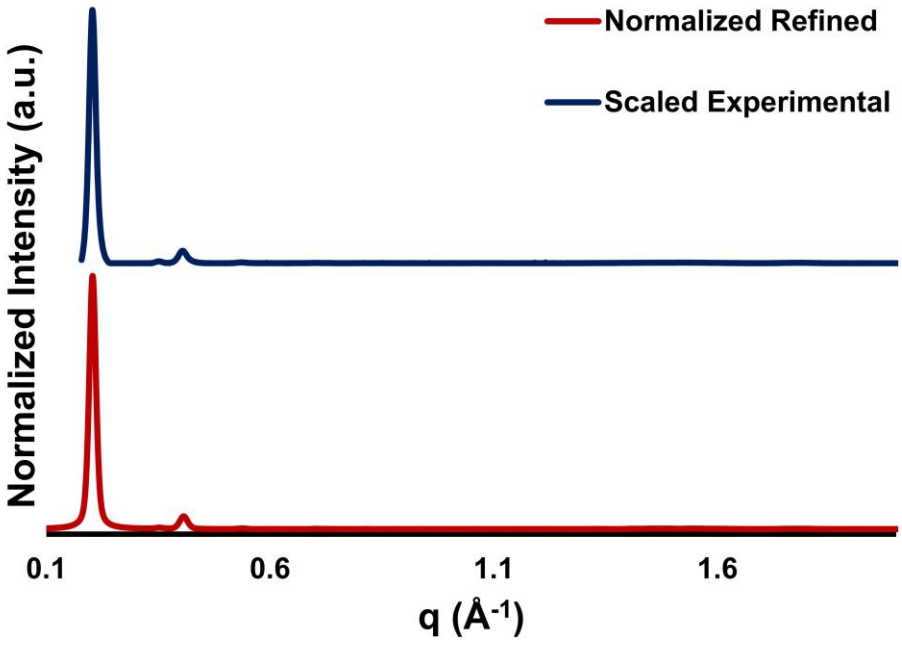

Figure S35. Comparison of refined diffraction pattern of TAPB-PDA-NH_2 COF.

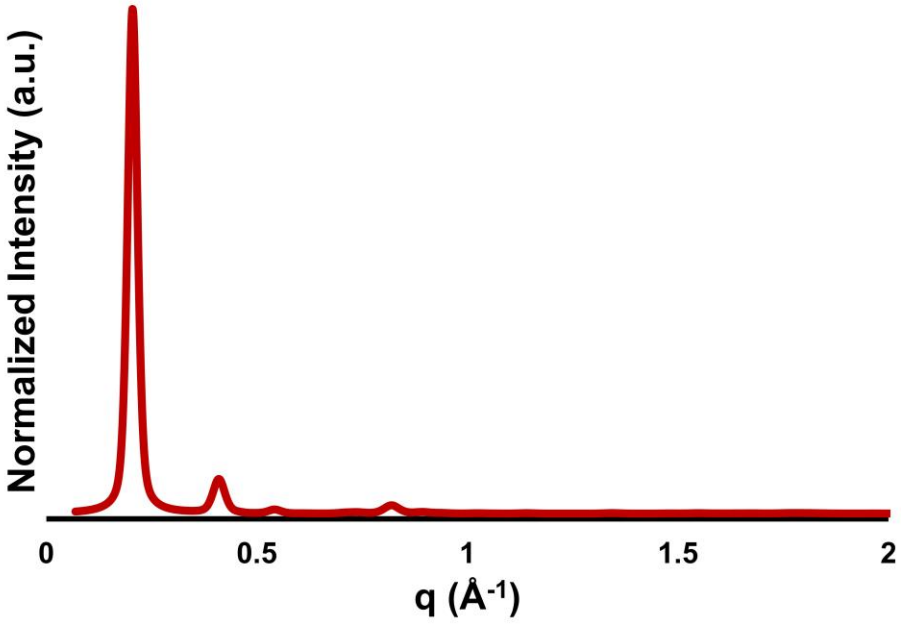

Figure S36. Refined diffraction pattern of TAPB-PDA-Br COF.

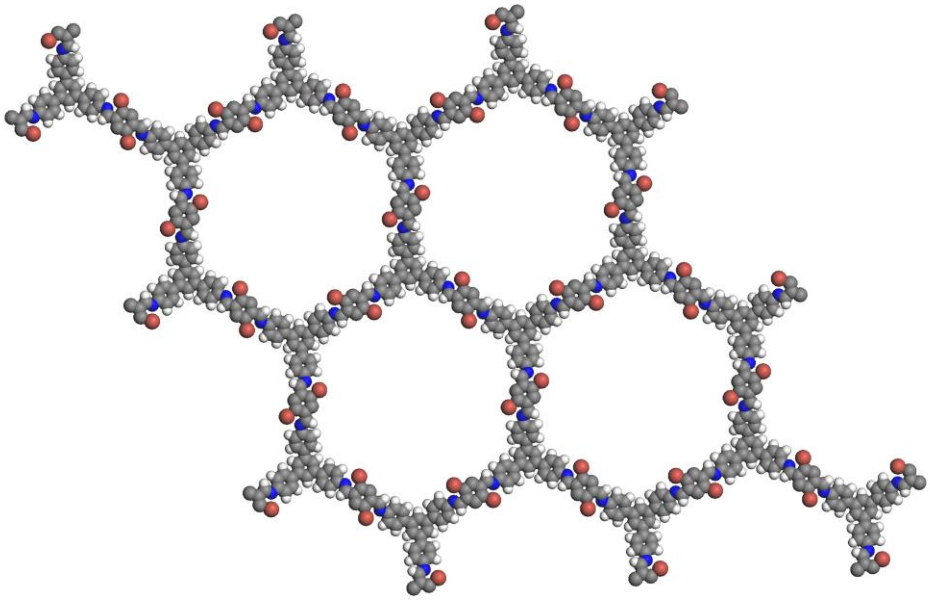

Figure S37. Refined structure of TAPB-PDA-Br COF.

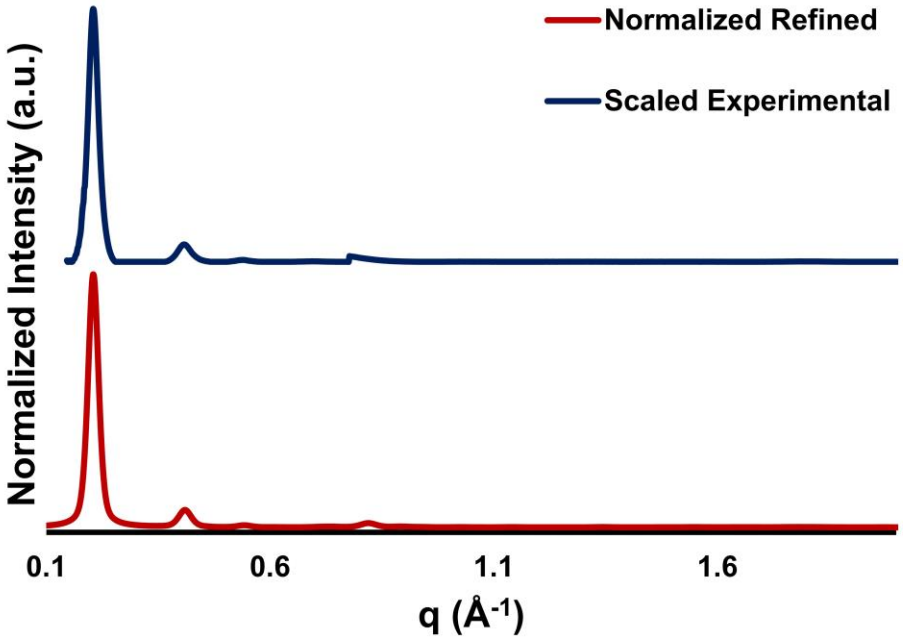

Figure S38. Comparison of refined diffraction pattern of TAPB-PDA-Br COF.

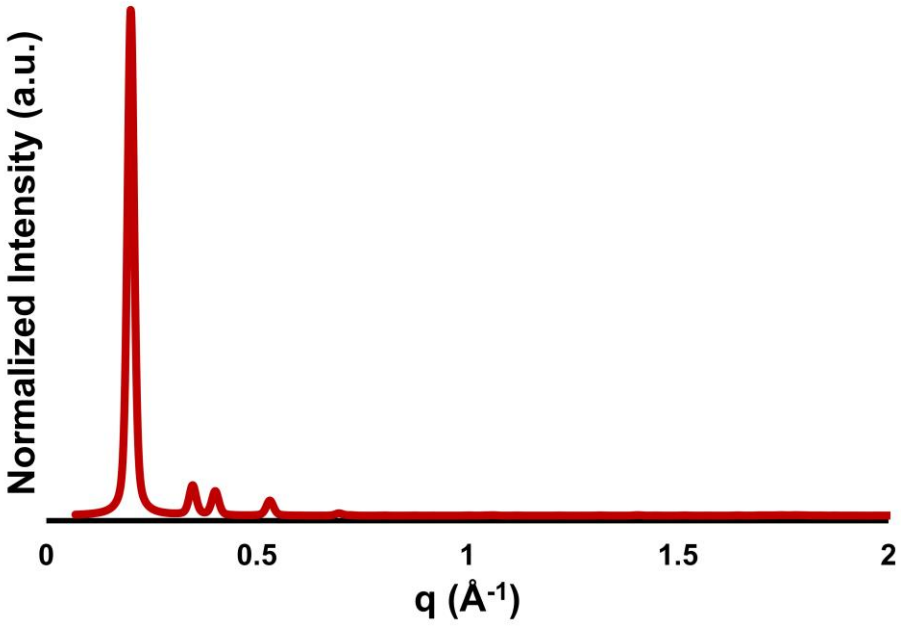

Figure S39. Refined diffraction pattern of TAPB-PDA-Me COF.

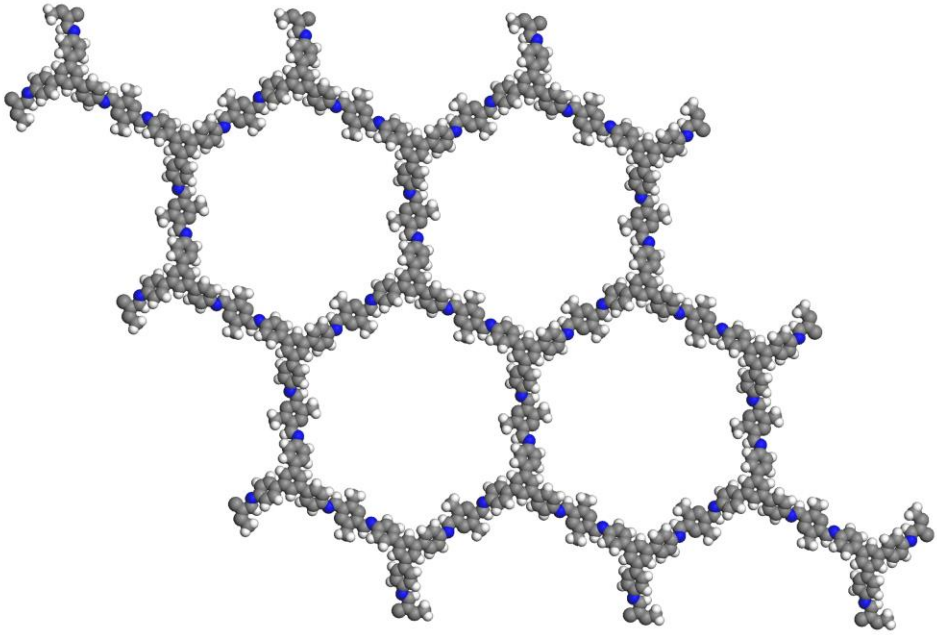

Figure S40. Refined structure of TAPB-PDA-Me COF.

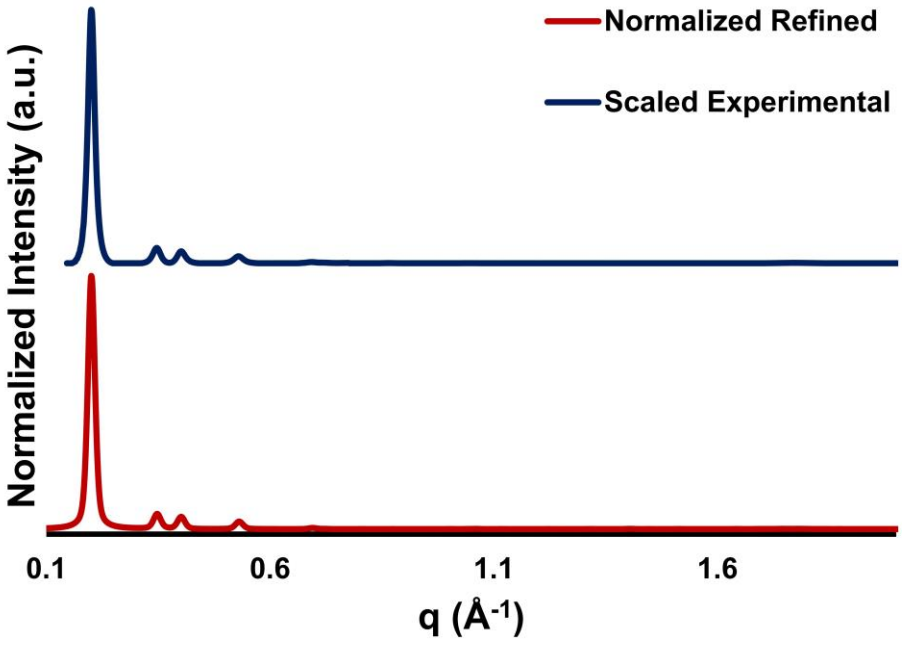

Figure S41. Comparison of refined diffraction pattern of TAPB-PDA-Me COF.

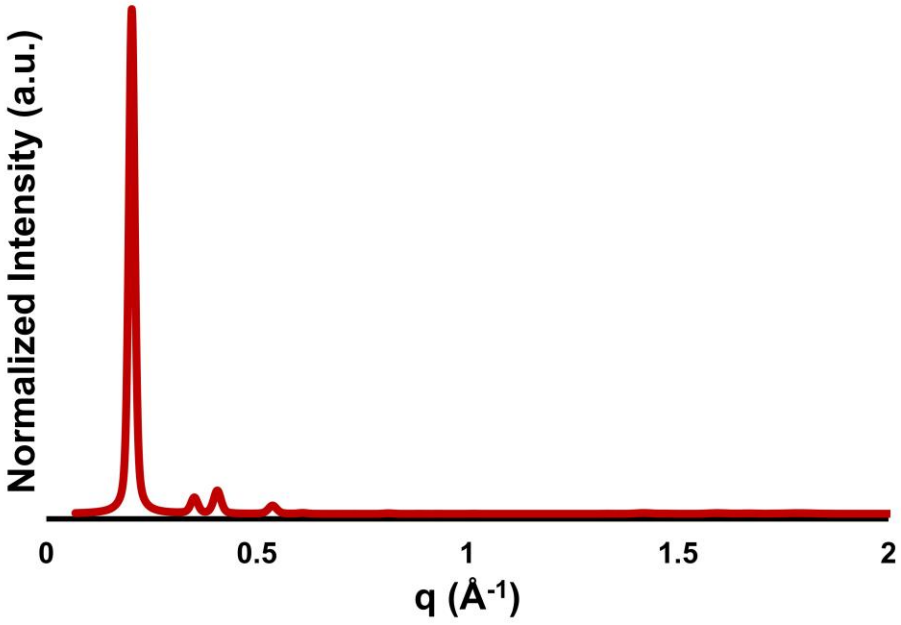

Figure S42. Refined diffraction pattern of TAPB-PDA-Et COF.

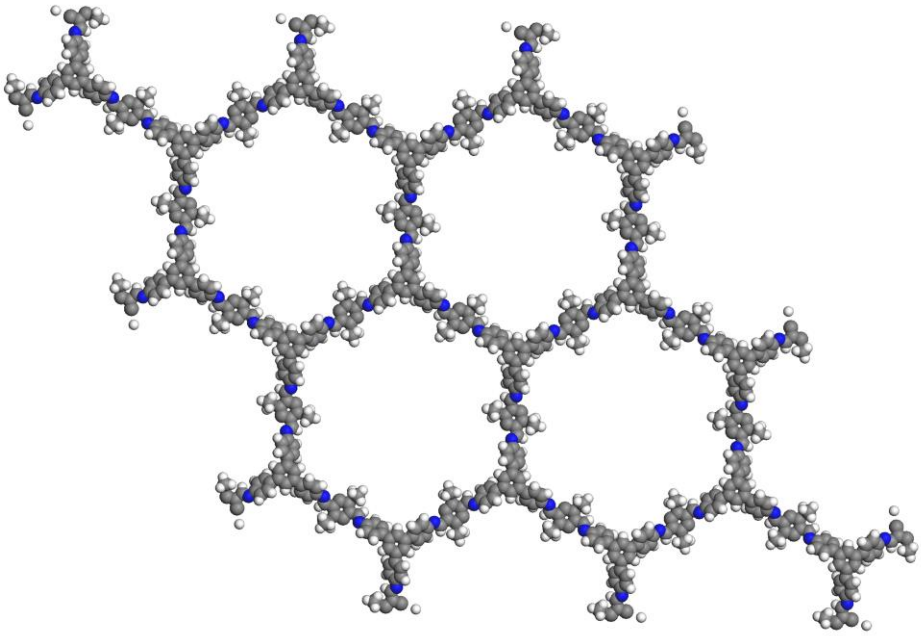

Figure S43. Refined structure of TAPB-PDA-Et COF.

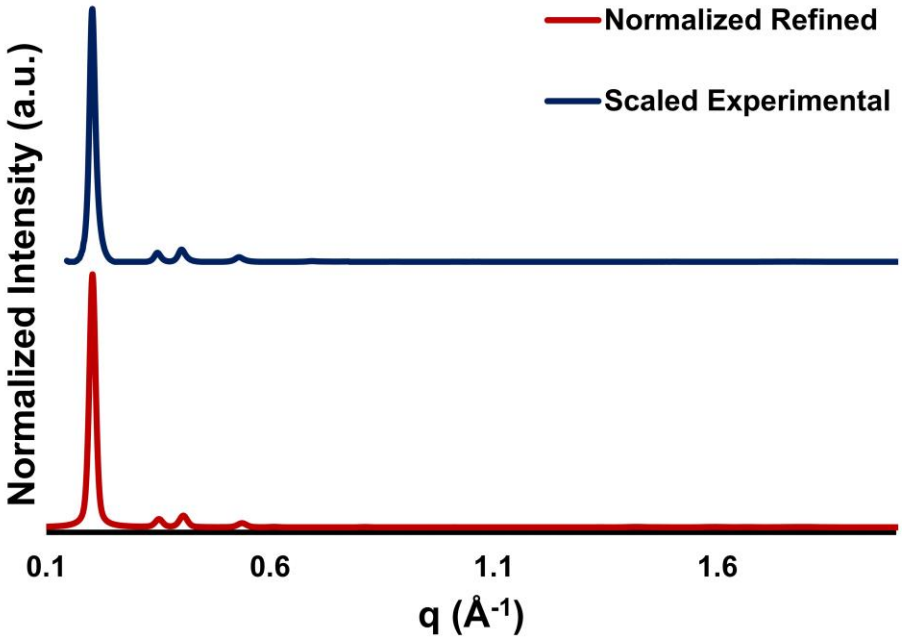

Figure S44. Comparison of refined diffraction pattern of TAPB-PDA-Et COF.

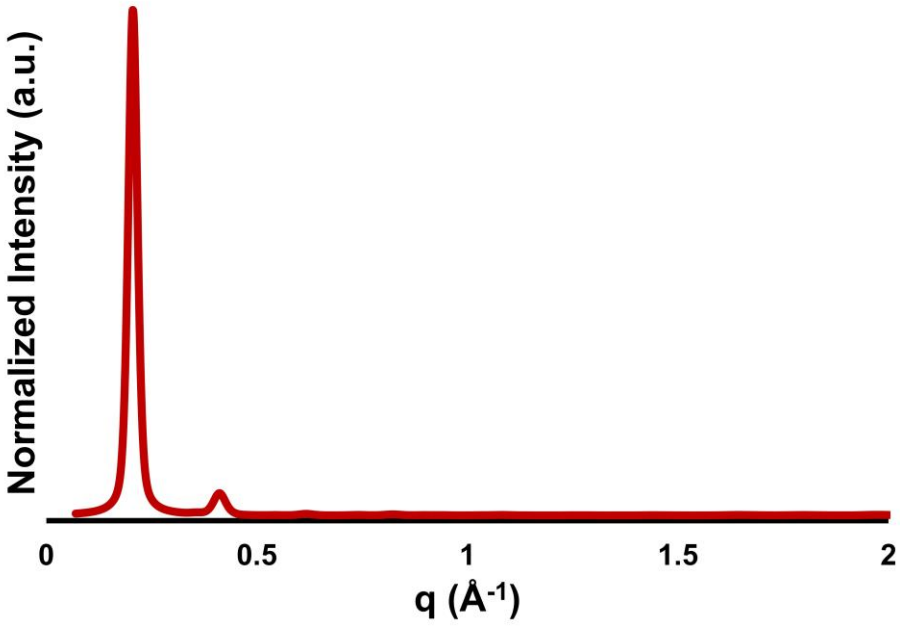

Figure S45. Refined diffraction pattern of TAPB-PDA-SMe COF.

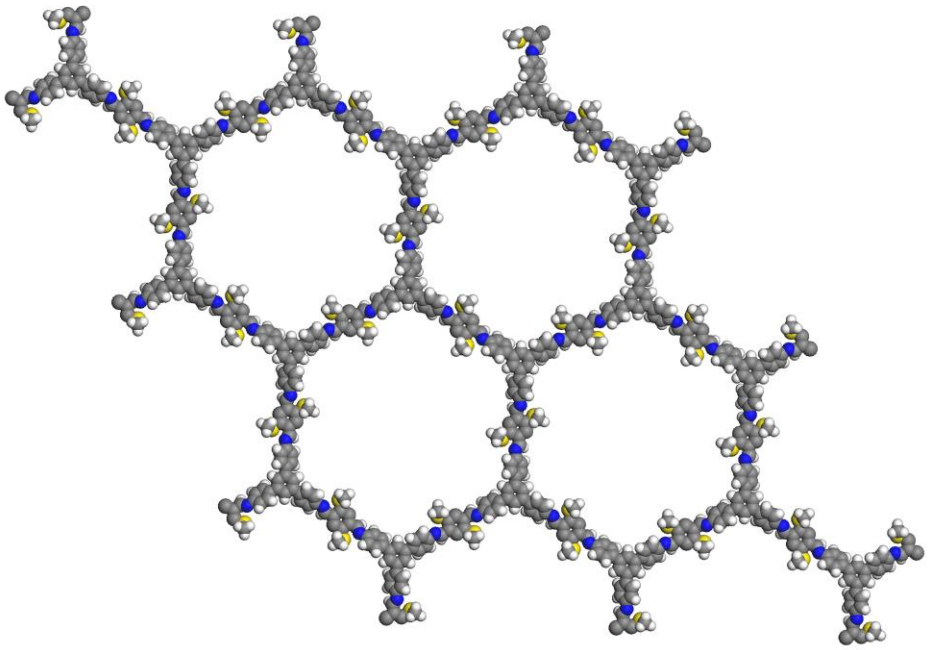

Figure S46. Refined structure of TAPB-PDA-SMe COF.

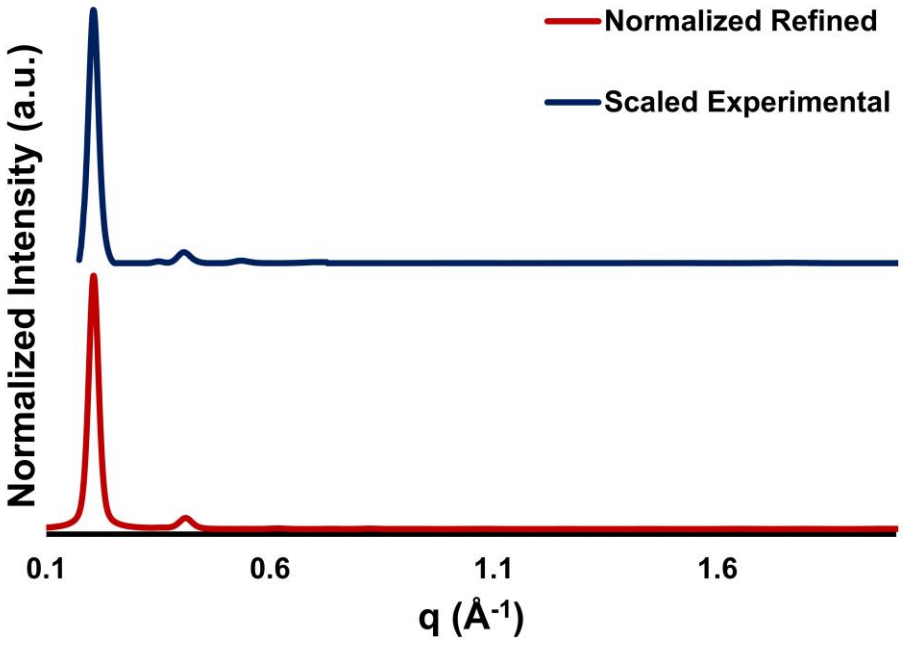

Figure S47. Comparison of refined diffraction pattern of TAPB-PDA-SMe COF.

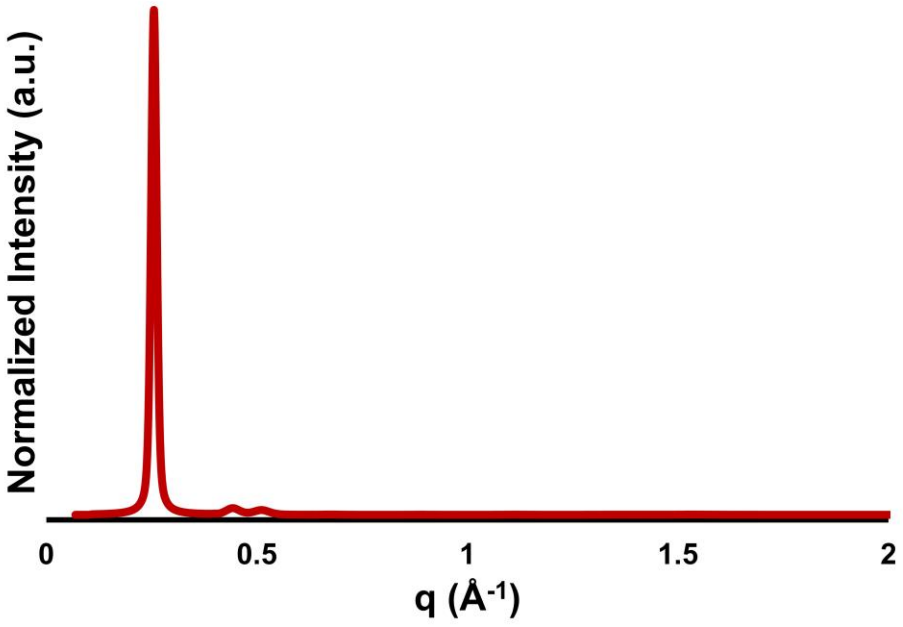

Figure S48. Refined diffraction pattern of BND-TFB COF.

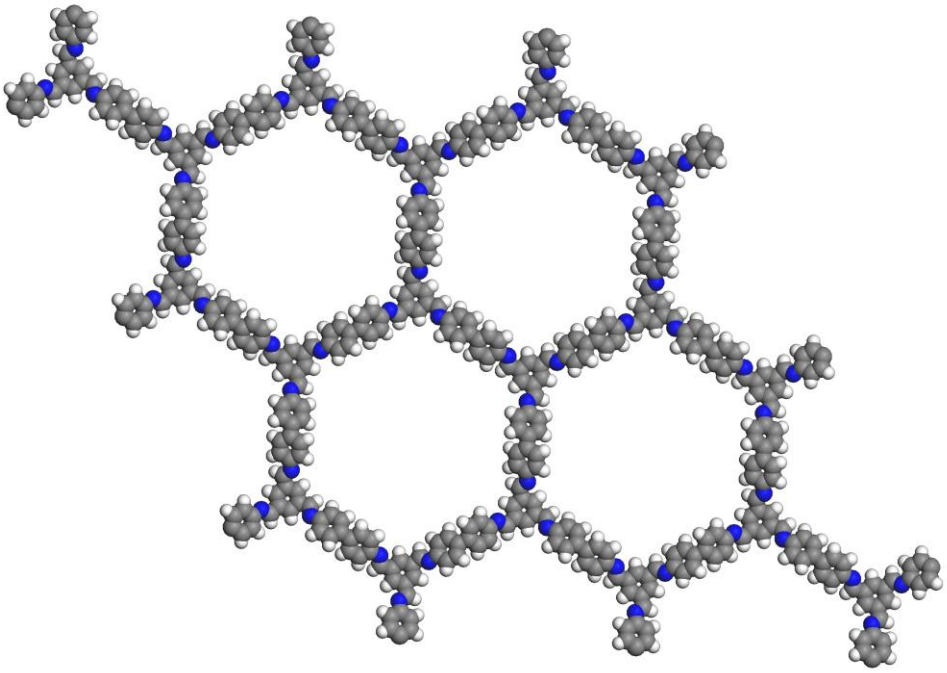

Figure S49. Refined structure of BND-TFB COF.

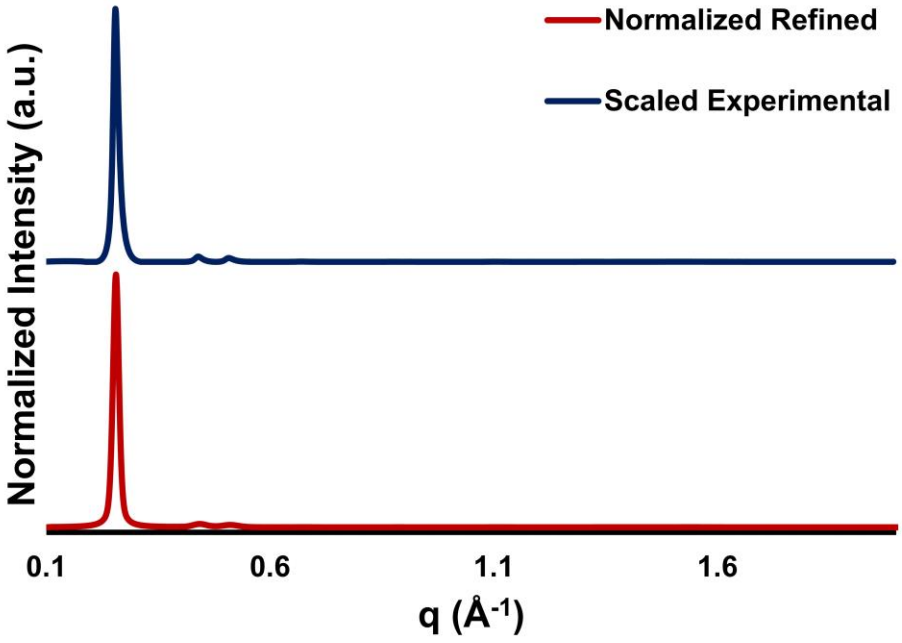

Figure S50. Comparison of refined diffraction pattern of BND-TFB COF.

E. Nitrogen Sorption Measurements

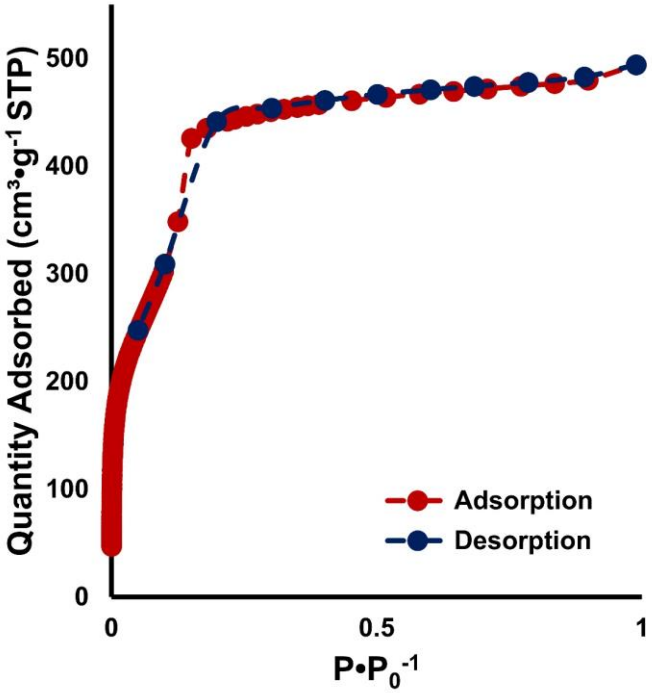

Figure S51. Nitrogen isotherm recorded at 77 K for HHTP-PBBA COF.

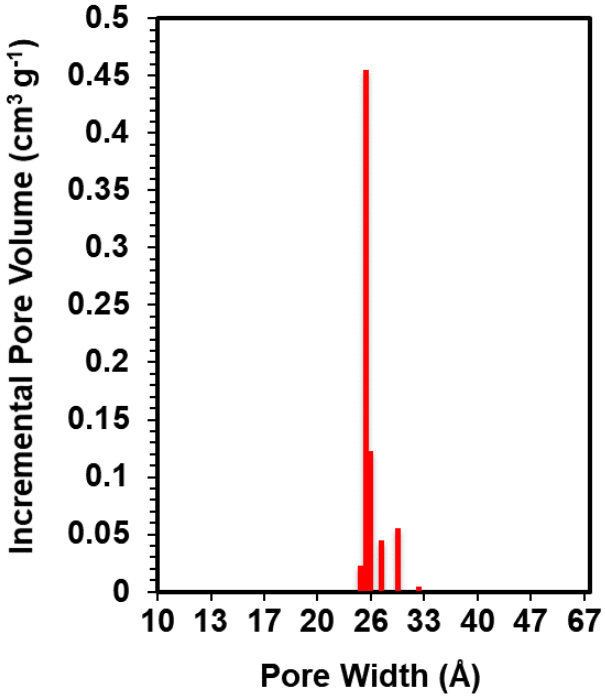

Figure S52. Pore size distribution of HHTP-PBBA COF.

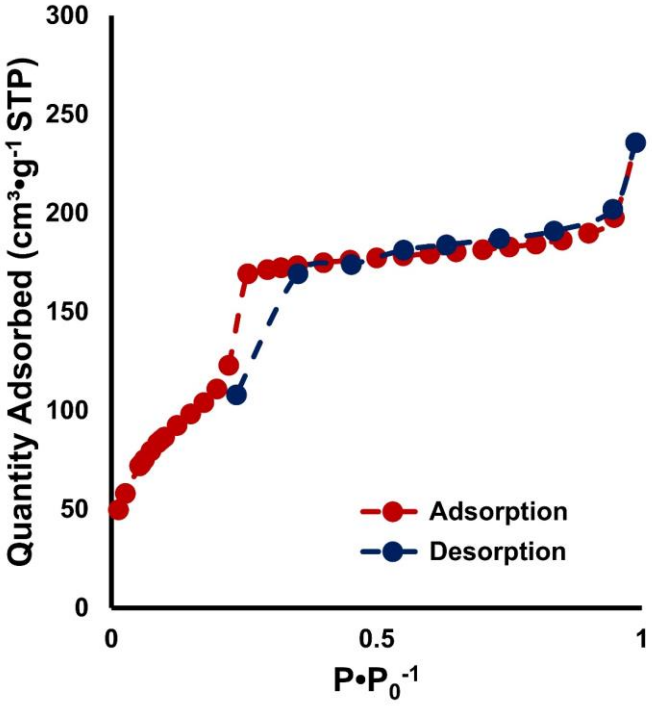

Figure S53. Nitrogen isotherm recorded at 77 K for HHTP-BBBA COF.

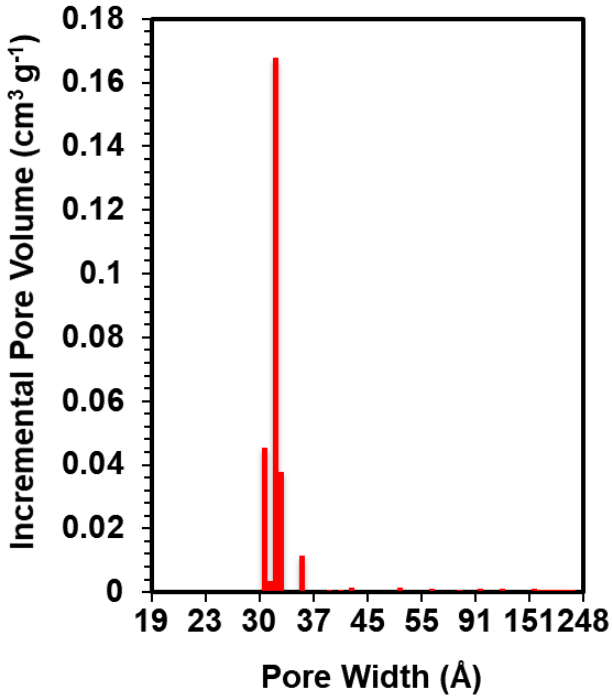

Figure S54. Pore size distribution of HHTP-BBBA COF.

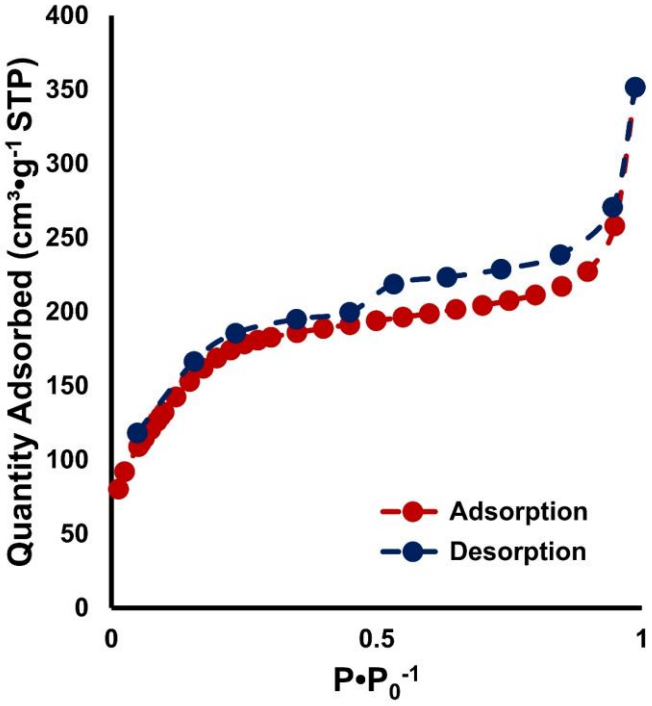

Figure S55. Nitrogen isotherm recorded at 77 K for TAPB-PDA COF.

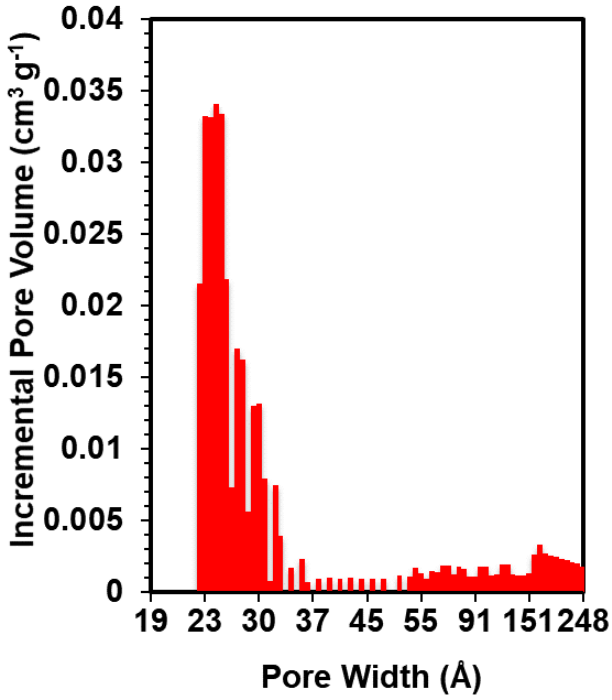

Figure S56. Pore size distribution of TAPB-PDA COF.

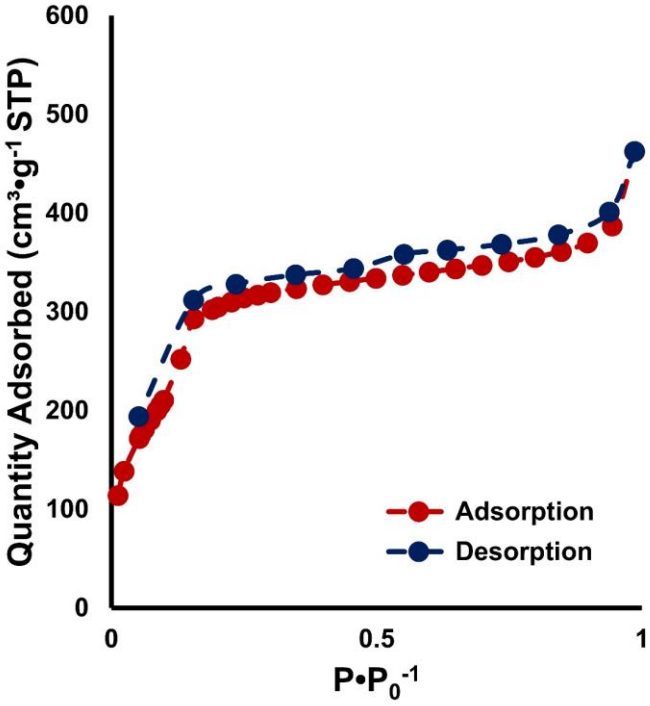

Figure S57. Nitrogen isotherm recorded at 77 K for TAPB-PDA-N_3 COF.

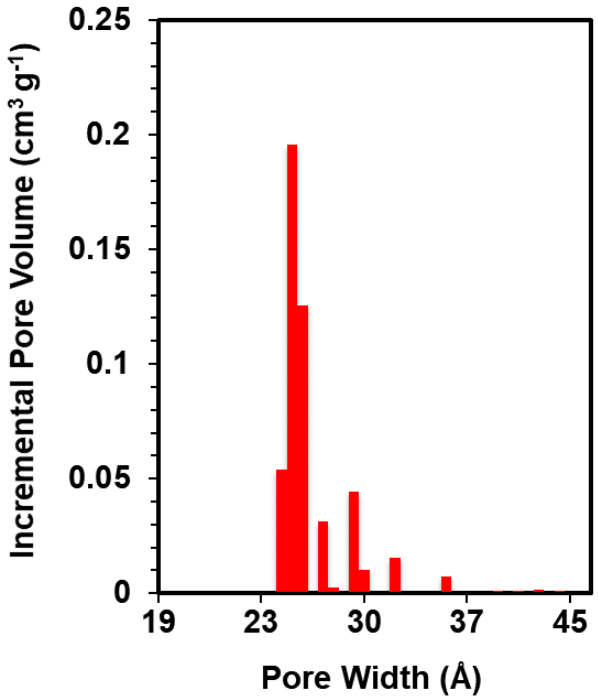

Figure S58. Pore size distribution of TAPB-PDA-N_3 COF.

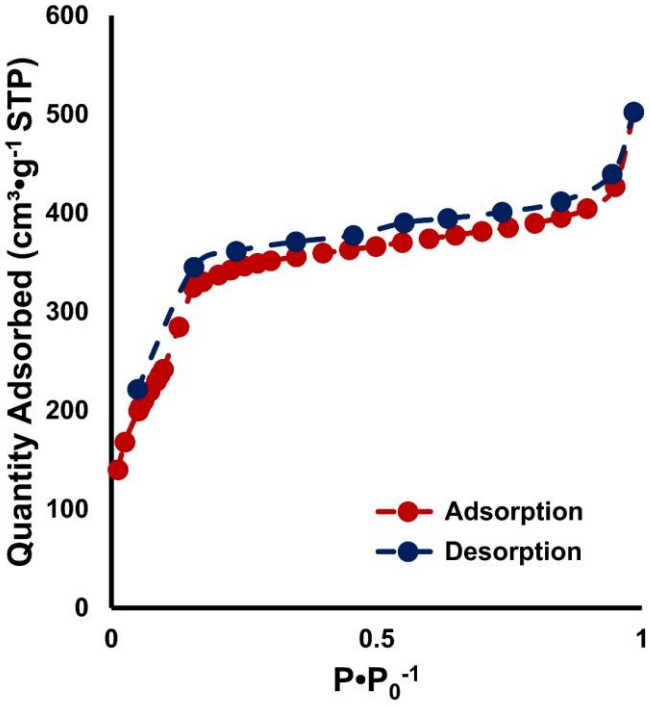

Figure S59. Nitrogen isotherm recorded at 77 K for TAPB-PDA-NH_2 COF.

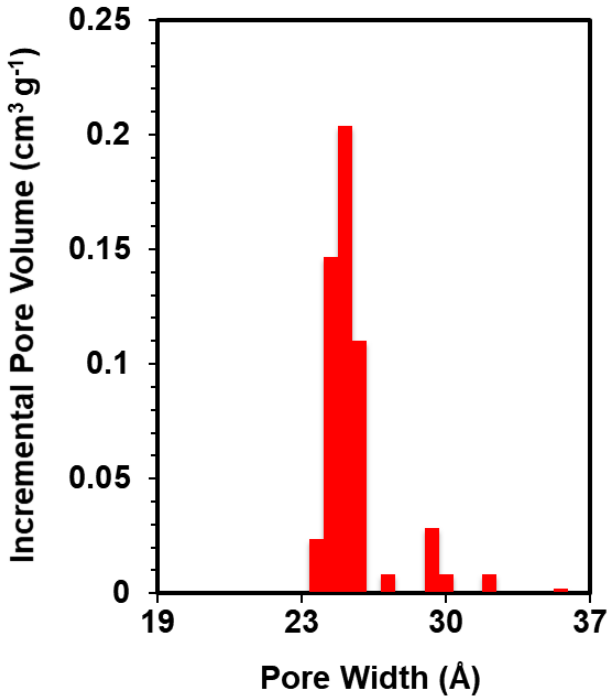

Figure S60. Pore size distribution of TAPB-PDA-NH_2 COF.

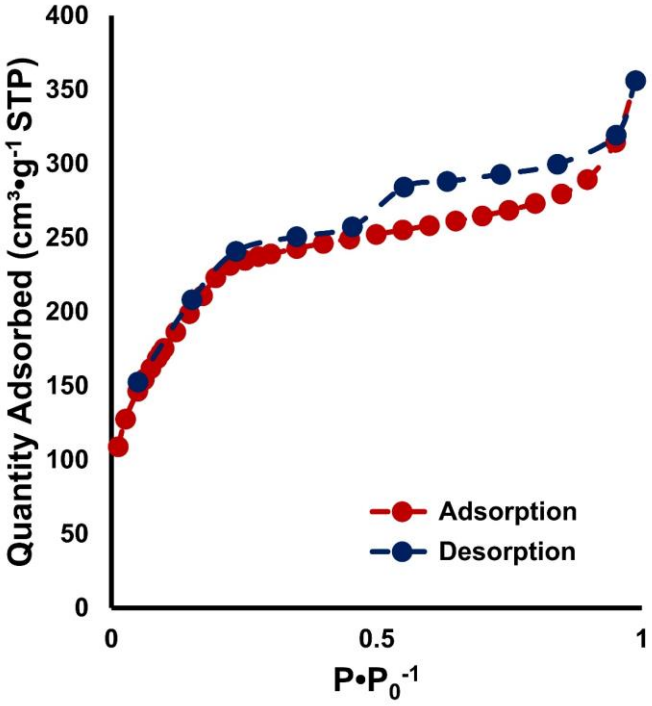

Figure S61. Nitrogen isotherm recorded at 77 K for TAPB-PDA-Br COF.

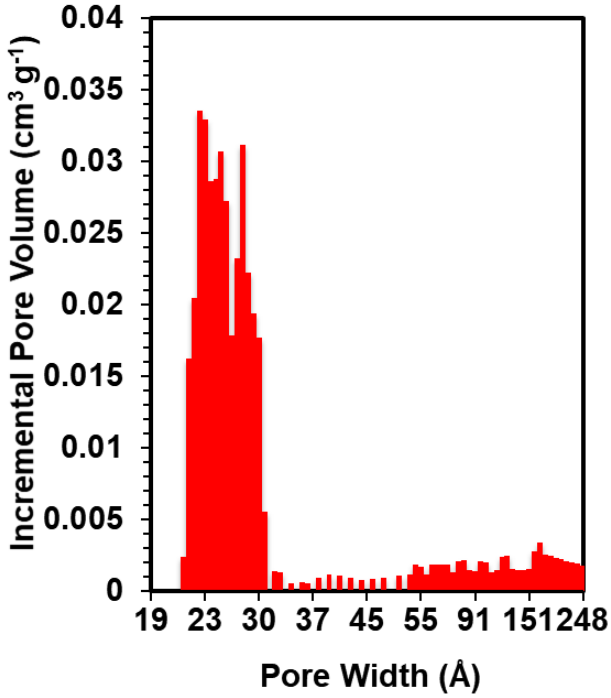

Figure S62. Pore size distribution of TAPB-PDA-Br COF.

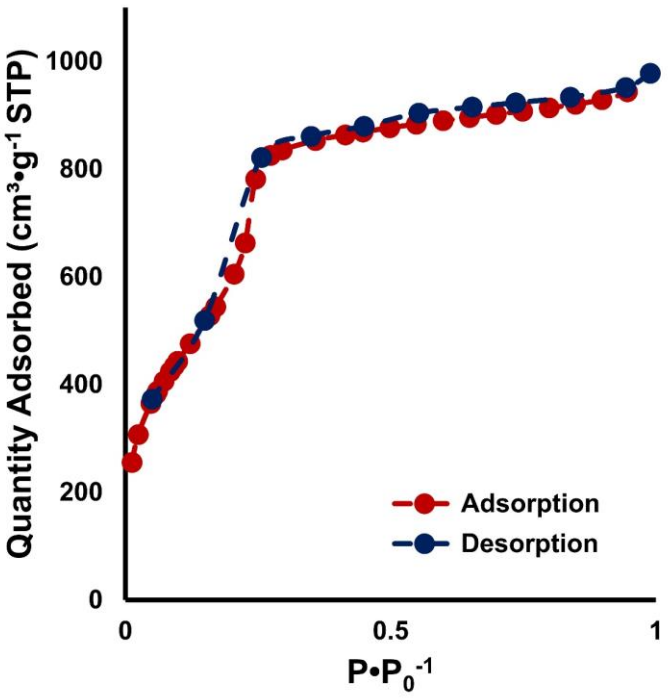

Figure S63. Nitrogen isotherm recorded at 77 K for TAPB-PDA-Me COF.

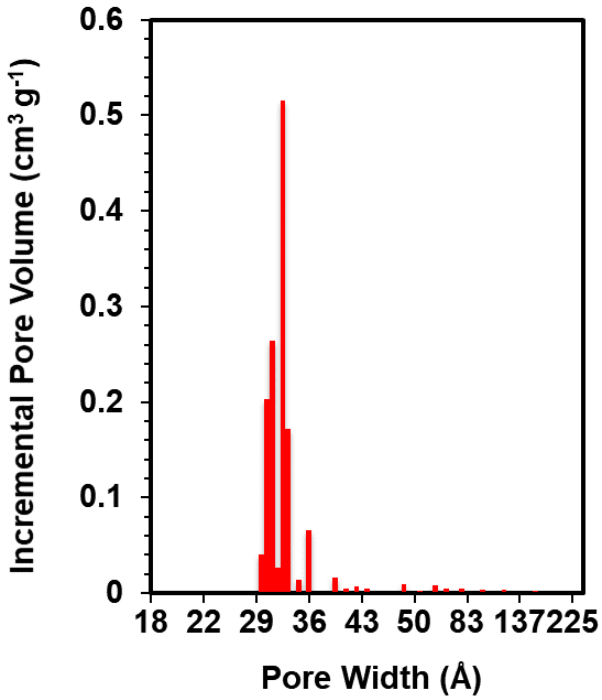

Figure S64. Pore size distribution of TAPB-PDA-Me COF.

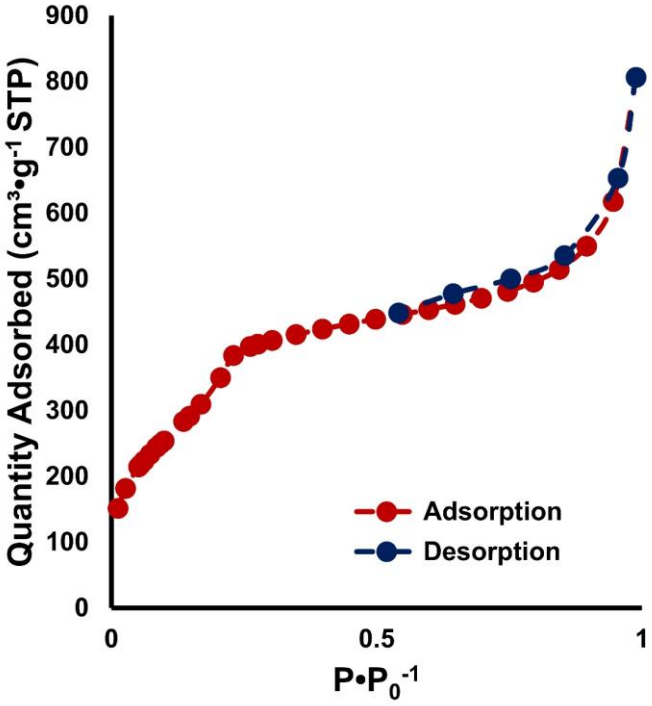

Figure S65. Nitrogen isotherm recorded at 77 K for TAPB-PDA-Et COF.

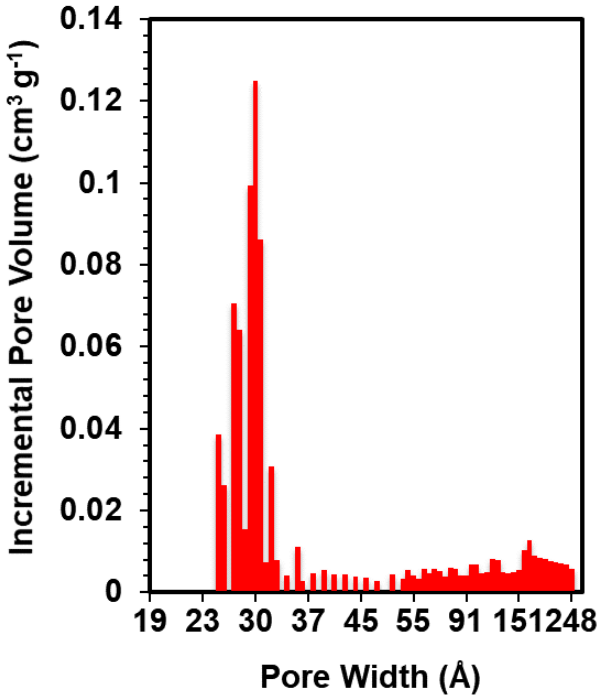

Figure S66. Pore size distribution of TAPB-PDA-Et COF.

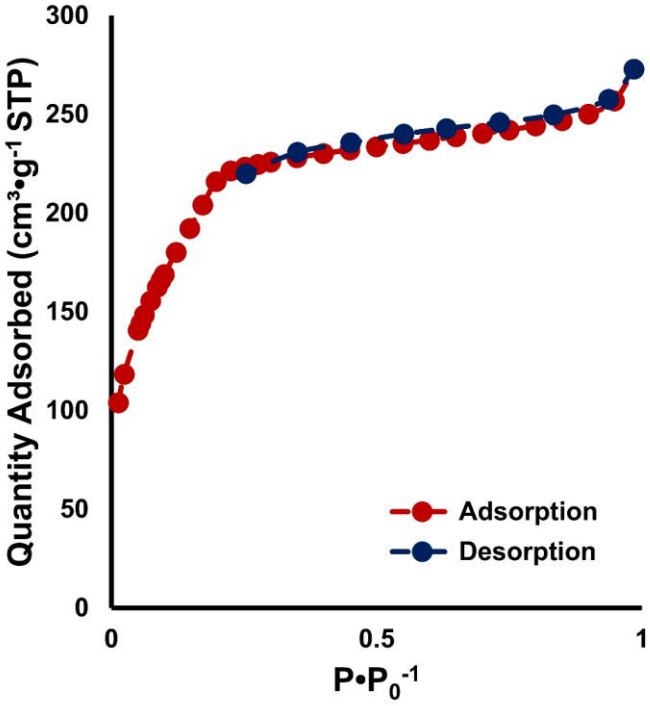

Figure S67. Nitrogen isotherm recorded at 77 K for TAPB-PDA-SMe COF.

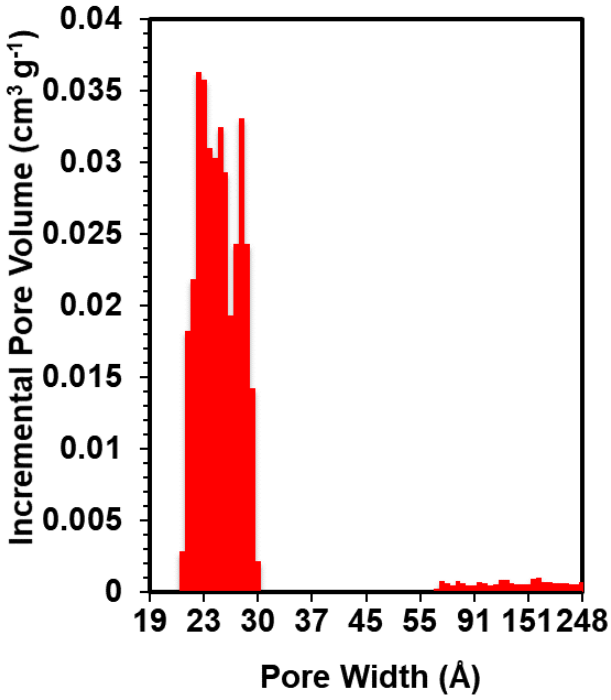

Figure S68. Pore size distribution of TAPB-PDA-SMe COF.

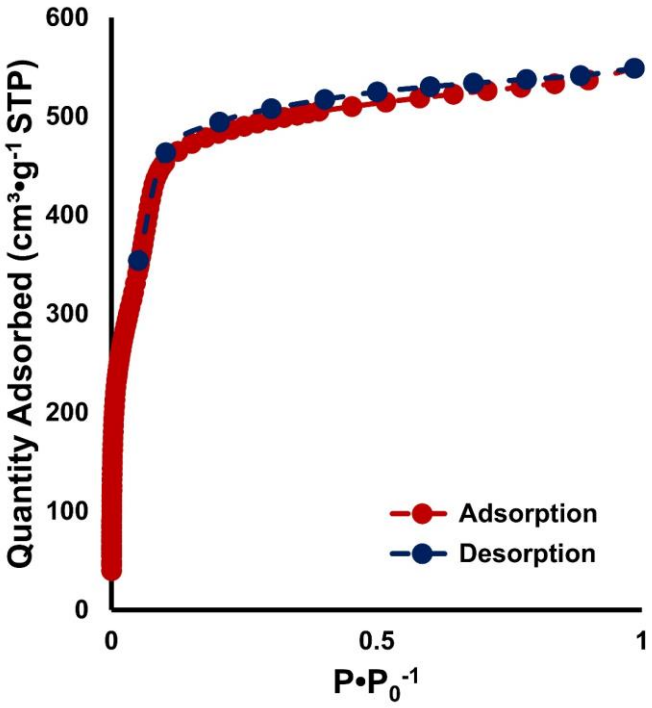

Figure S69. Nitrogen isotherm recorded at 77 K for BND-TFB COF.

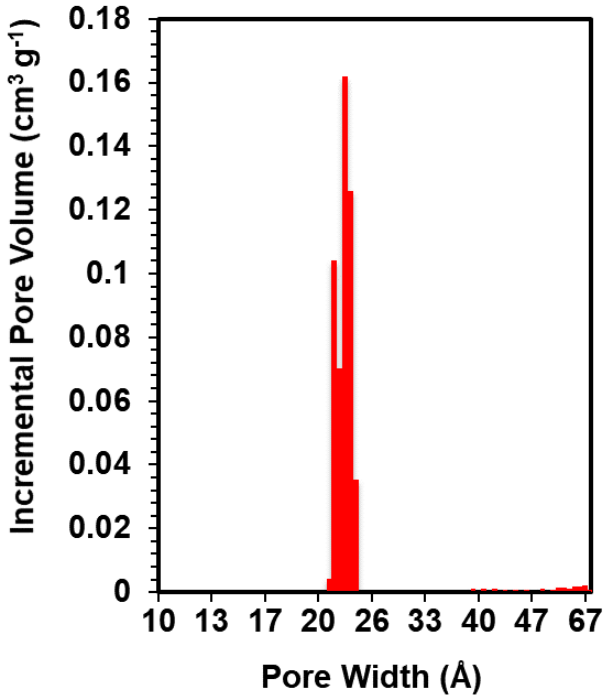

Figure S70. Pore size distribution of BND-TFB COF.

F. Fourier-Transfer Infrared Spectroscopy

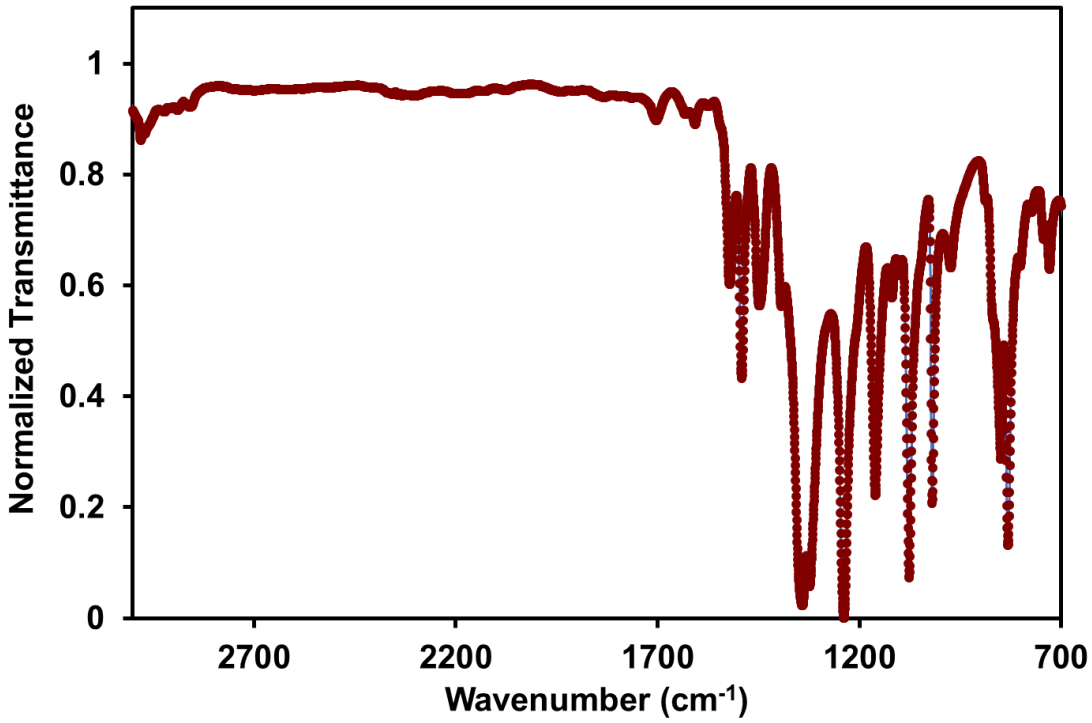

Figure S71. FT-IR Spectra of HHTP-PBBA COF.

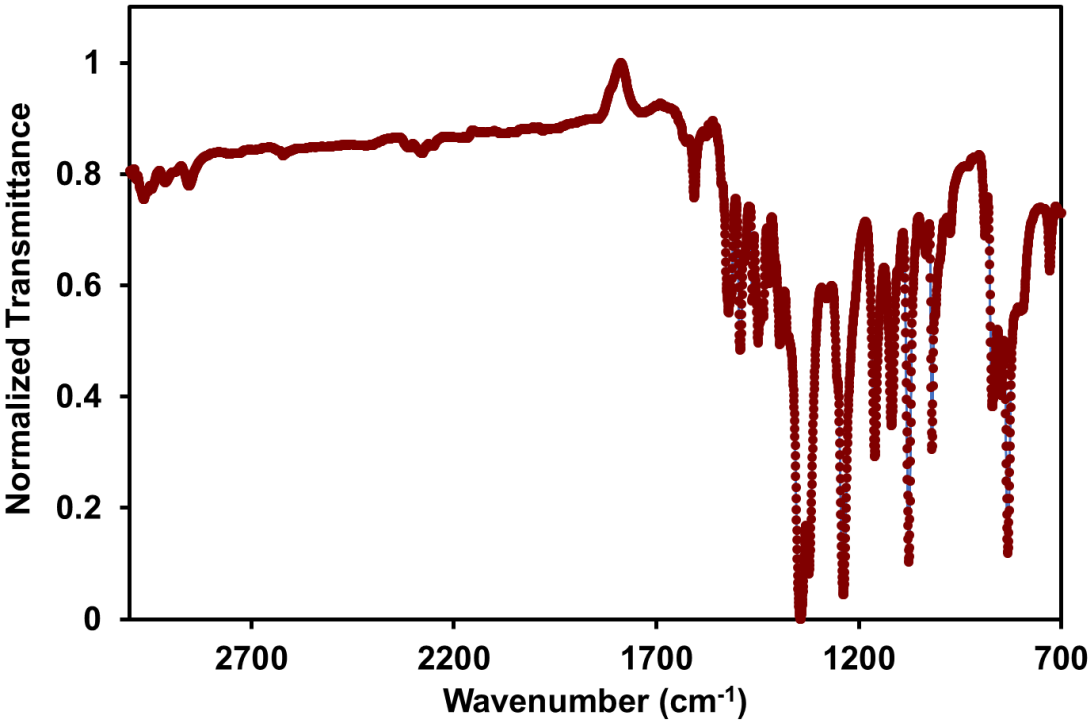

Figure S72. FT-IR Spectra of HHTP-BBBA COF.

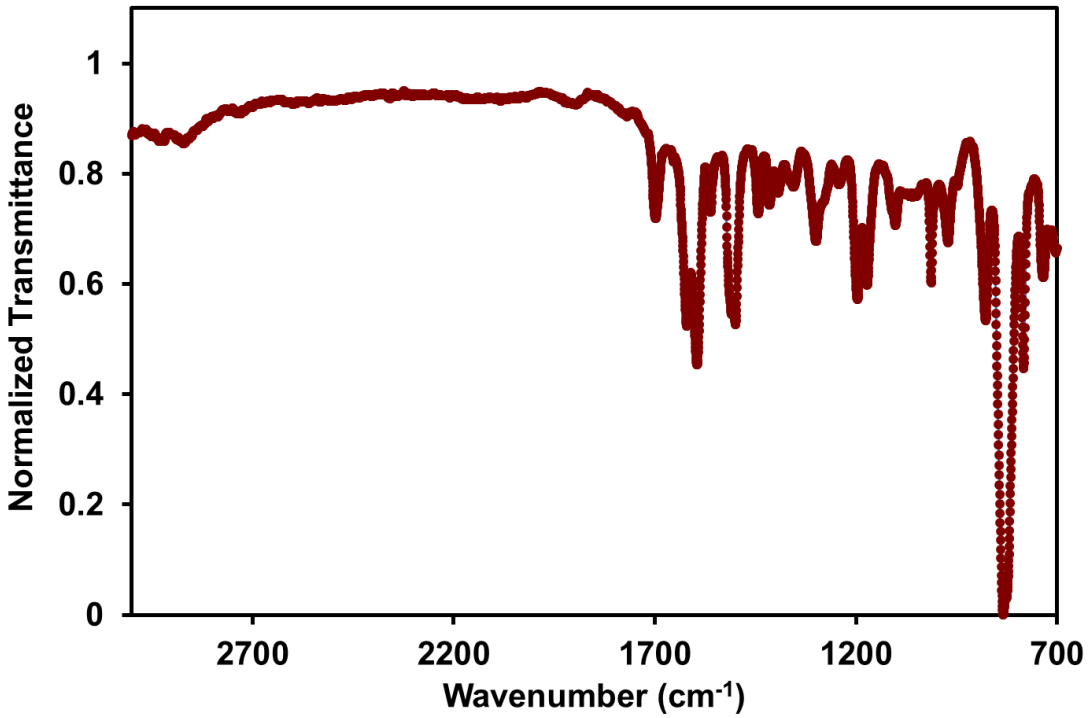

Figure S73. FT-IR Spectra of TAPB-PDA COF.

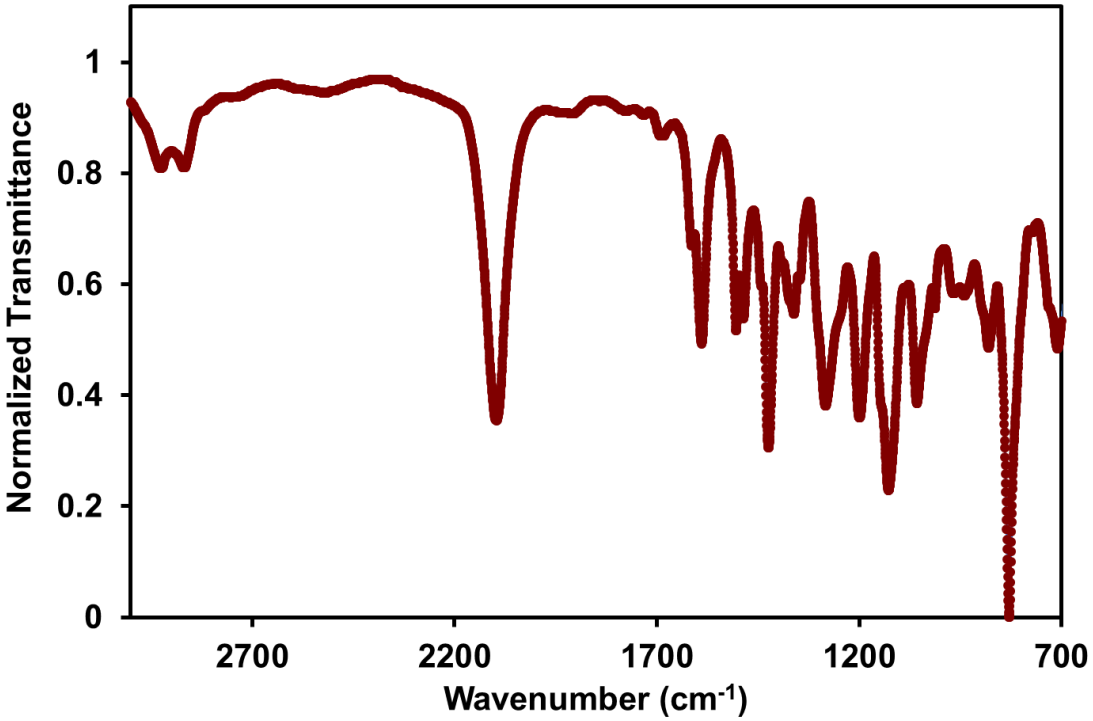

Figure S74. FT-IR Spectra of TAPB-PDA-N_3 COF.

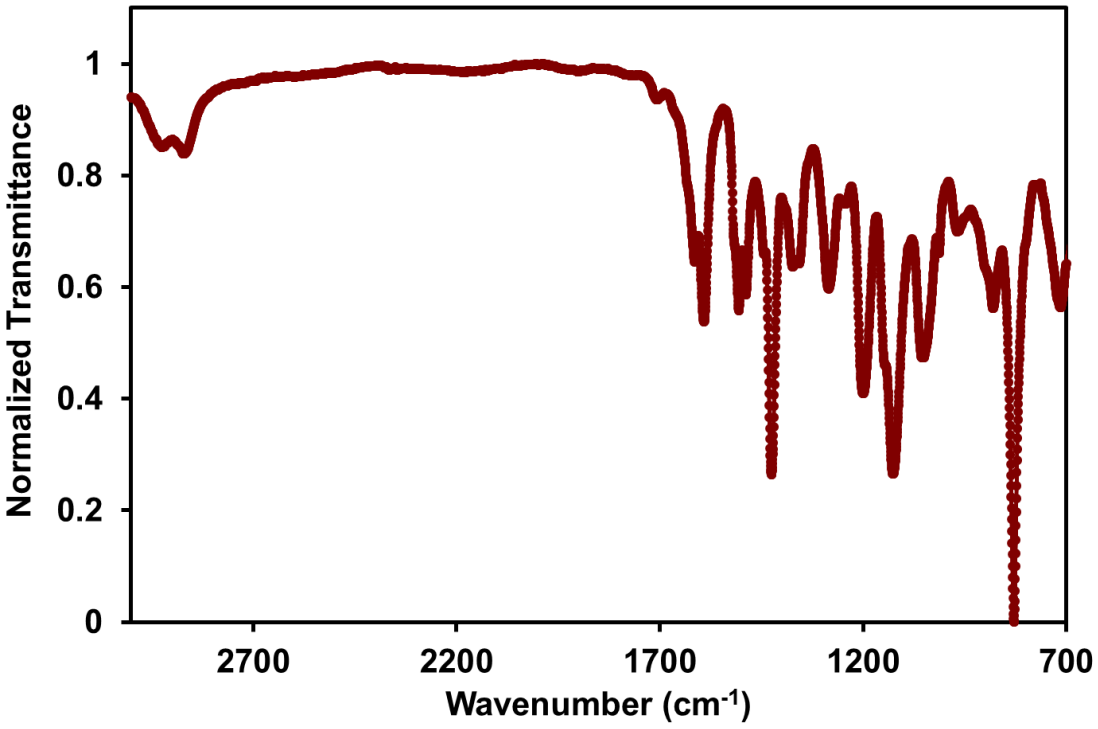

Figure S75. FT-IR Spectra of TAPB-PDA-NH_2 COF.

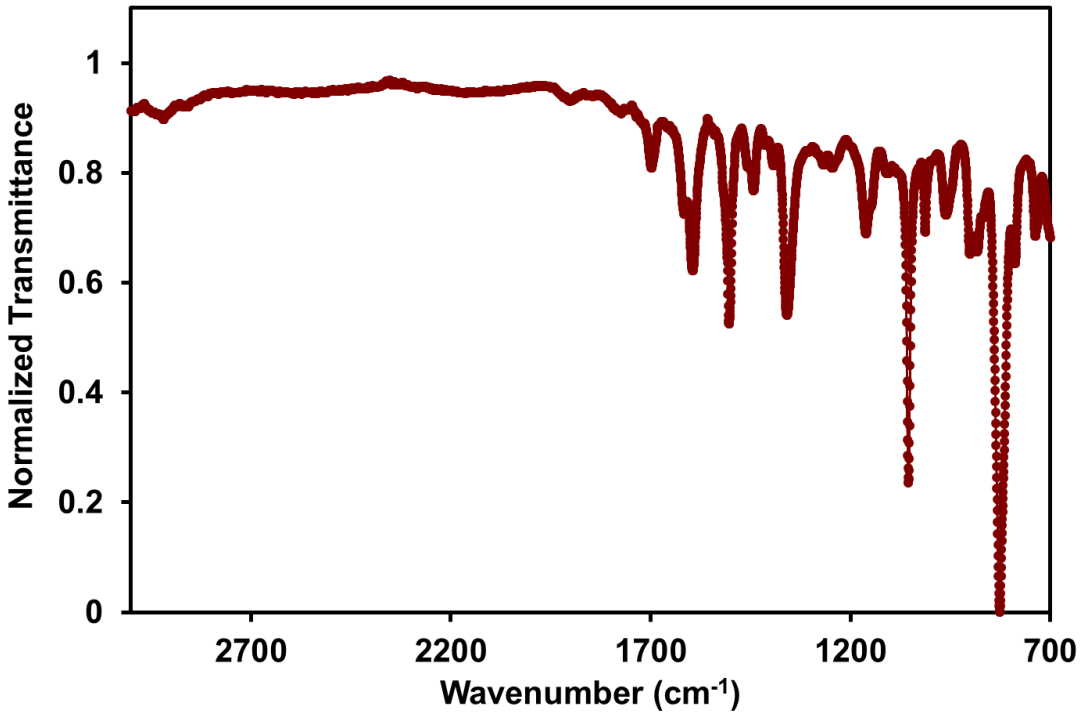

Figure S76. FT-IR Spectra of TAPB-PDA-Br COF.

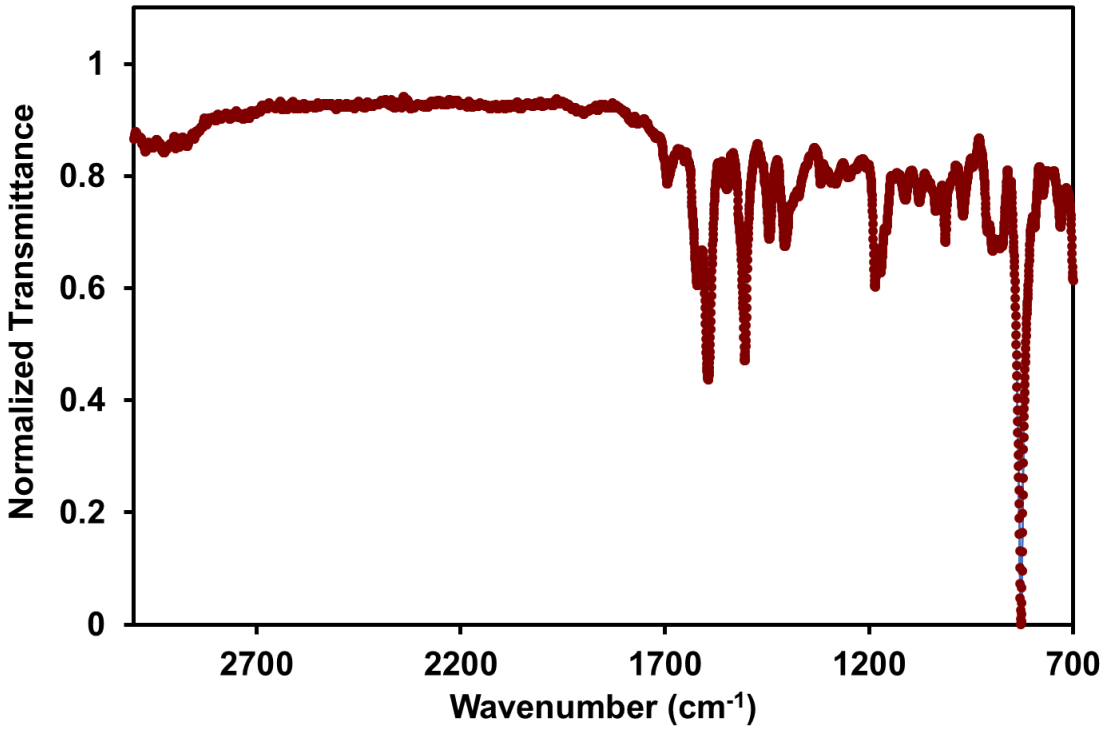

Figure S77. FT-IR Spectra of TAPB-PDA-Me COF.

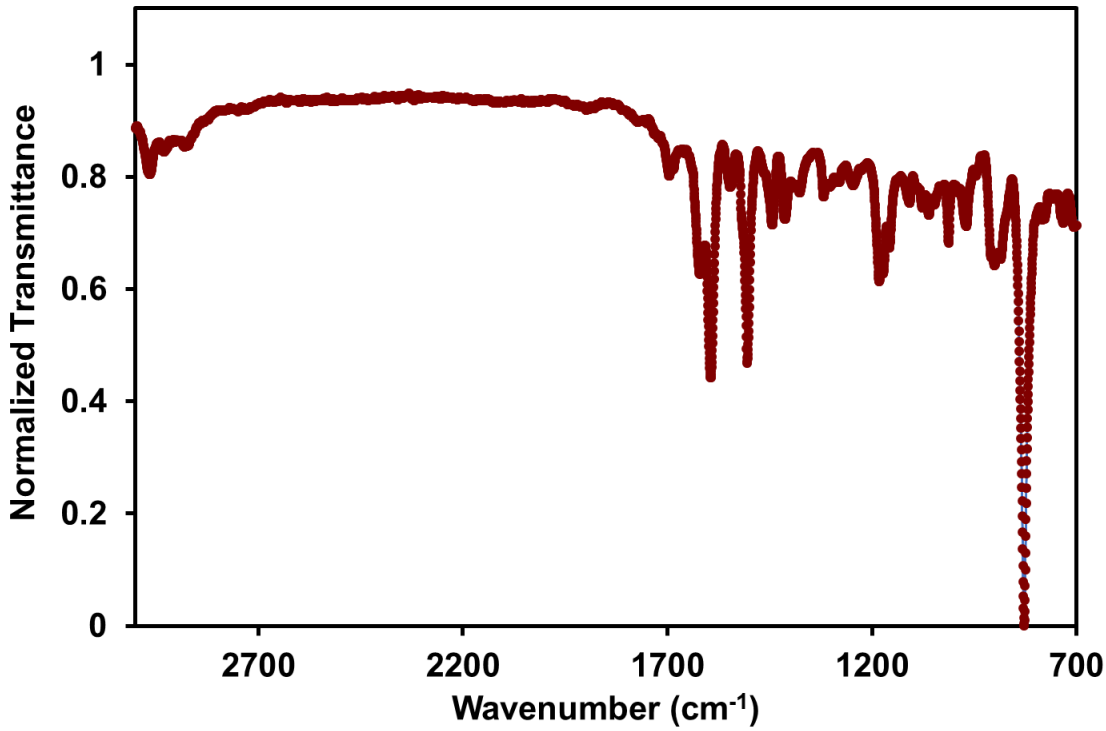

Figure S78. FT-IR Spectra of TAPB-PDA-Et COF.

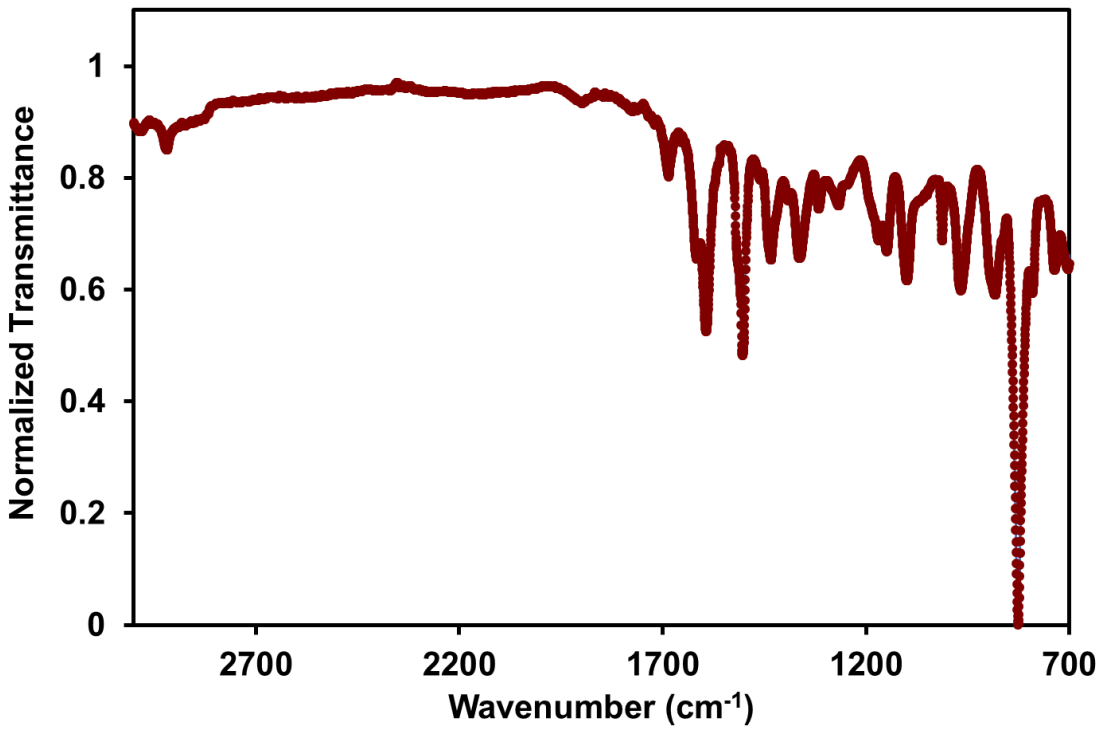

Figure S79. FT-IR Spectra of TAPB-PDA-SMe COF.

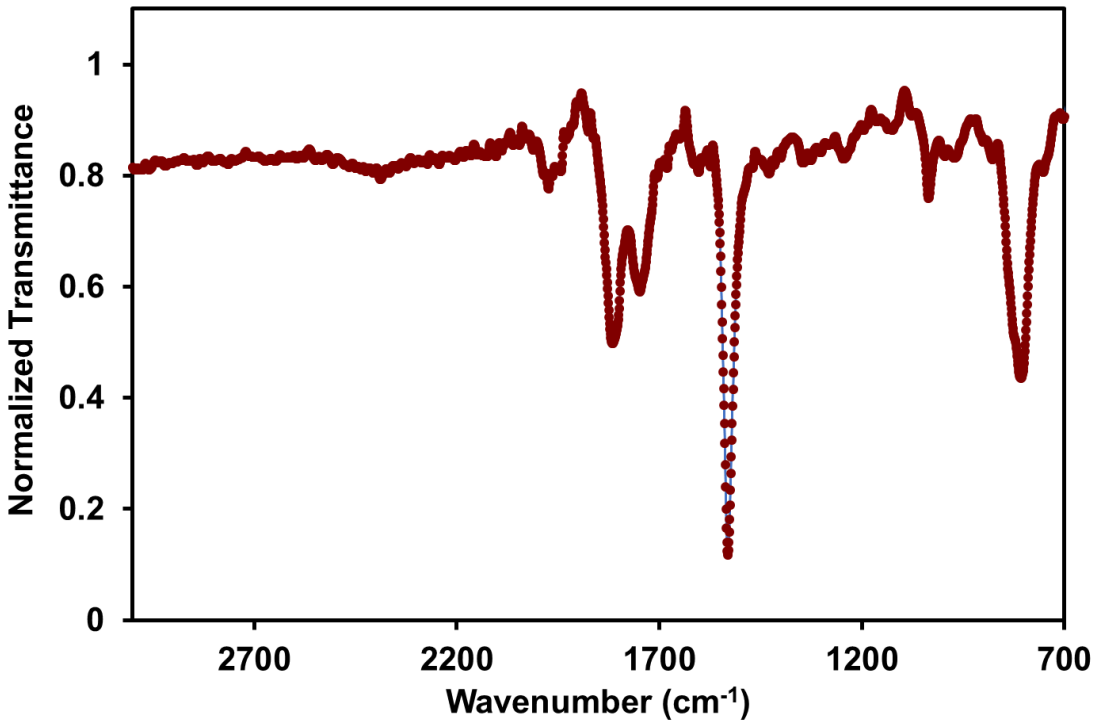

Figure S80. FT-IR Spectra of BND-TFB COF.

G. Diffuse Reflectance for Infrared Fourier Transform Spectroscopy

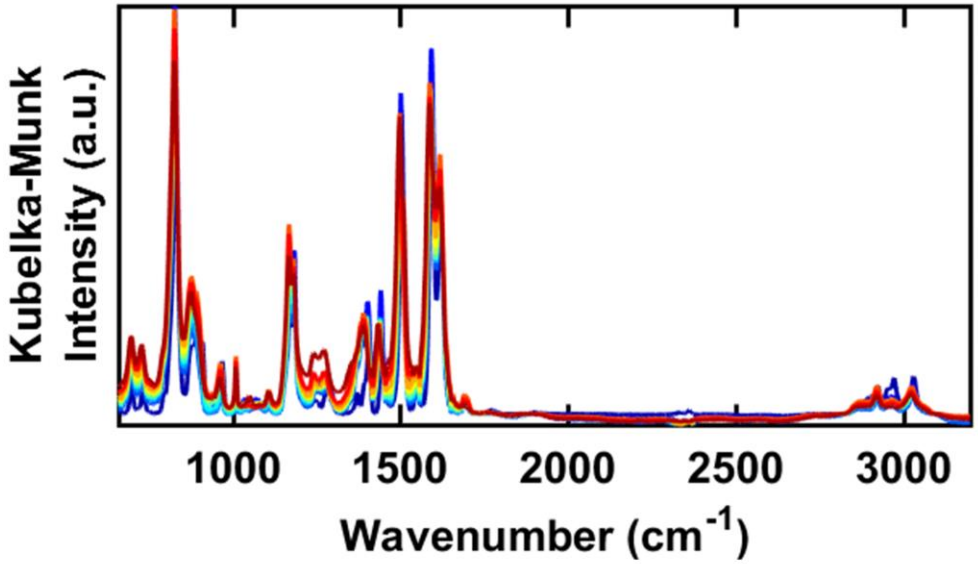

Figure S81. Full DRIFTS spectra of TAPB-PDA-Me COF.

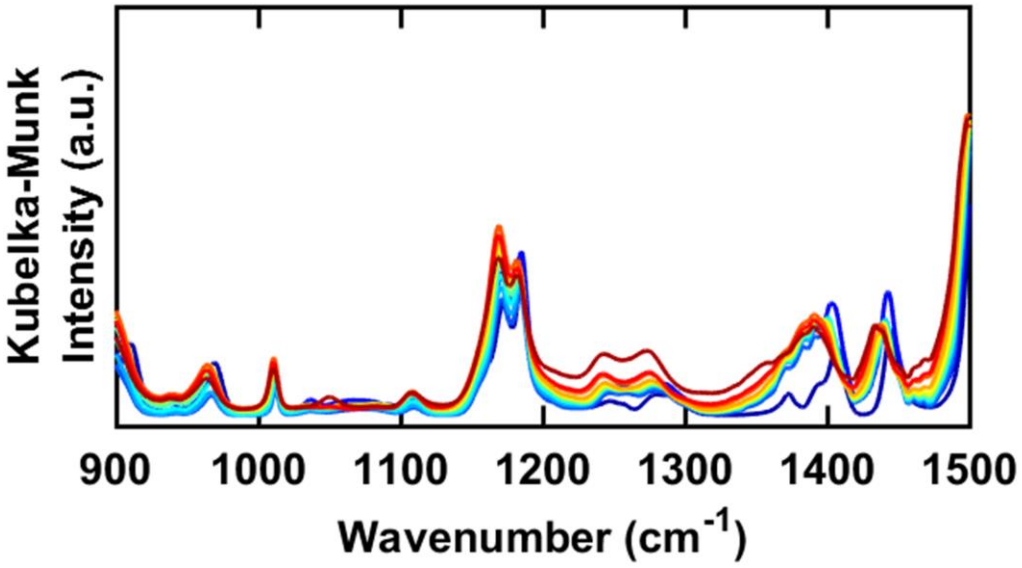

Figure S82. DRIFTS spectra of TAPB-PDA-Me COF from 900–1500 cm^{-1}.

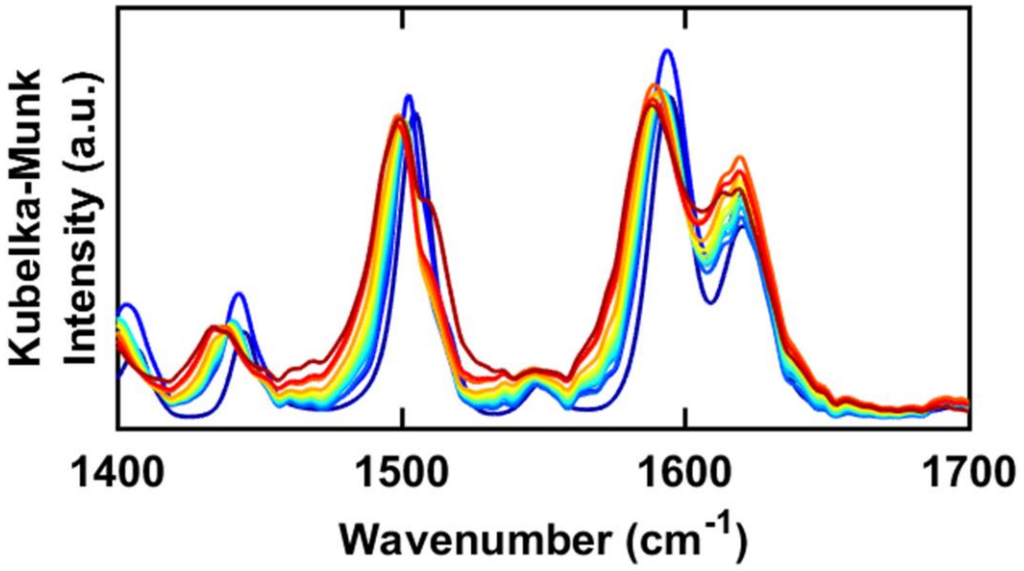

Figure S83. DRIFTS spectra of TAPB-PDA-Me COF from 1400–1700 cm^{-1}.

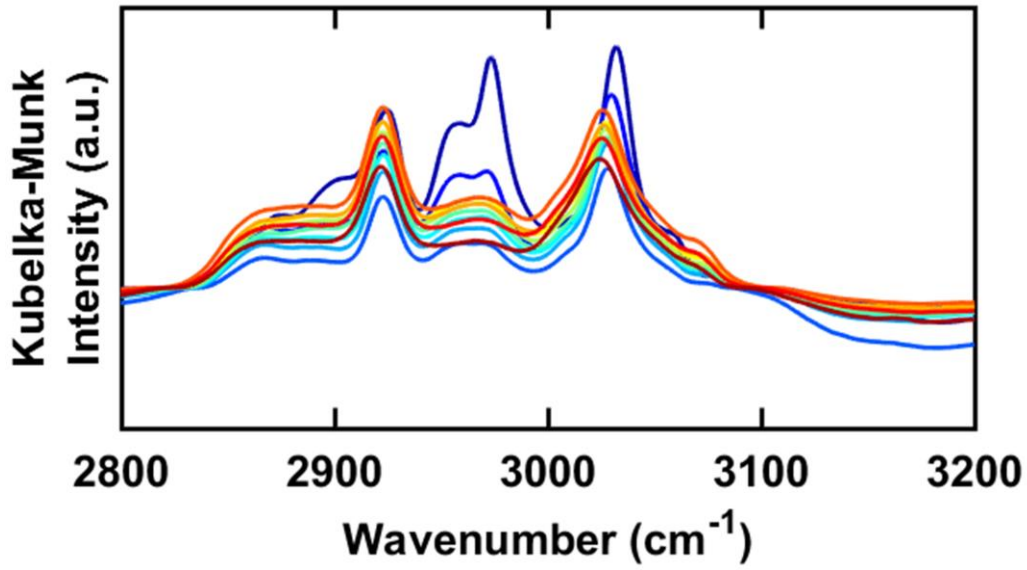

Figure S84. DRIFTS spectra of TAPB-PDA-Me COF from 2800–3200 cm^{-1}.

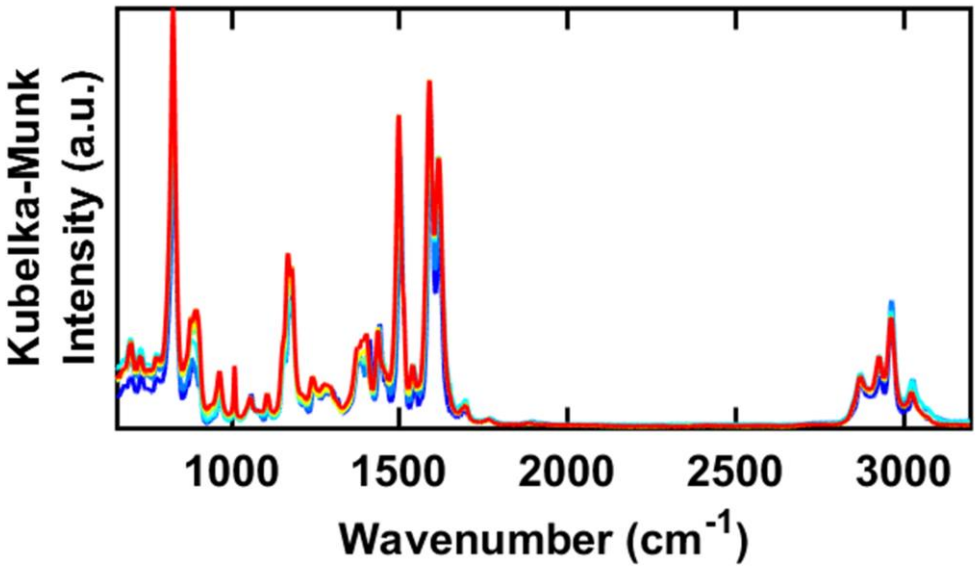

Figure S85. Full DRIFTS spectra of TAPB-PDA-Et COF.

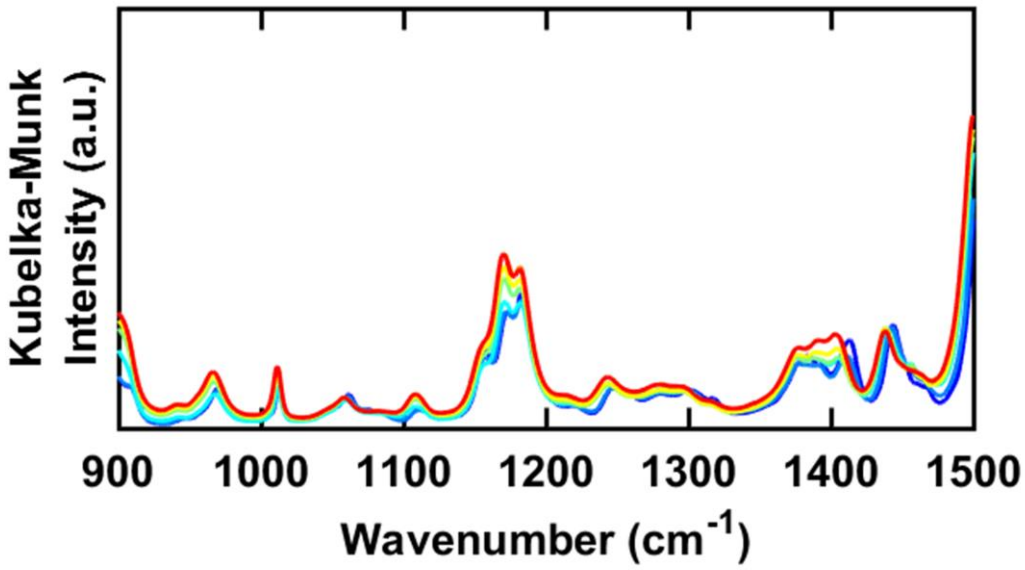

Figure S86. DRIFTS spectra of TAPB-PDA-Et COF from 900–1500 cm^{-1}.

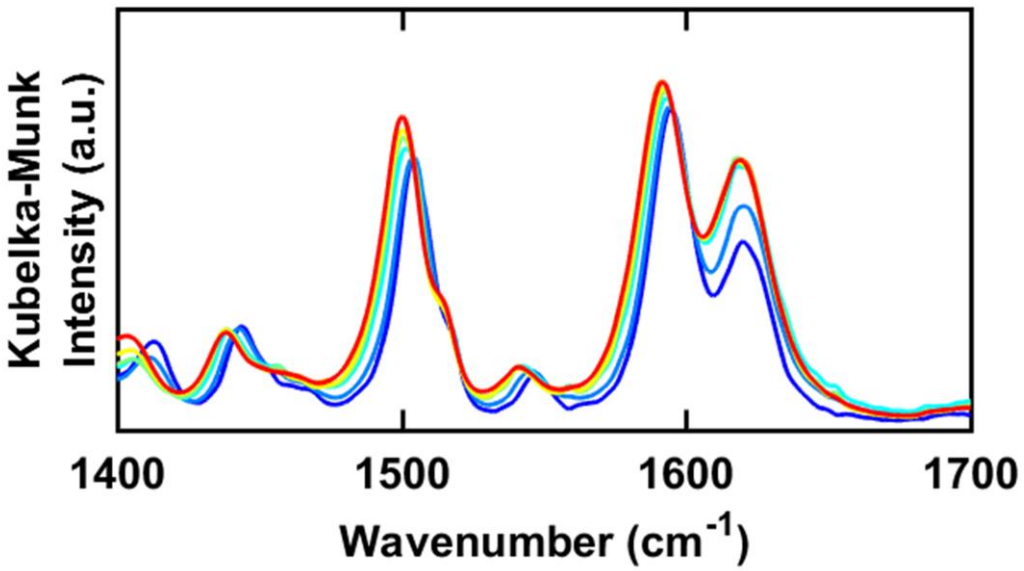

Figure S87. DRIFTS spectra of TAPB-PDA-Et COF from 1400–1700 cm^{-1}.

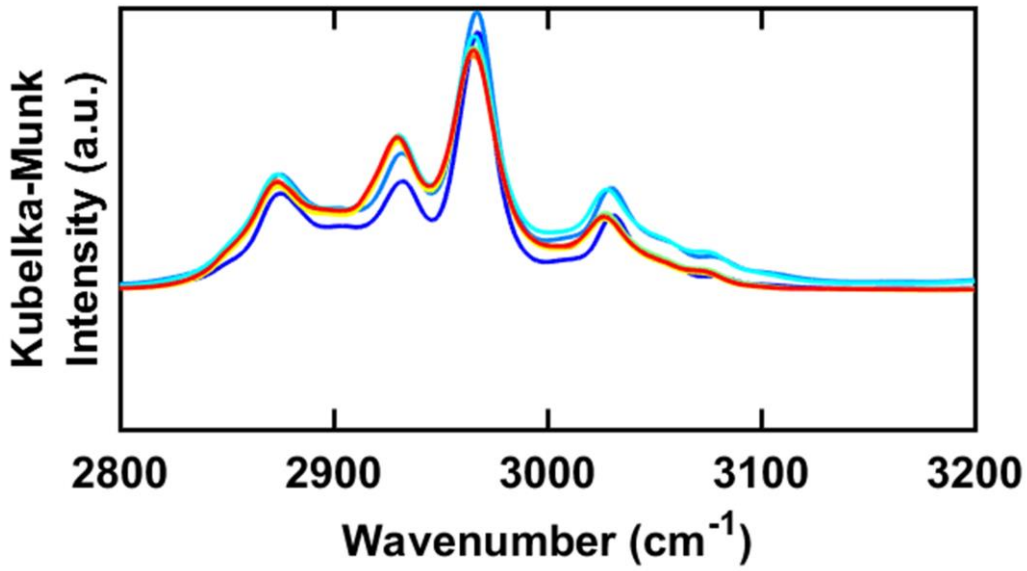

Figure S88. DRIFTS spectra of TAPB-PDA-Et COF from 2800–3200 cm^{-1}.

H. Thermal Gravimetric Analysis

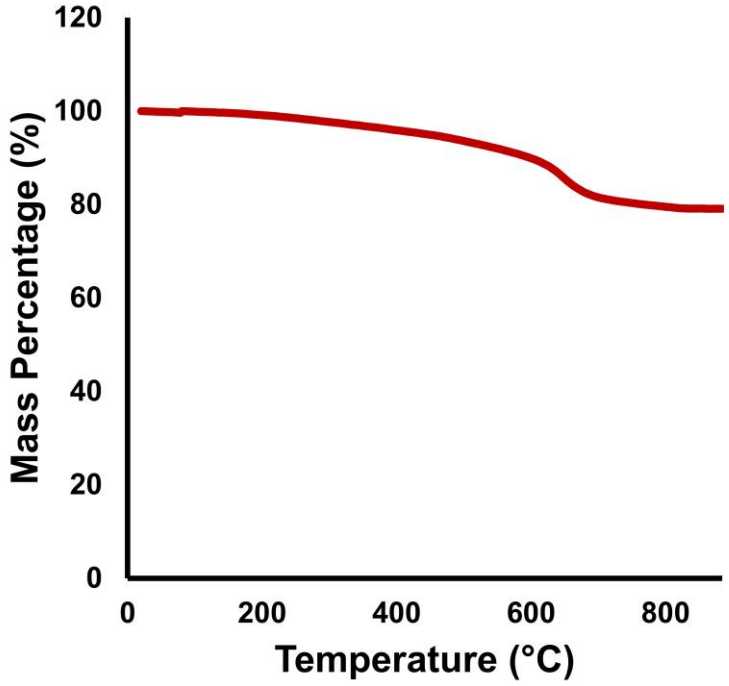

Figure S89. TGA of HHTP-PBBA COF.

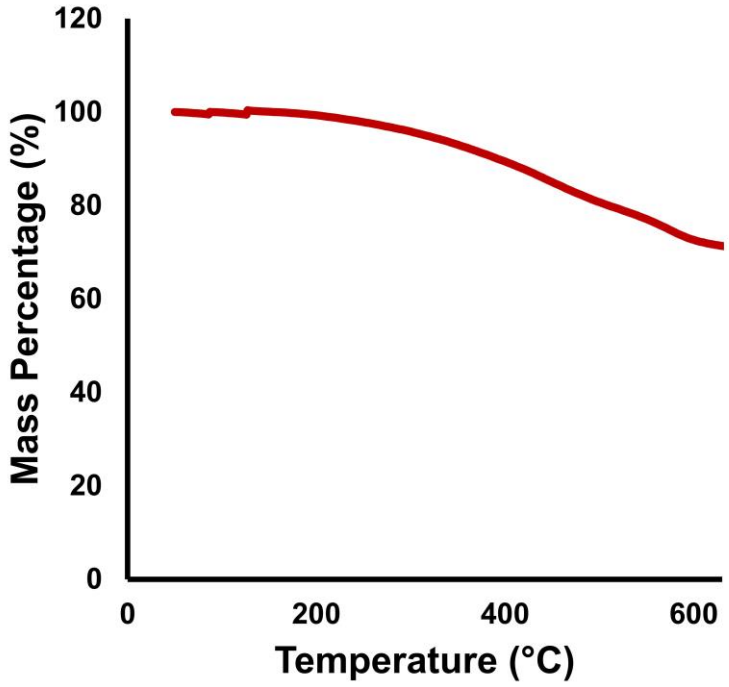

Figure S90. TGA of HHTP-BBBA COF.

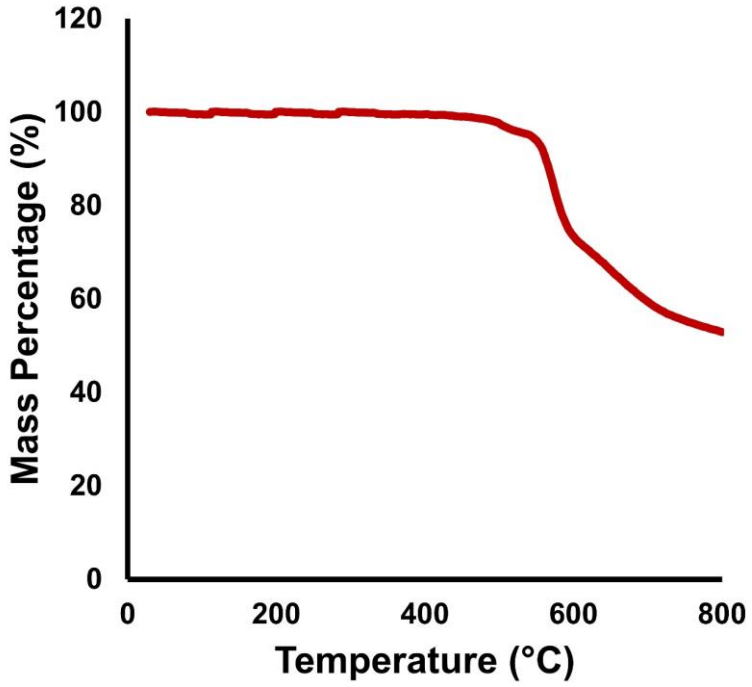

Figure S91. TGA of TAPB-PDA COF.

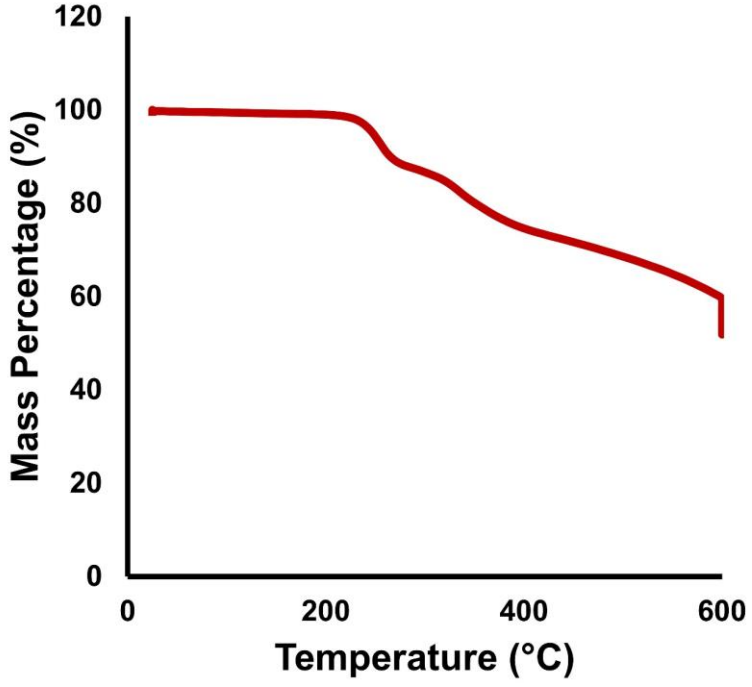

Figure S92. TGA of TAPB-PDA-N_3 COF.

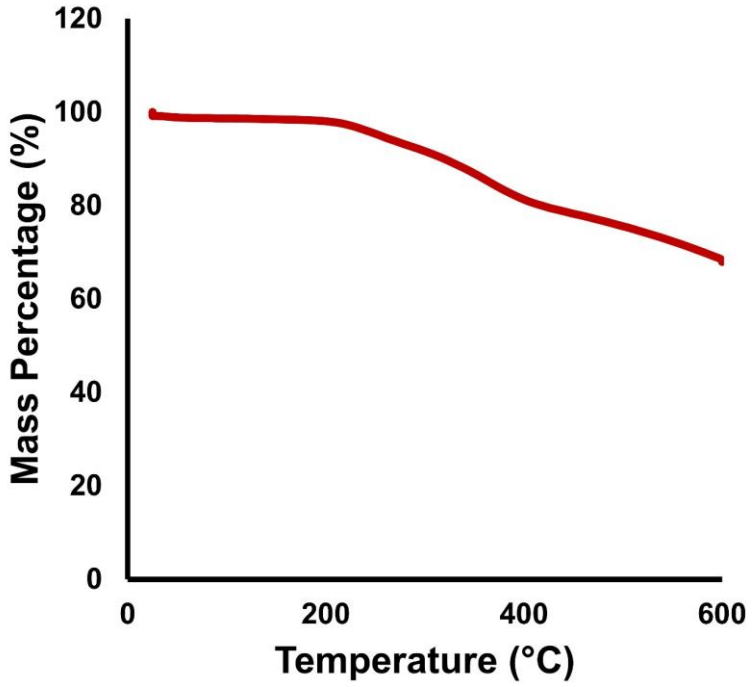

Figure S93. TGA of TAPB-PDA-NH_2 COF.

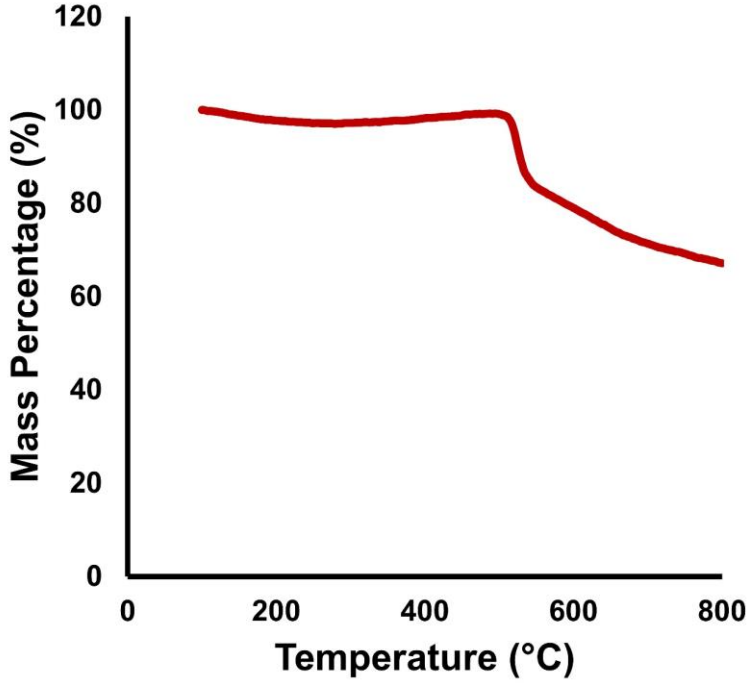

Figure S94. TGA of TAPB-PDA-Br COF.

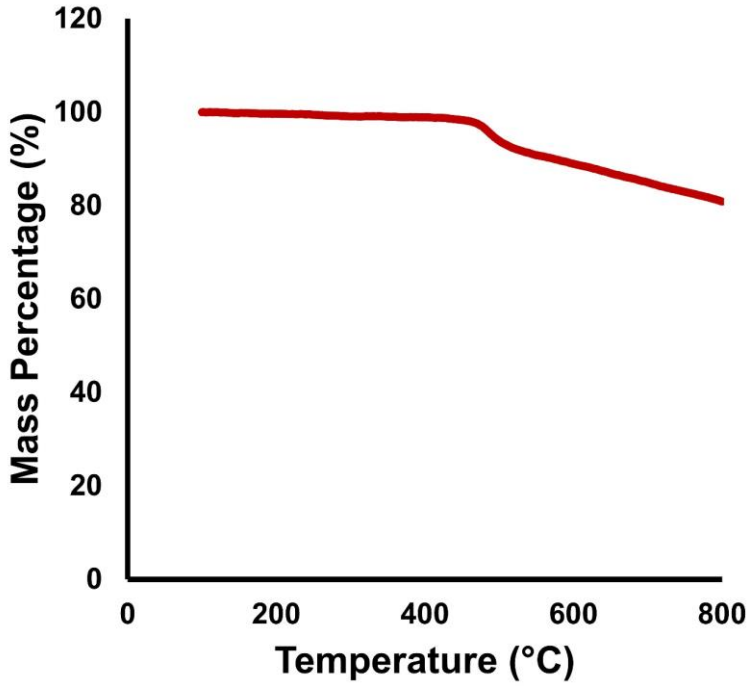

Figure S95. TGA of TAPB-PDA-Me COF.

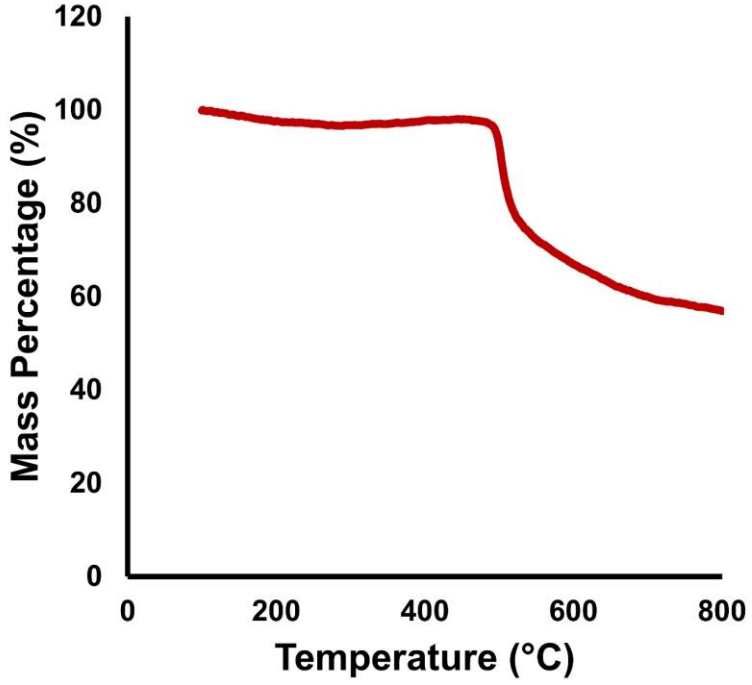

Figure S96. TGA of TAPB-PDA-Et COF.

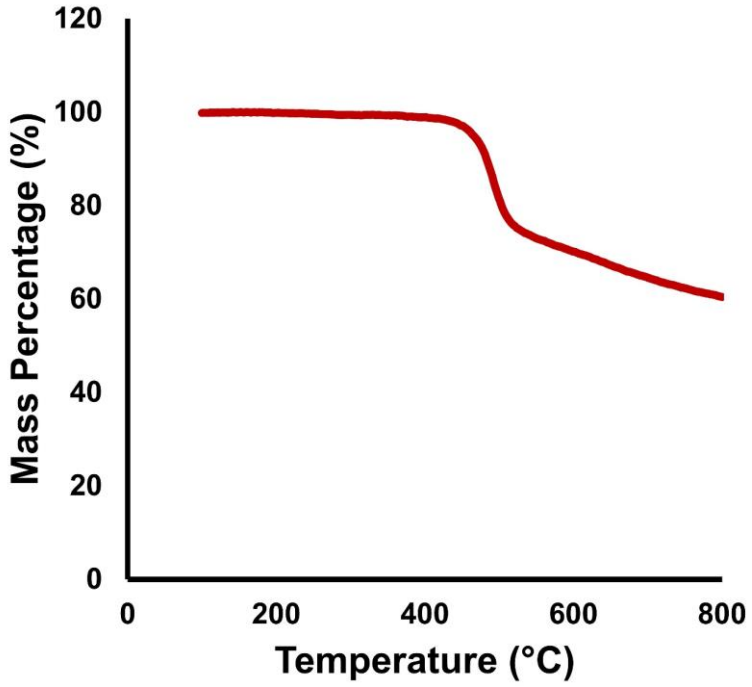

Figure S97. TGA of TAPB-PDA-SMe COF.

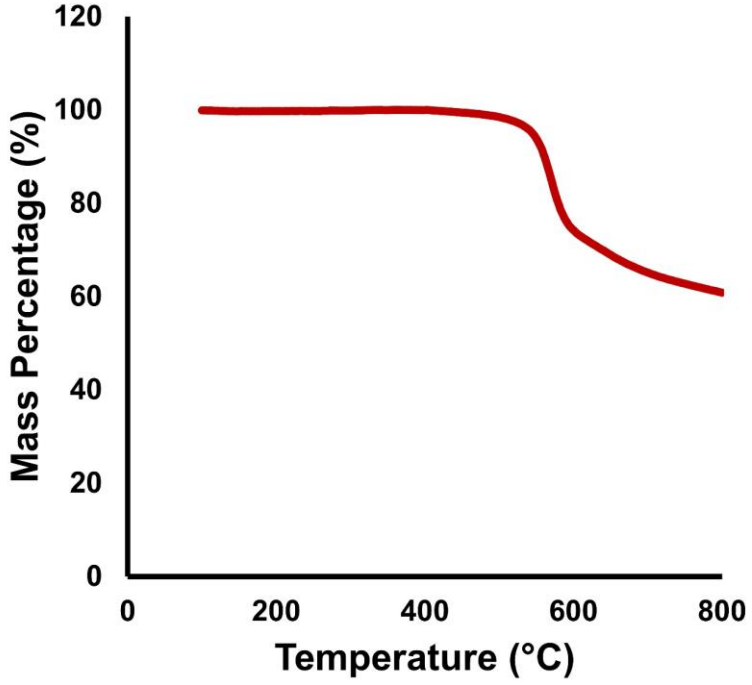

Figure S98. TGA of BND-TFB COF.

I. Density Functional Theory Calculations

Table S1. Summary of the calculated lattice parameters for TPB-PDA COF.

TAPB-PDA							
Phase	*Lattice parameters* (Å)						
	a	*b*	*c*	*α*	*β*	*γ*	Volume (Å^3)
Planar	37.20	37.20	4.04	90.0	90.0	120.0	4837
Deformed	37.03	37.25	4.05	97.8	85.3	120.0	4795
• The planar and deformed geometries have hexagonal and triclinic symmetry, respectively.							

Table S2. Summary of the calculated lattice parameters for TPB-PDA-Et COF.

TAPB-PDA-Et							
Phase	*Lattice parameters* (Å)						
	a	*b*	*c*	*α*	*β*	*γ*	Volume (Å^3)
Planar	37.04	37.04	4.10	90.0	90.0	120.0	4877
Deformed	37.48	37.34	4.08	70.7	109.0	121.1	4795
• The planar and deformed geometries have hexagonal and triclinic symmetry, respectively.							

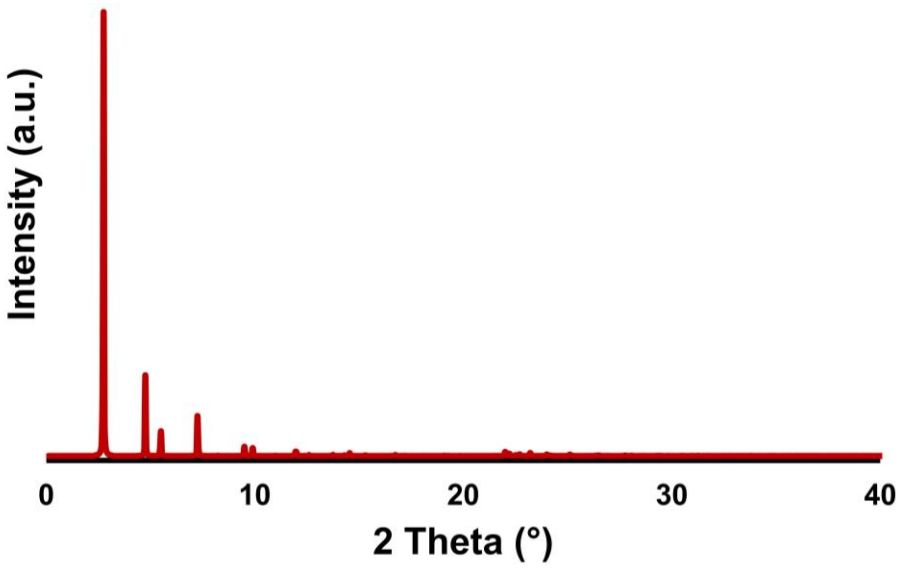

Figure S99. Simulated eclipsed XRD pattern of TAPB-PDA COF.

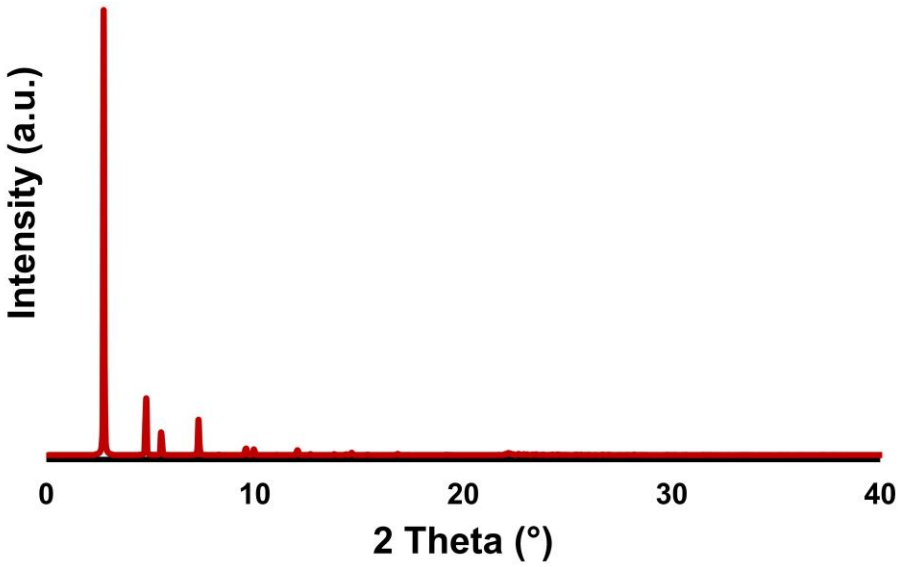

Figure S100. Simulated relaxed XRD pattern of TAPB-PDA COF.

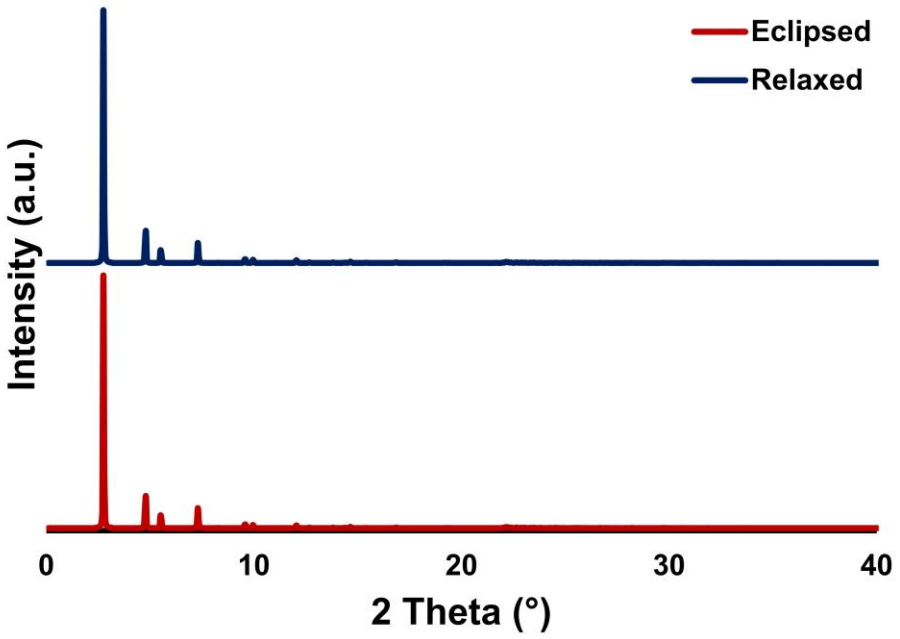

Figure S101. Comparison of simulated relaxed and eclipsed XRD patterns of TAPB-PDA COF.

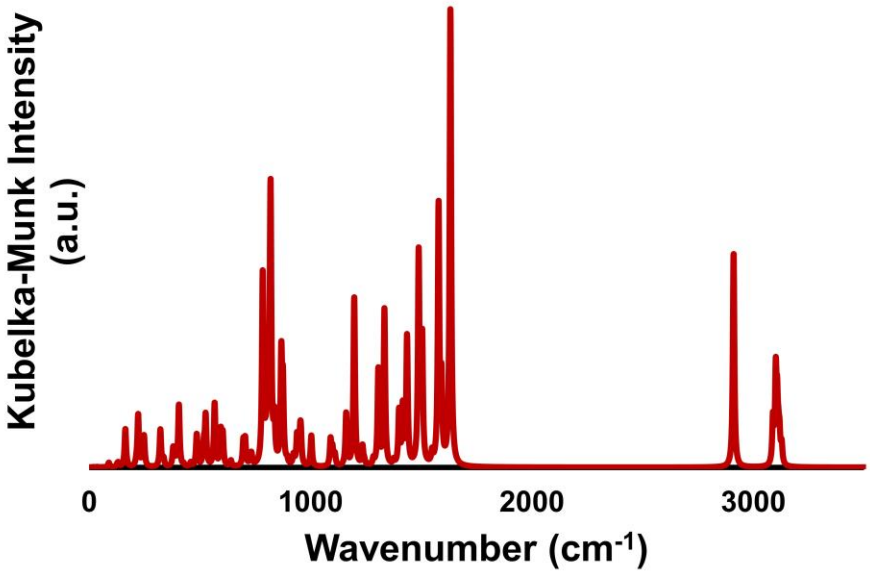

Figure S102. Full simulated IR spectra of TAPB-PDA COF.

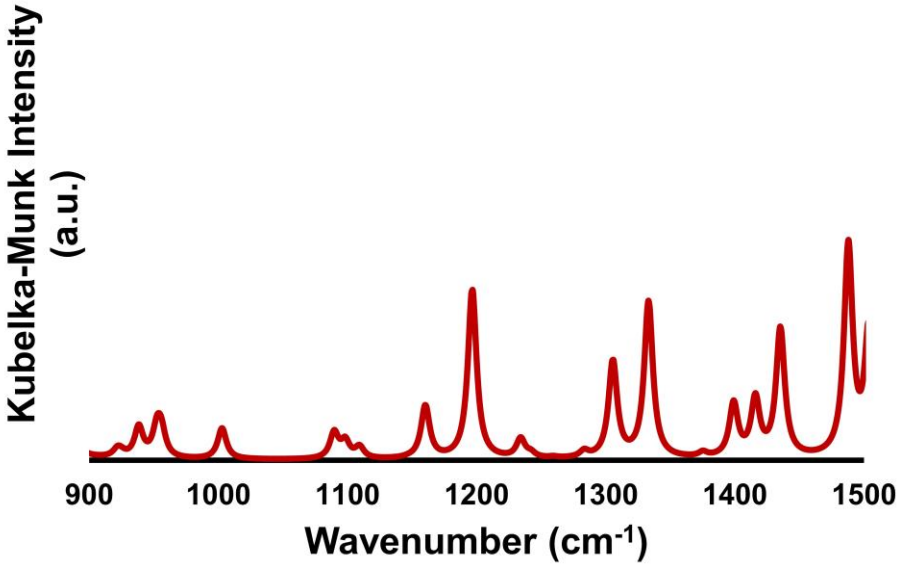

Figure S103. Simulated IR spectra of TAPB-PDA COF from 900–1500 cm^{-1}.

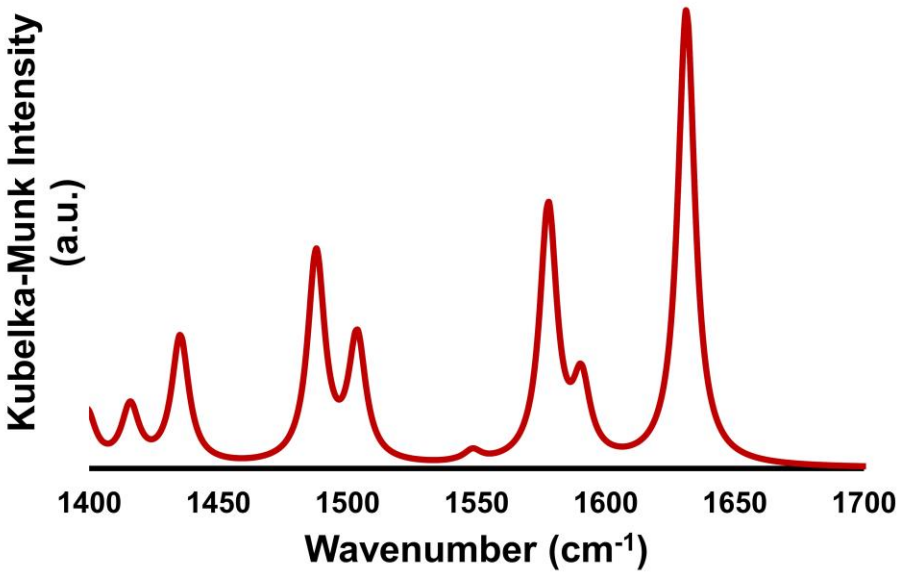

Figure S104. Simulated IR spectra of TAPB-PDA COF from 1400–1700 cm^{-1}.

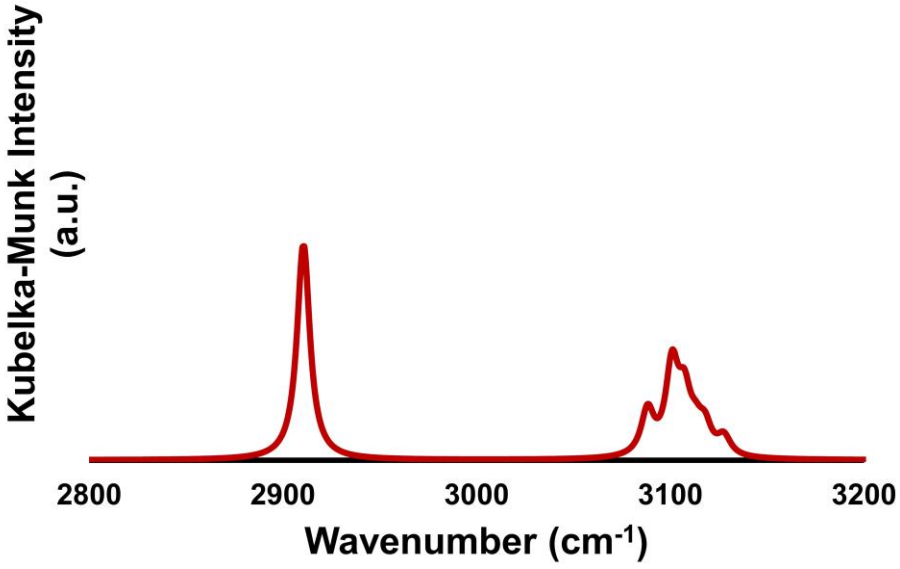

Figure S105. Simulated IR spectra of TAPB-PDA COF from 2800–3200 cm^{-1}.

J. PDA-NH_2 Self-Condensation Control Reaction

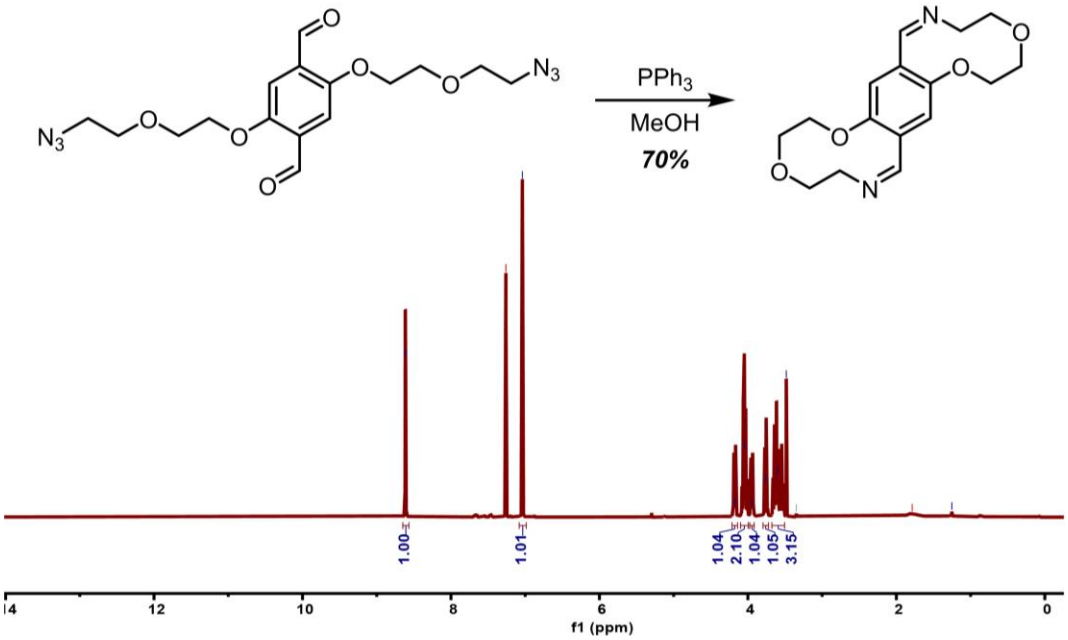

Figure S106. ^{1}H NMR ($CDCl_3$, 500 MHz, 298 K) of the self-condensation of PDA-NH_2 upon reduction of the azide starting material.

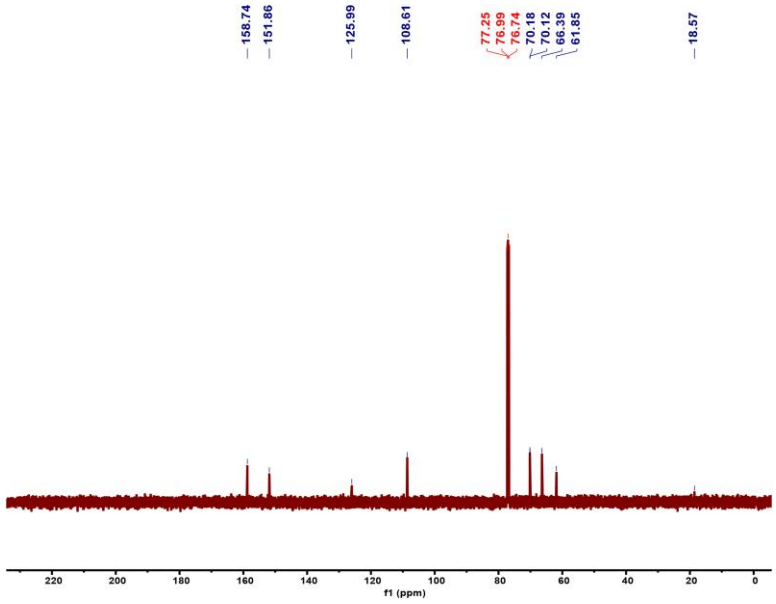

Figure S107. ^{13}C NMR ($CDCl_3$, 126 MHz, 298 K) of the self-condensation of PDA-NH_2 upon reduction of the azide starting material.

K. References

1. Dovesi, R.; Erba, A.; Orlando, R.; Zicovich-Wilson, C. M.; Civalleri, B.; Maschio, L.; Rerat, M.; Casassa, S.; Baima, J.; Salustro, S.; Kirtman, B., Quantum-mechanical condensed matter simulations with CRYSTAL. *Wires Comput Mol Sci* **2018,** *8* (4), e1360.
2. Perdew, J. P.; Burke, K.; Ernzerhof, M., Generalized Gradient Approximation Made Simple. *Phys. Rev. Lett.* **1996,** *77* (18), 3865-3868.
3. Grimme, S.; Antony, J.; Ehrlich, S.; Krieg, H., A consistent and accurate ab initio parametrization of density functional dispersion correction (DFT-D) for the 94 elements H-Pu. *J. Chem. Phys.* **2010,** *132* (15), 154104.
4. Ryder, M. R.; Maul, J.; Civalleri, B.; Erba, A., Quasi-Harmonic Lattice Dynamics of a Prototypical Metal–Organic Framework. *Advanced Theory and Simulations* **2019,** *2* (11), 1900093.
5. Ryder, M. R.; Van de Voorde, B.; Civalleri, B.; Bennett, T. D.; Mukhopadhyay, S.; Cinque, G.; Fernandez-Alonso, F.; De Vos, D.; Rudic, S.; Tan, J. C., Detecting Molecular Rotational Dynamics Complementing the Low-Frequency Terahertz Vibrations in a Zirconium-Based Metal-Organic Framework. *Phys. Rev. Lett.* **2017,** *118* (25), 255502.
6. Ryder, M. R.; Civalleri, B.; Bennett, T. D.; Henke, S.; Rudic, S.; Cinque, G.; Fernandez-Alonso, F.; Tan, J. C., Identifying the role of terahertz vibrations in metal-organic frameworks: from gate-opening phenomenon to shear-driven structural destabilization. *Phys. Rev. Lett.* **2014,** *113* (21), 215502.
7. Broyden, C. G., The Convergence of a Class of Double-rank Minimization Algorithms 1. General Considerations. *J. Inst. Maths Applics* **1970,** *6* (1), 76-90.
8. Broyden, C. G., The Convergence of a Class of Double-rank Minimization Algorithms: 2. The New Algorithm. *J. Inst. Maths Applics* **1970,** *6* (3), 222-231.
9. Fletcher, R., A New Approach to Variable Metric Algorithms. *Comput. J.* **1970,** *13* (3), 317-322.
10. Goldfarb, D., A Family of Variable-Metric Methods Derived by Variational Means. *Math. Comput.* **1970,** *24* (109), 23-26.
11. Shanno, D. F., Conditioning of Quasi-Newton Methods for Function Minimization. *Math. Comput.* **1970,** *24* (111), 647-656.
12. Noel, Y.; Zicovich-Wilson, C. M.; Civalleri, B.; D'Arco, P.; Dovesi, R., Polarization properties of ZnO and BeO:Anab initiostudy through the Berry phase and Wannier functions approaches. *Phys. Rev. B* **2001,** *65* (1).
13. Abellán-Flos, M.; Tanç, M.; Supuran, C. T.; Vincent, S. P., Exploring carbonic anhydrase inhibition with multimeric coumarins displayed on a fullerene scaffold. *Org Biomol Chem* **2015,** *13* (27), 7445-7451.
14. Ji, W.; Xiao, L.; Ling, Y.; Ching, C.; Matsumoto, M.; Bisbey, R. P.; Helbling, D. E.; Dichtel, W. R., Removal of GenX and Perfluorinated Alkyl Substances from Water by Amine-Functionalized Covalent Organic Frameworks. *Journal of the American Chemical Society* **2018,** *140* (40), 12677-12681.
15. Okada, Y.; Sugai, M.; Chiba, K., Hydrogen-Bonding-Induced Fluorescence: Water-Soluble and Polarity-Independent Solvatochromic Fluorophores. *The Journal of Organic Chemistry* **2016,** *81* (22), 10922-10929.
16. Xie, Z.; Yang, B.; Liu, L.; Li, M.; Lin, D.; Ma, Y.; Cheng, G.; Liu, S., Experimental and theoretical studies of 2,5-diphenyl-1,4-distyrylbenzenes with all-cis- and all-trans double bonds: chemical structure determination and optical properties. *Journal of Physical Organic Chemistry* **2005,** *18* (9), 962-973.
17. Corcos, A. R.; Levato, G. A.; Jiang, Z.; Evans, A. M.; Livingston, A. G.; Mariñas, B. J.; Dichtel, W. R., Reducing the Pore Size of Covalent Organic Frameworks in Thin-Film Composite Membranes Enhances Solute Rejection. *ACS Materials Letters* **2019,** *1* (4), 440-446.
18. Wessig, P.; Gerngroß, M.; Freyse, D.; Bruhns, P.; Przezdziak, M.; Schilde, U.; Kelling, A., Molecular Rods Based on Oligo-spiro-thioketals. *The Journal of Organic Chemistry* **2016,** *81* (3), 1125-1136.

19. Yamamoto, T.; Nishimura, T.; Mori, T.; Miyazaki, E.; Osaka, I.; Takimiya, K., Largely π-Extended Thienoacenes with Internal Thieno[3,2-b]thiophene Substructures: Synthesis, Characterization, and Organic Field-Effect Transistor Applications. *Organic Letters* **2012,** *14* (18), 4914-4917.
20. Vitaku, E.; Dichtel, W. R., Synthesis of 2D Imine-Linked Covalent Organic Frameworks through Formal Transimination Reactions. *Journal of the American Chemical Society* **2017,** *139* (37), 12911-12914.
21. Côté, A. P.; Benin, A. I.; Ockwig, N. W.; O'Keeffe, M.; Matzger, A. J.; Yaghi, O. M., Porous, Crystalline, Covalent Organic Frameworks. *Science* **2005,** *310* (5751), 1166-1170.
22. Matsumoto, M.; Dasari, R. R.; Ji, W.; Feriante, C. H.; Parker, T. C.; Marder, S. R.; Dichtel, W. R., Rapid, Low Temperature Formation of Imine-Linked Covalent Organic Frameworks Catalyzed by Metal Triflates. *Journal of the American Chemical Society* **2017,** *139* (14), 4999-5002.
23. Xu, H.; Gao, J.; Jiang, D., Stable, crystalline, porous, covalent organic frameworks as a platform for chiral organocatalysts. *Nature Chemistry* **2015,** *7* (11), 905-912.